A Non-filtering Gear Fault Detection Method

Elise Mayo

Thesis submitted to the Faculty of Graduate and Postdoctoral Studies

in partial fulfillment of the requirements for the degree of

Master of Applied Science
in Mechanical Engineering

Ottawa-Carleton Institute for Mechanical and Aerospace Engineering

University of Ottawa

Ottawa, Ontario

March 2016

Abstract

Rotating elements, including gears, are one of the most problematic elements in machinery. It is not preferable to monitor their condition visually considering time and money is required to take apart the machine to observe the parts. Monitoring of gears is important because the failure of such elements can cause major damage to machinery. A few non-invasive methods are proposed, however vibration analysis is, so far, the most efficient way to monitor the condition of the gear. Vibrations are caused by the continuous contact between the two rotating gears. When a fault occurs, the signal is modified in different ways depending on the type of fault - distributed or local. Many fault detection methods are effective for one type of fault or the other. In this thesis, several methods are proposed with the objective of finding an efficient method for both types of faults. The calculus enhanced energy operator (CEEO), previously designed for bearing fault detection, is proposed here for the first time on gears. Two other methods, the EO123 and EO23, are derived based on the original energy operator. The proposed methods are filter free, simple and can handle a certain level of noise and interference. With the exception of low rotational frequencies of the gears, it can be concluded from simulated and experimentally-obtained signals that the CEEO method can handle noise better than the other proposed methods and that the EO23 method can handle interference better than the others. Different conditions determine the effectiveness of the methods.

Acknowledgments

I would like to express my sincere gratitude to my supervisor, Professor Ming Liang, who has steered me and taught me about the field throughout my work. I would also like to thank immensely my co-supervisor, Professor Natalie Baddour, who guided my work and generously gave her time in order to help me reach my goal.

As well, I am grateful to Professors Chuan Li and Zhipeng Feng for collection of the experimental data from the gearbox dynamic test rig of our laboratory, used in Chapters 4 and 5, respectively.

I would also like to thank my colleagues that have made this hard task more enjoyable. Finally, I am grateful for the support my family has given me throughout the two years needed to complete my Masters of Applied Science.

Contents

List of Figures

List of Tables

Chapter 1 Introduction

There is a lot of interest in the detection of faults in gears. These rotating components work under load and in strenuous environments such as factories or moving vehicles. With the appearance of a fault, time and continuous use leads to the increase in size of the fault and eventually a system failure will ensue. It is therefore important to detect gear faults as early as possible. The difficulty is that gears are inside a closed box, which makes it difficult to visually identify a fault. To visually observe the gear's condition, the machine in question needs to be stopped. In a factory, this would result in a reduction of production time and would require additional workforce; it is therefore an expensive maintenance. Another example to consider is the maintenance of gears in helicopter gearboxes. If a fault occurs during flight and results in a failure of the gearbox, the whole system will be compromised. Therefore, being able to monitor a gear, while the system is running, lessens the cost and time needed for machine maintenance.

A widely used method to monitor the health of a gear is vibration analysis of the signal acquired with an accelerometer [1]–[7]. This acquired vibration signal is a combination of impulses caused by gear meshing, noise, interfering signals, in addition to the impulses caused by faults. The main goal of the processing of this acquired signal is to enhance the fault components of the signal and reduce the other components of the signal. There are many challenges faced to achieve this.

The objective of this thesis is to find an effective method of gear vibration signal processing that does not require initial information about the gear's condition. Therefore, a non-filtering fault detection method is developed. The methods employed are inspired by the energy

operator (EO) developed by Teager [8]. A frequency-domain analysis is then performed. More precisely; the Fourier Transform is applied to the time domain signals processed by the proposed methods to identify the pertinent frequencies.

Three proposed methods are compared to the original energy operator approach. These methods are first examined using simulation data for both distributed faults and local faults with impulsive signal features. In both cases, the methods' ability to handle noise and interfering signals is observed. Finally, to prove the efficiency of these methods, they have to be tested on experimental faulty signals. These also include interferences and noise. The advantages and disadvantages of the methods are then discussed.

1.1 Outline of the thesis

The thesis is structured as follows. Chapter 2 contains a literature review of gearbox fault detection. The theory behind the proposed methods is explained in Chapter 3. There are two types of faults on gears that affect the signal differently, local faults and distributed faults. The efficiency of fault detection methods on distributed faults and local faults is observed in Chapter 4 and Chapter 5 respectively.

1.2 Contributions of the thesis

The calculus enhanced energy operator (CEEO) is a fault detection method originally proposed for fault detection in bearings. It is studied here for the first time for fault detection in gears. Two other variations of the energy operator (EO), the EO123 and the EO23, are developed and proposed here for the first time.

Chapter 2 Literature review

There are different methods used for gearbox fault detection. Many use vibration analysis [1]–[4], [8], [9], others use wear debris analysis [5], [6] or thermal imaging [10]. Thermal imaging or thermography works by converting infrared radiation scanned with an infrared camera into an electrical signal [11]. To get accurate fault detection, the 'thermal signature' of a healthy gear needs to be stored. Wear debris analysis has been shown to be effective simply for the detection of wear [5], [12]. This method does not detect other types of fault such as cracks and fractures unless it is used in conjunction with the monitoring of the vibration signal [6].

As gears rotate and the gear teeth come into contact with each other, cracks, spalls or wear wilcause vibration features that are each identifiable if an effective data analysis method is available. The resulting vibration signal can include two different types of faults, distributed and local faults. Spatially distributed faults such as wear result in distributed features in the vibration signal, as shown in Figure 2.1 (c). These features have particular characteristics that can be detected by some fault detection methods. The other type of fault in gears is spatially localized faults. Local faults result in impulsive vibration features in the signal – signals that are also localized in time. These are caused by spatially-localized faults such as cracks or spalls, for example. In Figure 2.1 (a), the peaks in the time-domain signal generated by a local fault are narrower than the peaks observed in Figure 2.1 (c), the time-domain signal generated by distributed faults. Spatially distributed faults result in temporally-distributed features in the vibration signal, whereas spatially-localized faults results in temporally-localized signal features. In the frequency domain, the signal generated by a local fault, Figure 2.1 (b) shows single peaks

at the meshing frequency and its harmonics and smaller sidebands showing the presence of faults. On the other hand, distributed faults in the frequency domain, as shown in Figure 2.1 (d), include large sidebands around the meshing frequency and its harmonics.

Vibration analysis for fault detection is the most widely used method [1]–[4], [8], [9]. To extract the data for spectral analysis, an accelerometer is placed on the gear box such that the lateral vibration movement of the rotating element, in this case the gear, can be detected. It is possible to recognize fault features and extract the fault feature from the vibration signal. The signal is then processed either in the time domain, the frequency domain or the time-frequency domain to enable more detailed analysis.

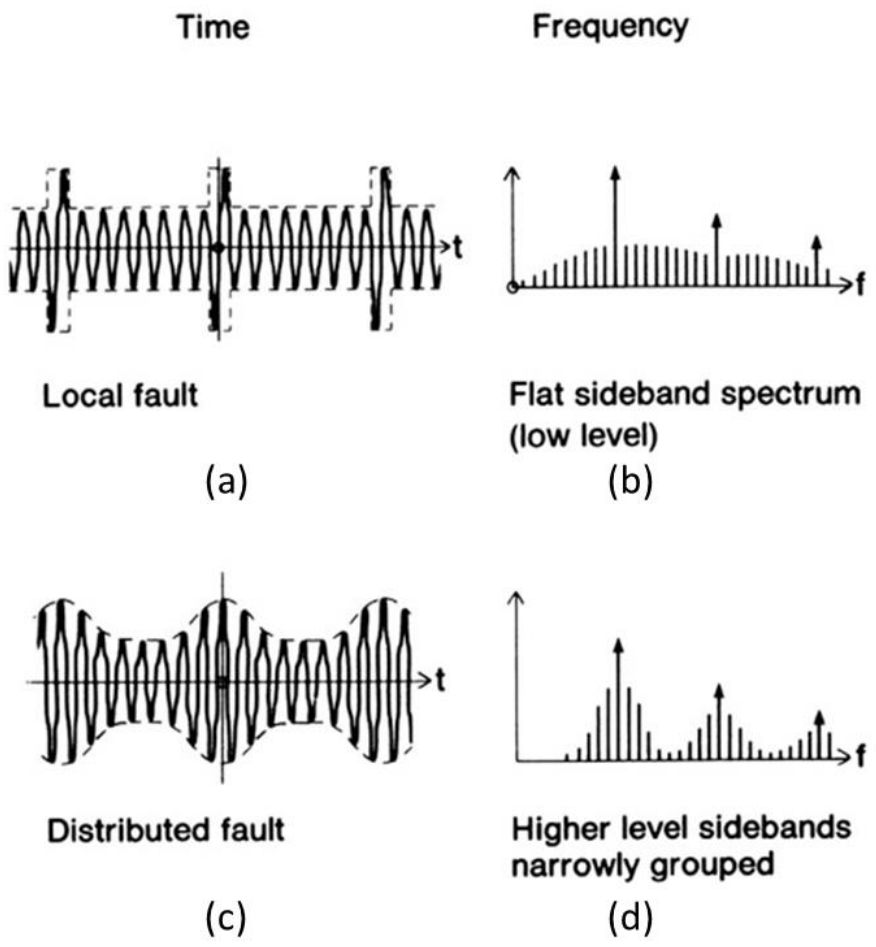

Figure 2.1: Time and frequency domain signals for local and distributed faults [4]

2.1 **Time domain**

Time domain signal processing fault detection methods have a statistical approach. The information of the gear is compared to the characteristics obtained at its original state.

Different time domain methods, such as root mean square (RMS) or Kurtosis, use statistical equations to determine if the presence of a fault is indicated. These methods require a priori information about the healthy state of the gear to extract the faulty features [7].

Synchronous averaging is an example of a time-domain fault detection method. This method extracts the periodic signal from the noise. To extract the periodic signal, the operating

frequency has to be known prior to the analysis [7]. A few fault detection methods use synchronous averaging, such as synchronous averaged time signals [1], the residual signal [2] [3], cepstrum of the synchronous averaging signal [13], time-frequency distribution of synchronous averaging [9], [14] and demodulation [7]. While capable of detecting distributed faults, the methods mentioned above are not effective with local faults. All these methods work differently; however, they all have the same disadvantages. First, considering that the sampling frequency is a multiple of the rotational frequency, at a high rotational frequency, the Nyquist theorem still has to be respected. Therefore, when the rotational frequency is large, the required Nyquist sampling rate becomes too high for efficient computation. Second, changes of phase in the signal can cause non-linearity in the peaks [15], [16]. This is an issue for this type of fault detection. These changes of phase are caused by common things such as rotating under load and varying speed. The non-linear deformity of the signal means the periodic feature cannot be extracted.

Time domain fault detection methods are simple and effective for de-noising [7]; however, some a priori information is generally required for the fault detection to be effective.

2.2 **Frequency domain**

Fault detection in the frequency domain is also widely used [17]–[21]. Methods such as the Hilbert Huang Transform (HHT) or the High Frequency Resonance approach [22] are examples of fault detection methods in the frequency domain. Different disadvantages result from these methods.

The Hilbert-Huang transform (HHT) fault detection method and its variations are widely used methods [17, 18, 20, 23, 21, 24]. The HHT is implemented via computer by performing a

time adaptive decomposition operation, which results in signal separation into components. Applying the Hilbert Transform to one of those components, called the intrinsic mode function (IMF), results in the HHT signal [19]. The HHT is not efficient at differentiating low-energy components from signal interferences. Some unwanted features are enhanced while low-energy faults tend to be reduced. This method is widely used mostly because of its computational simplicity. Also, it is used to detect the amplitude of the meshing harmonics as well as their sidebands. The Hilbert-Huang transform has been shown to be ineffective when tested on local faults such as cracks [19].

The high frequency resonance is the most widely used frequency domain method for obtaining the envelope spectrum [22]. The concept behind this method is that when a fault occurs, large impulses in the time domain appear in the signal. This large impulse is distributed over a wide range of frequencies in the frequency domain, over several harmonics [25]. However, this makes it difficult to detect faults in presence of interferences caused by other components in the machinery. From this method, noise is concentrated around the system's resonant frequency. To remove the noise, a bandpass filter needs to be designed around the resonant frequency. The main drawback of the method is the determination of the parameters to design the bandpass filter, namely the centre frequency and the bandwidth and the required bandpass filter. Some methods then further process the signal with the Hilbert Transform [26], [27, p. 33], [28]. Other methods automatically select parameters that facilitate the design of the filter for the user [29]–[34]. However, these parameters are dependent on the environment or situation, and information is needed for their selection [35]. The parameters defined initially do not remain optimal throughout the lifetime of the gear. When calibrations and maintenance are done throughout the use of gears, the original bandpass filter becomes no longer efficient since

the value of the resonant frequency changes. This can produce inaccurate results. Also, the methods related to the High Frequency Resonance approach do not take into consideration noise and interference close to the resonant frequency. The peaks around the resonant frequency caused by noise and interference also tend to falsify the fault detection results. Furthermore, this method has been shown to be inefficient for the detection of distributed faults. Local faults cause amplitude demodulation therefore they can be detected with this method [35].

Hence, frequency domain fault detection methods have been designed for use with either local faults or distributed faults. Furthermore, some methods also require initial information to be effective.

2.3 **Time-frequency domain**

While in the time domain, initial information is required, and in the frequency domain most methods are effective for either one type of fault or the other, but mostly not both, the time-frequency domain fault detection methods concentrate on periodic peaks of faults [35]. A few methods have become common: the Short-Time Fourier Transform (STFT), the Wavelet Transform and the Wigner-Ville Distribution (WVD).

The Short-time Fourier transform works by decomposing the signal into smaller sections that are locally stationary [36]. The Fast Fourier Transform (FFT) is then applied to the segments. The energy density is calculated for each of the results and finally they are all assembled to form the time-frequency distribution [36]. The main disadvantage of this method is that there is loss of resolution either in the time or the frequency domain.

The same logic is used to apply the Wavelet Transform. The signal is once again decomposed into segments; however, their lengths are variable. The advantage of this is that the

resolution in both the time and frequency domains can be controlled. Therefore, the resolution can be improved at a specific place in the signal for analysis [36]. However, the Wavelet Transform also has disadvantages such as loss of energy, deformation of borders and overlapping [25].

The Wigner-Ville Distribution consists of a bilinear transform, the Fourier transform of the signal's instantaneous auto-correlation [36]. This method does not result in low resolution; however, it does have two main disadvantages. First, the results can be non-positive. Considering that the signal represents a form of energy, the negative terms cannot be interpreted. The second disadvantage is that considering it is bilinear, there are cross terms. These cross terms are not squared, therefore they aren't the energy. These create interfering peaks [36].

In summary, most existing fault detection methods suffer from the disadvantages of complexity, applicability to only one type of fault and/or the necessity of prior information. It is advantageous for a fault detection method for gears to be as simple as possible. The benefit of using a fault detection method that does not require initial information is that there is no additional error uncertainty and less data needs to be stored. The continuous changing environment conditions can also add to the uncertainty of the values set for a healthy gear. Another advantage of having a simple method is that the system is less expensive with respect to time and cost. If a large memory is needed, a more costly system is required. If a complicated fault detection method is used, it is less appealing for users to acquire it.

The energy operator (EO) or Teager energy operator [8], [35] is a method that has previously been proposed and has shown to be effective with both types of faults, distributed and local. This is explained by the ability of the EO to extract all signal features [35]. The EO is also

filter free; therefore, no initial information is needed and it is a simple algorithm. While it is an efficient method, its capacity to handle noise and interference could be improved [35].

Faghidi and Liang recently proposed a new fault detection method for bearings derived from the energy operator [25], known as the Calculus Enhanced Energy Operator. They demonstrated that the calculus enhanced energy operator (CEEO) method can handle noise and interference better than the EO. In Faghidi and Liang's work, the CEEO was proposed and evaluated for the detection of faults in bearings but has so far not been applied to the detection of faults in gears.

Chapter 3 The Energy Operator and its variants

In this chapter, non-parametric methods for vibration analysis for the detection of gear faults are proposed. The Calculus Enhanced Energy Operator (CEEO) method is adopted for fault detection on gear boxes for the first time. This method was proposed in [25] and has been proposed and evaluated for bearing fault detection [37]. However, it has not been proposed and evaluated for fault detection in gears to date. Two other methods are derived from the energy operator, proposed and evaluated here for the first time.

First, to evaluate a method of fault detection, the set of simulated gear signals used for the evaluation process needs to be complete. Therefore, the equation chosen to simulate the gear signals on which the fault detection method is to be tested needs to be realistic. Secondly, many different conditions need to be simulated, such as worn gears and gears with cracked, chipped, or broken teeth. White noise and interferences are also added to the vibration signal to simulate the signals acquired in real life. Different fault detection methods can then be investigated so that they can be compared to the proposed method. Noise and interferences have to be dealt with to obtain a reliable fault detection method.

3.1 Energy operator fault detection methods

The energy operator had been shown to be an efficient approach to fault detection in gears; however, it has a few downfalls. Therefore, in this section the objective is to outline this method and to modify it to obtain a method that better handles noise and interference.

3.1.1 The Energy Operator

The Energy Operator (EO) is a non-parametric fault detection method [3]. This fault detection method calculates the energy of the oscillations in a signal. Its effectiveness can be demonstrated with the steps below. Firstly, from Newton's second law of motion, the second-order differential equation describing simple harmonic oscillations in a signal is given by [8]

$$\frac{d^2x}{dt^2} + \frac{k}{m}x = 0, \tag{3.1}$$

where x is the displacement, t is time, k is the spring constant and m is the mass. The solution of this differential equation is given by

$$x(t) = A\cos(\omega t + \phi) \tag{3.2}$$

where A is the amplitude, ω is the frequency (in radians/s) and ϕ is the initial phase of the system. The frequency of oscillation, ω, is given by

$$\omega = \left(\frac{k}{m}\right)^{1/2}, \tag{3.3}$$

and can be substituted into the equation of total energy. The total energy in a system is the sum of the potential and kinetic energies and can be written as

$$E = \frac{1}{2}kx^2 + \frac{1}{2}m\dot{x}^2. \tag{3.4}$$

By substituting equation (3.2) into (3.4), the total energy is given by

$$E = \frac{1}{2}m\omega^2A^2 \propto \omega^2A^2. \tag{3.5}$$

The square of the frequency of oscillation ω and amplitude of oscillation *A* are thus shown to be proportional to the total energy of the system.

The Energy Operator (EO) algorithm is found first by determining the equations at three discrete points:

$$\begin{aligned} x_n &= A\cos\left(nh\omega+\phi\right) \\ x_{n+1} &= A\cos\left(\left(n+1\right)h\omega+\phi\right) \\ x_{n-1} &= A\cos\left(\left(n-1\right)h\omega+\phi\right). \end{aligned} \tag{3.6}$$

where *n* is the sample number, and h is the time between samples. By multiplying two of the points, x_{n+1} and x_{n-1}, then

$$x_{n+1}x_{n-1} = \frac{A^2}{2}\left[\cos\left(2nh\omega+2\phi\right)+\cos\left(2h\omega\right)\right]. \tag{3.7}$$

Furthermore, by substituting x_n, equation (3.7) then becomes

$$x_{n+1}x_{n-1} = x^2{}_n - A^2\sin^2\left(\omega\right). \tag{3.8}$$

The final step to isolate the energy *E* is to approximate for small values of ω, $\sin\left(\omega\right)\approx\omega$. The energy defined in equation (3.5) can then be isolated in the previous equation, (3.8), as

$$x_n{}^2 - x_{n+1}x_{n-1} \approx A^2\omega^2 \propto E. \tag{3.9}$$

The discrete form of the energy operator is now defined formally as

$$\Psi_D(x_n) = x_n^2 - x_{n-1}x_{n+1} \tag{3.10}$$

where $\Psi_D(x_n)$ is the discrete form of the energy operator of the discrete vibration signal x_n. A first-order continuous approximation to the discrete form of the energy operator can be represented in continuous form as [1]

$$\Psi_C\left(x(t)\right) = \left(\frac{dx(t)}{dt}\right)^2 - x(t)\frac{d^2x(t)}{dt^2} \quad . \tag{3.11}$$

where $\Psi_C\left(x(t)\right)$ is the continuous form of the energy operator of the continuous signal $x(t)$. It can be shown that the energy operator extracts the amplitude modulation and frequency modulation of a signal [1].

As Bozchalooi and Liang [35] demonstrated, the advantage of using the EO for fault detection is its increased amplitude modulation and increased Signal-to-Interference Ratio (SIR). Most methods will do one while compromising the other. For example, before using the High Frequency Resonance fault detection method [26], a filter needs to be applied to the signal to solve this problem. The inconvenience of the EO is the lack of enhancement of the SNR. Therefore, a new non-filtering method will be proposed to obtain a better success rate in gear fault detection.

3.1.2 The Calculus Enhanced Energy Operator

The calculus enhanced energy operator (CEEO) method is a variation of the energy operator. This method has previously been proposed and optimized for bearing fault detection. In this section, the advantages and drawbacks of this method are outlined. It has been previously shown that the energy operator does not perform well with noise [25]. However, it improves the signal to interference ratio (SIR). Instead of applying the EO directly to the vibration signal, in the

CEEO method, a layer operator (LO) [25] is proposed and used on the vibration signal prior to the application of the EO.

The motivation behind using the layer operator (LO) is to improve the signal to noise ratio (SNR) when applying the energy operator. The LO includes differentiation as well as integration.

3.1.2.1 The differentiation operator

As demonstrated in [25] and [39], differentiation reduces the relative strength of low-frequency signal components but increases the relative strength of high-frequency components. This implies that it improves the SIR because the frequencies of the interferences are mostly much lower than those of the resonance excited by the impact of the fault. However, the high-frequency noise can also be magnified by differentiation and hence differentiation cannot be used to improve the SNR. Differentiation of a discrete gear vibration signal is expressed by

$$D(x_n) = \frac{x_n - x_{n-1}}{h} \tag{3.12}$$

where h is the step of time. The simplified equation becomes

$$hD(x_n) = x_n - x_{n-1}. \tag{3.13}$$

3.1.2.2 The integration operator

The backward integration of x_n, as explained in [25], is represented by

$$I(x_n) = h\frac{(x_n + x_{n-1})}{2}. \tag{3.14}$$

The simplified discrete integration operator is given by

$$\frac{2I\left(x_n\right)}{h} = x_n + x_{n-1}. \tag{3.15}$$

3.1.2.3 The Layer Operator

The layer operator is defined as the sequential application of a differentiation and integration operator. This operation can apply the differentiation and integrations in either order. This is demonstrated in the following. First, the differentiation operator given in equation (3.13) is applied to the signal. Then, the integration operator given in equation (3.15) is applied, which completes the application of the layer operator, defined as

$$LO_1\left(x_n\right) = 2I\left(D\left(x_n\right)\right) = x_n - x_{n-1} + x_{n-1} - x_{n-2} = x_n - x_{n-2}. \tag{3.16}$$

The same result is obtained if the differentiation is done following integration, given by

$$LO_1\left(x_n\right) = D\left(2I\left(x_n\right)\right) = \left(x_n + x_{n-1}\right) - \left(x_{n-1} + x_{n-2}\right) = x_n - x_{n-2}. \tag{3.17}$$

In both cases we observe that the steps h cancel out and the factor of 2 simply scales the signal, therefore it does not need to be considered.

The second order layer operator, as shown in [37], is defined as two successive applications of the layer operator and is given by

$$LO_2\left(x_n\right) = LO_1\left(LO_1\left(x_n\right)\right) = x_n - 2x_{n-2} + x_{n-4}. \tag{3.18}$$

3.1.2.4 CEEO Applied to Gears

The calculus enhanced energy operator (CEEO) was proposed in [25] and applied to bearing fault detection. It is defined as

$$\Psi_{CEEO}\left(x_n\right) = LO_1^2\left(x_n\right) - x_n LO_2\left(x_n\right) = x_n^2 - x_{n-2}x_{n+2}. \tag{3.19}$$

CEEO was shown to improve the efficiency of fault detection and therefore reduce computation time. It has never been tested on gears even though it has been shown to be effective with bearing fault detection. Bearing fault signals only include additive fault features. These are also present in gear fault signals. However, the main difference between bearing and gear signals is that gear fault signals also include multiplicative features. The effect of the CEEO fault detection method on additive features is shown in [25].

3.1.3 Higher order continuous approximations

Two new fault detection methods are proposed in this section. They have been obtained with the mathematical steps shown below. The continuous equation in equation (3.11) is an approximation of the discrete form in equation (3.10). It is approximated using the Taylor series expansion. In this section, the second order terms in the Taylor series are kept in order to obtain a better approximation to the discrete energy operator. Using a truncated higher-order Taylor series, the terms in equation (3.10) can be written in terms of their Taylor series expansion as

$$\begin{aligned} x_n &= x\left(t\right) \\ x_{n+1} &= x\left(t+h\right) = x(t) + x'(t)h + \frac{x''(t)h^2}{2} + \frac{x'''(t)h^3}{6} + \frac{x''''(t)h^4}{24} \\ x_{n-1} &= x\left(t-h\right) = x(t) - x'(t)h + \frac{x''(t)h^2}{2} - \frac{x'''(t)h^3}{6} + \frac{x''''(t)h^4}{24} \end{aligned} \tag{3.20}$$

Substituting equation (3.20) into (3.10), the second order continuous energy operator becomes:

$$\Psi_{C2'}\left(x(t)\right) = x^2(t) - \left(x(t) + x'(t)h + \frac{x''(t)h^2}{2} + \frac{x'''(t)h^3}{6} + \frac{x''''(t)h^4}{24} \right) \times \left(x(t) - x'(t)h + \frac{x''(t)h^2}{2} - \frac{x'''(t)h^3}{6} + \frac{x''''(t)h^4}{24} \right) \tag{3.21}$$

Expanding (3.21) and keeping only terms of order h^4 and lower gives

$$\Psi_{C2}\left(x(t)\right) = h^2\left(x'(t)^2 - x(t)x''(t)\right) - \frac{h^4}{3}\left(x''(t)^2 - x'(t)x'''(t)\right) + \frac{h^4}{12}\left(x''(t) - x(t)x''''(t)\right) \tag{3.22}$$

where $\Psi_{C2}(\ )$ refers to the continuous form of the energy operator with only terms of order h^4 and lower.

Equation (3.22) can be considered to contain first order terms in h^2 (terms multiplied by h^2) and second order terms in h^2 (terms multiplied by h^4), where h is the time-step size. Considering that the value of h is very small, the second order terms are much smaller than the first order. It would be pertinent to analyse this equation and different combinations of the terms.

Proceeding with equation (3.22), the corresponding discrete form is found using the finite difference representation of differentiation. Differentiation of the gear vibration signal is expressed by

$$x'(t) = \frac{x_n - x_{n-1}}{h} \tag{3.23}$$

Substituting (3.23) and equivalent expressions for higher derivatives into equation (3.22) and then grouping terms, the discrete equivalent of equation (3.22) becomes

$$\Psi_{D2}\left(x_n\right) = \overbrace{x_{n+1}^2 - x_{n+2}x_n}^{\text{EO at } (n+1)} - \frac{1}{3}\overbrace{\left[x_n^2 - x_{n+1}x_{n-1}\right]}^{\text{EO at } (n)} + \frac{1}{12}\overbrace{\left[x_n^2 - x_{n+2}x_{n-2}\right]}^{CEEO \text{ at } (n)} \tag{3.24}$$

In equation (3.24), we can identify the first set of terms as the energy operator evaluated at time $t=(n+1)h$ or equivalently at discrete counter $n+1$, the second set of terms represents the energy operator at *n* and finally the third set of terms is the energy operator at *n* with a distance 2, which has been proposed as the Calculus Enhanced Energy Operator (CEEO) [25], Equation (3.19).

The CEEO method has not been applied to gears as a fault detection method to date. Hence, in this thesis, its effectiveness will be investigated for the application to fault detection for gears. The EO (introduced in equation (3.10)) is used as a reference, to compare the efficiency of the other proposed methods. The EO is also the first set of terms in equation (3.24). The second set of terms in equation (3.24) is also the energy operator but shifted backwards by one time step with respect to the first set of terms. The last term in equation (3.24) is the energy operator with steps of two. As previously mentioned, this has been proposed previously as the calculus enhanced energy operator. In Table 3.1, the studied methods are listed. The last two methods in Table 3.1 have never been proposed before, they are two new approaches proposed in this thesis for the first time. The EO123 is defined as the sum of all three sets of terms from equation (3.24). Considering that the last two sets of terms are considerably smaller than the first (because they are second order terms in h^2), it is expected that the results of this method will be very close to the results from using the EO only. The second new proposed method is the EO23 method. It is proposed as the sum of all the second order terms from equation (3.24). The terms in the EO23 are all at a similar scale, it is therefore interesting to observe the method's ability to detect fault in the presence of noise and interferences.

The fault detection methods that are proposed and analysed in this thesis are listed in Table 3.1 and Table 3.2.

Fault detection methods	Equations
EO	$\Psi_{EO}(x_n) = x_n^2 - x_{n+1}x_{n-1}$
CEEO	$\Psi_{CEEO}(x_n) = x_n^2 - x_{n+2}x_{n-2}$
EO123	$\Psi_{EO123}(x_n) = x_{n+1}^2 - x_{n+2}x_n - \frac{1}{3}\left[x_n^2 - x_{n+1}x_{n-1}\right] + \frac{1}{12}\left[x_n^2 - x_{n+2}x_{n-2})\right]$
EO23	$\Psi_{EO23}(x_n) = -\frac{1}{3}\left[x_n^2 - x_{n+1}x_{n-1}\right] + \frac{1}{12}\left[x_n^2 - x_{n+2}x_{n-2})\right]$

Table 3.1: Discrete equations for fault detection methods

The third method in Table 3.1 and Table 3.2, EO123, is the full expression of Equations (3.22) and(3.24). It includes the first and second order terms. The fourth method of the tables is formed with only the second order terms. The continuous equivalents of the fault detection methods shown in Table 3.1 are shown in Table 3.2.

Fault detection methods	Equations
EO	$\Psi_{EO}(x(t)) = x'(t)^2 - x(t)x''(t)$
CEEO	$\Psi_{CEEO}(x(t)) = x''(t) - x(t)x''''(t)$

EO123	$\Psi_{EO123}(x(t)) = h^2\left(x'(t)^2 - x(t)x''(t)\right) - \frac{h^4}{3}\left(x''(t)^2 - x'(t)x'''(t)\right) + \frac{h^4}{12}\left(x''(t) - x(t)x''''(t)\right)$
EO23	$\Psi_{EO23}(x(t)) = -\frac{h^4}{3}\left(x''(t)^2 - x'(t)x'''(t)\right) + \frac{h^4}{12}\left(x''(t) - x(t)x''''(t)\right)$

Table 3.2: Continuous equations for fault detection methods

The EO and the CEEO have been used in previous work [1], [25]. The EO is currently used in many fault detection situations [1], [8]. As previously mentioned, the CEEO method proposed by Faghidi and Liang [25] was previously analyzed on bearing fault detection; however, it has not yet been applied to faulty gear signals.

Chapter 4 Evaluation of fault detection with distributed gear faults

The effectiveness of the methods proposed in the previous chapter is evaluated via simulations and also experimentally acquired gear vibration signals. To build a relevant bank of simulated signals, the simulation models, parameters, noise and interferences need to be chosen carefully. The bank of signals will then be used to numerically evaluate the proposed fault detection methods. Subsequently, evaluation will be performed using real signals collected by Professor Chuan Li at a mechanical engineering lab at University of Ottawa.

4.1 Simulated study

The vibration signal of healthy gears rotating at a constant speed and under a constant load can be simulated via [1]

$$x_{healthy}(t) = \sum_{p=0}^{M} X_p \cos\left(p\omega_m t + \phi_p \right) \tag{4.1}$$

where X_p is the amplitude of the pth meshing harmonic, ω_m is the meshing frequency of the driving gear and ϕ_p is the initial phase of the pth meshing harmonic. The meshing gear signal $x_{healthy}(t)$ varies with time, t, and is summed M times depending on the number of harmonics. The faults are then added into this basic equation to simulate the harmonics added by different faults such as worn, cracked or chipped teeth.

4.1.1 Fault simulation

To simulate multiple faults such as a cracked, chipped or worn gears, McFadden [1], proposes a non-filtering method adding amplitude and phase modulations to Equation (4.1). The equation for simulating a faulty gear then becomes

$$x_{faulty}(t) = \sum_{p=0}^{M} X_p \left(1 + a_p(t)\right) \cos\left(p\omega_m t + \phi_p + b_p(t)\right) \tag{4.2}$$

where $a_p(t)$ and $b_p(t)$ are the amplitude and phase modulations. The Amplitude Modulation (AM) and Phase Modulation (PM) are calculated via

$$a_p(t) = \sum_{n=0}^{N_a} A_{pn} \cos\left(n\omega_{rt} t + \alpha_{pn}\right) \tag{4.3}$$

and

$$b_p(t) = \sum_{n=0}^{N_b} B_{pn} \cos\left(n\omega_{rt} t + \beta_{pn}\right) \tag{4.4}$$

where A_{pn} and B_{pn} are respectively the amplitudes of the AM and PM and α_{pn} and β_{pn} are their phases. For the amplitude and phase modulations, the number of harmonics N_a and N_b represent the number of sidebands on either side of the meshing component in the frequency domain. If this number is high, the harmonic effect is local. For example, for a spatially-localized fault N could be 10. This occurs when there is a chip or a spall in the gear. On the other hand, with a small number of harmonics, the fault is spatially distributed on the gear. For example, this would be used to simulate a worn tooth [35].

The approach using AM and PM is often applied to model faults such as wear [35]. It is not used to simulate impulses caused by single breaks or fractures, where a different modelling approach must be used. The modelling of impulsive faults will be considered in the next chapter.

4.1.2 Fault analysis

The amplitude and phase modulations can be used to model distributed faults such as wear. Single profile changes such as those produced by a cracked tooth [35] require another simulation equation, which is considered in Chapter 5.

4.1.2.1 Amplitude and Phase modulated signals

Amplitude modulated faults can easily be approximated using McFadden's Equation (4.2) and equation (4.3). To show mathematically that the method can yield accurate results, the simplest example of an amplitude modulated signal is considered for further analysis. Consider the following representative term

$$x_{AM}(t) = X\left(1 + A\sin(\omega_{rt}t)\right)\sin(\omega_m t) \tag{4.5}$$

where ω_{rt} and ω_m are the rotational frequency and the meshing frequency of the pinion respectively, M is 1, N_a is 1 and there is no phase modulation.

In order to simulate the simplest plot of an amplitude modulated signal containing one harmonic M, an amplitude of a fault A of 0.9 on the driving gear, the amplitude X is of value 1, the rotational frequency of the driving gear is set to 12 Hz and the driving gear contains 32 teeth.

Equation (4.5) is not a realistic model for a faulty gear because of the single harmonic; however, it is simple enough to permit mathematical manipulations to show the basic result of the fault simulation equation. Further, since Equation (4.5) contains one term in the Fourier

series, it can demonstrate how the fault detection methodology behaves with one term, the sum of such terms representing the modelled faulty gear signal. The continuous time domain signal of equation (4.5) is shown in Figure 4.1(a). From equation (4.5) it can be concluded that the plot obtained in Figure 4.1(b) for the Fourier transform of the time domain signal in Equation (4.5) is what can be expected. Peaks are at the rotational frequency and at its second harmonic as expected after the Fourier transform is applied. Applying the FFT to distributed functions such as sinusoidal functions results in peaks at the value within the parentheses such as $(\omega_{rt}t)$ or $(\omega_m t)$ in equation (4.5).

Applying the equations from Table 3.2 to the previous function, equation (4.5), the peaks representing the faults can theoretically be located. First, the EO is used to transform the signal and the result is

$$\Psi_{EO}\left(x_{AM}\right) \approx X^2 \left[\begin{array}{l} A\left(2\omega_m^2 + \frac{\omega_{rt}^2}{2}\right)\sin\left(\omega_{rt}t\right) + \frac{A^2\omega_{rt}^2}{2}\cos\left(2\omega_{rt}t\right) - \frac{A\omega_{rt}^2}{2}\sin\left(\omega_{rt}t\right)\cos\left(2\omega_{rt}t\right) + \\ +A^2\omega_{rt}^2\sin\left(\omega_m t\right) + \mathrm{DC} \end{array} \right] \quad (4.6)$$

The first two terms in equation (4.6) are the first and second harmonics of the rotational frequency. The last three terms are higher order terms that are situated higher than the fundamental meshing harmonic or constants [35]. Therefore, peaks are expected at the first and second harmonic of the rotational frequency of the driving gear ω_{rt} after applying the Fourier Transform. When the other methods, EO123, EO23 and CEEO, are applied to the amplitude modulated signal shown in equation (4.5), the first and second harmonics are located at the rotational frequency ω_{rt} and its second harmonic. This is shown in Figure 4.2 (b) for the CEEO,

(c) for the EO123 and (d) for the EO23. The amplitude modulated signal is illustrated by the peaks in

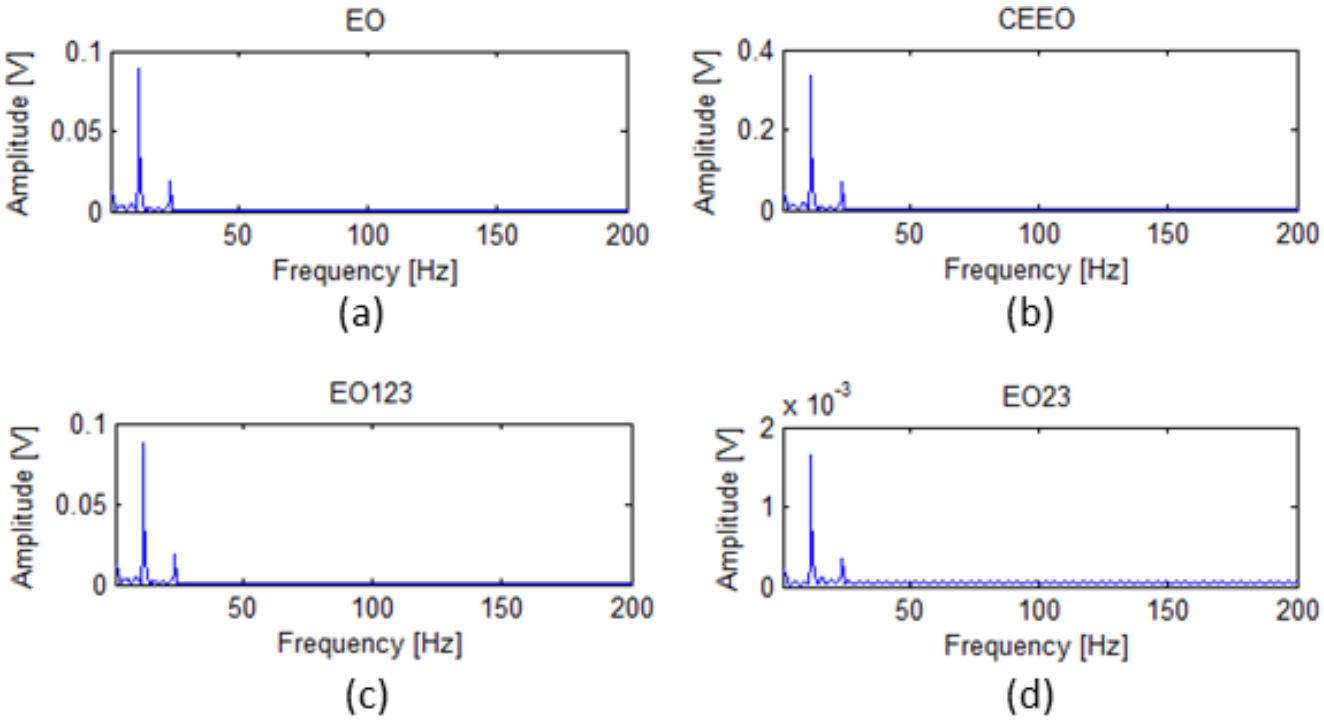

Figure 4.2 that are at the rotational frequency of the pinion and its second harmonic. The plots in, as expected, support the mathematical results.

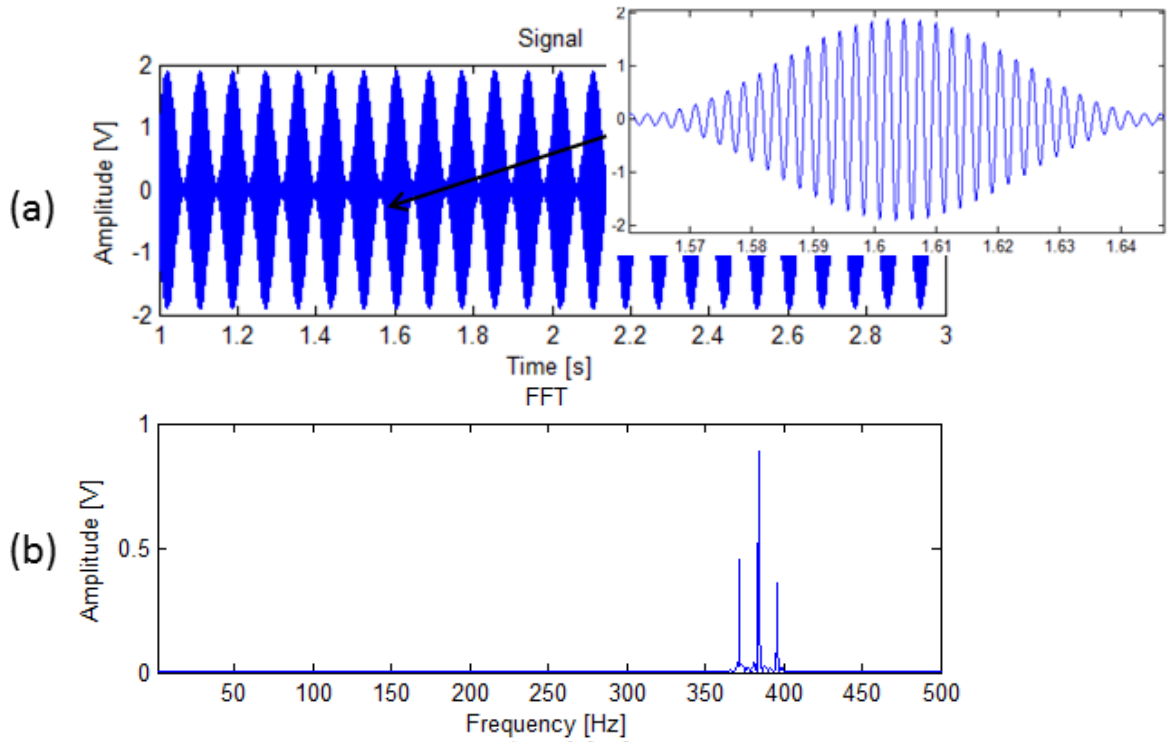

Figure 4.1: (a) Time domain signal and (b) its Fourier Transform of a single harmonic of an amplitude modulated fault

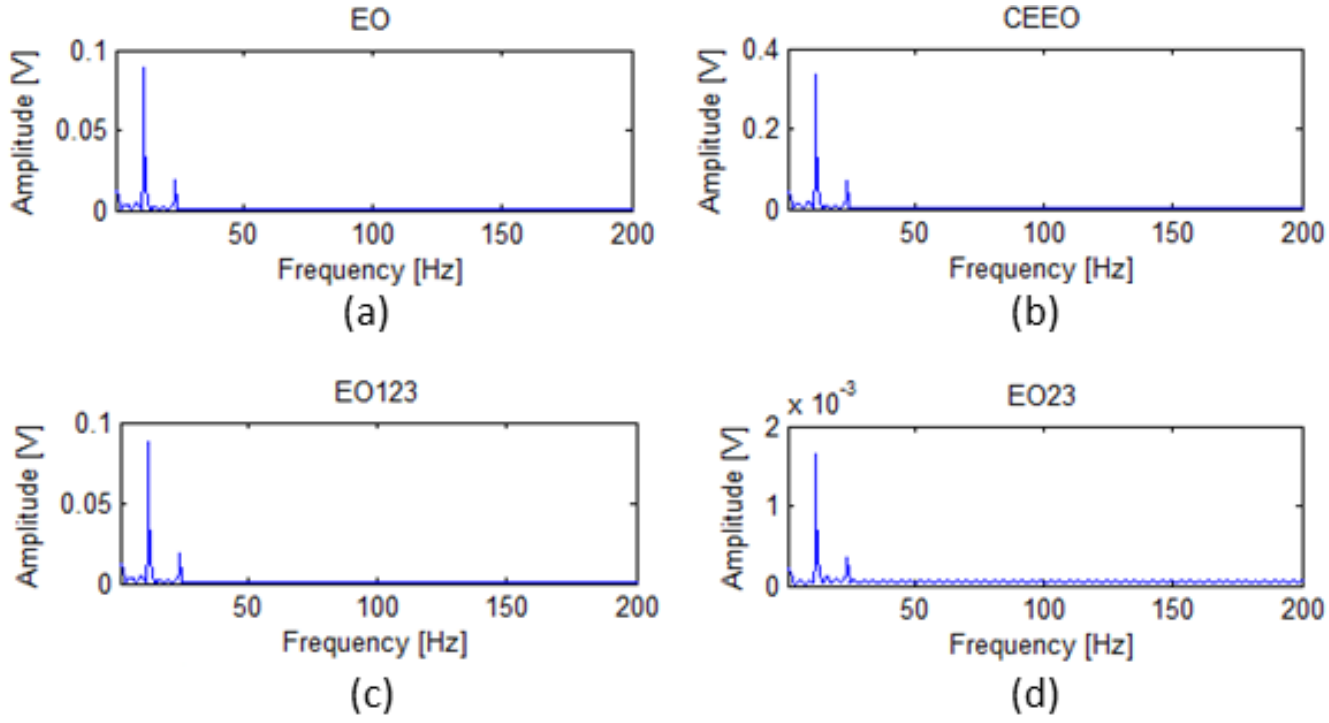

Figure 4.2: (a) EO (b) CEEO (c) EO123 (d) EO23 fault detection methods applied to a single harmonic of an amplitude modulated fault

The same can be seen in the signal generated by a fault causing phase modulation. The signal of a phase modulated fault can be simulated by

$$x_{PM}(t) = X\sin(\omega_m t + B\sin(\omega_{rt} t)). \tag{4.7}$$

where ω_{rt} and ω_m are the rotational frequency and the meshing frequency of the pinion respectively, M is 1, N_b is 1 and there is no amplitude modulation. The result of the EO transform applied to equation (4.7), a phase modulated signal, is given by

$$\begin{aligned}\Psi_{EO}\left(x_{PM}\right) \approx X^2\omega_{rt}\left[2B\omega_m\cos\left(\omega_{rt}t\right)+\frac{B^2\omega_{rt}}{2}\cos\left(2\omega_{rt}t\right)\right]+X^2\omega_{rt}^2\left[2B\sin\left(\omega_{rt}t\right)\cos\left(\omega_m t\right)\right.\\ \cos\left(B\sin\omega_{rt}t\right)\times\left(\cos\left(B\sin\omega_{rt}t\right)\sin\left(\omega_m t\right)+\cos\left(\omega_m t\right)\sin\left(B\omega_{rt}t\right)\right)\Big]X^2\omega_{rt}^2 B\sin\left(\omega_{rt}t\right)\\ \left[\sin\left(B\sin\omega_{rt}t\right)\cos\left(B\sin\omega_{rt}t\right)-\sin\left(\omega_m t\right)\cos\left(\omega_m t\right)\right]+\mathrm{DC}\end{aligned} \tag{4.8}$$

The first terms in equation (4.8), as shown for the amplitude modulated signal, are situated at the first and second harmonic of the rotational frequency of the pinion. To simulate the simplest plot of a phase modulated signal containing one harmonic *M*, an amplitude of a fault B of 0.9 on the driving gear, the amplitude X is of value 1, the rotational frequency of the driving gear is set to 12 Hz and the driving gear contains 32 teeth. The time domain signal generated by a single harmonic of a phase modulated fault is simulated in Figure 4.3 (a). The Fourier Transform is then generated in Figure 4.3 (b).

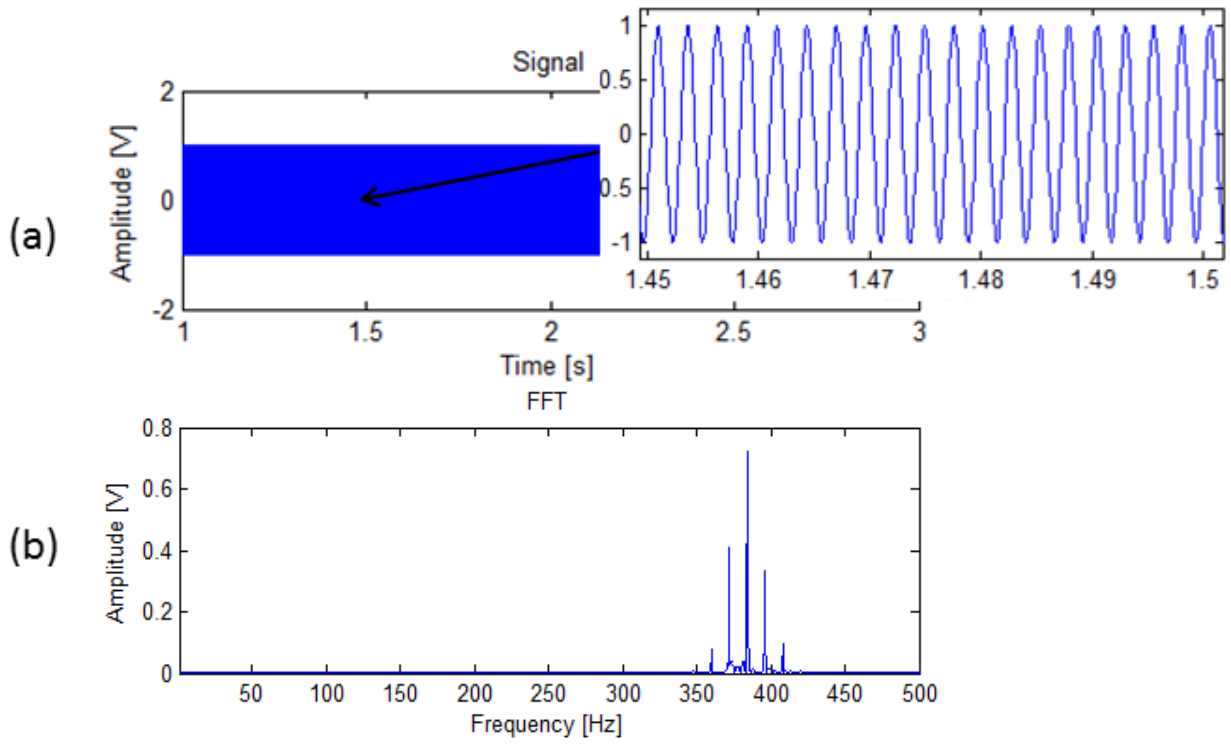

Figure 4.3: (a) Time domain signal and (b) its Fourier Transform of a single harmonic of a phase modulated fault

The results of applying all the methods, EO, EO123, EO23 and CEEO to the phase modulated signal are shown in Figure 4.4. With phase modulation, the results of the fourth method, EO23, are different from

the rest of the fault detection methods, as shown in

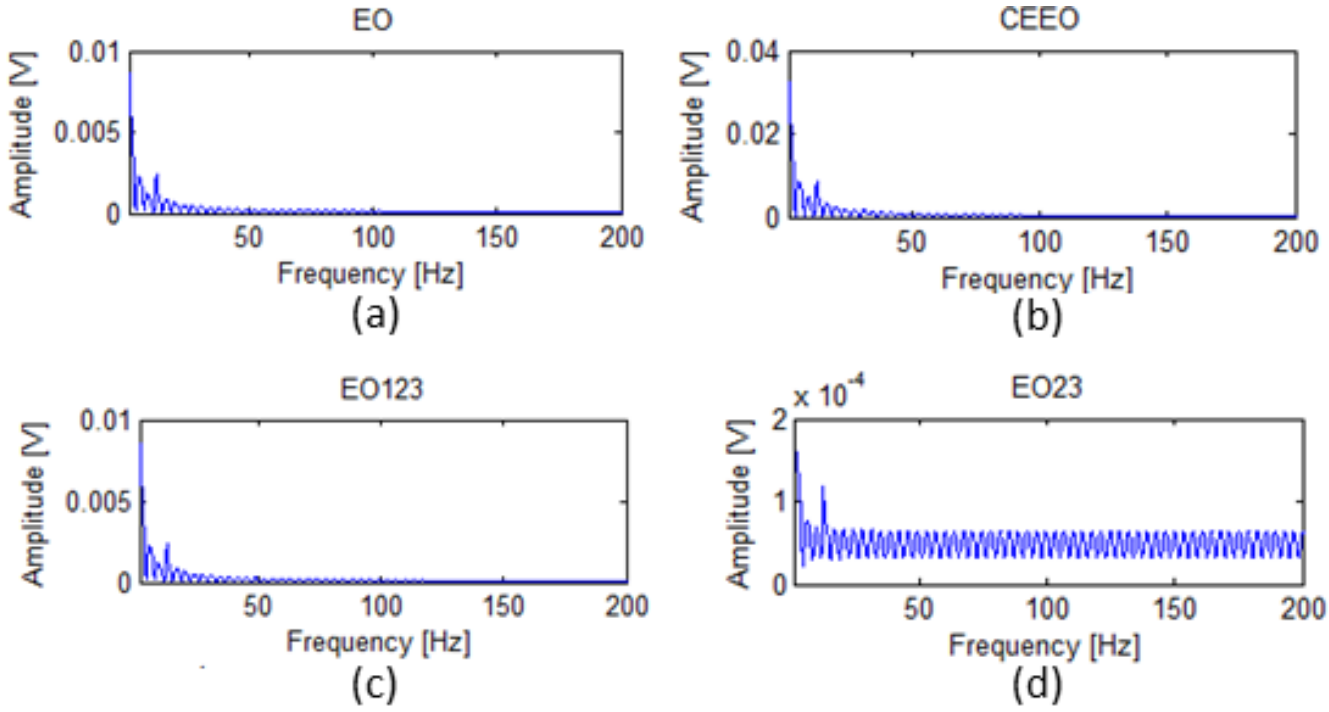

Figure 4.4.

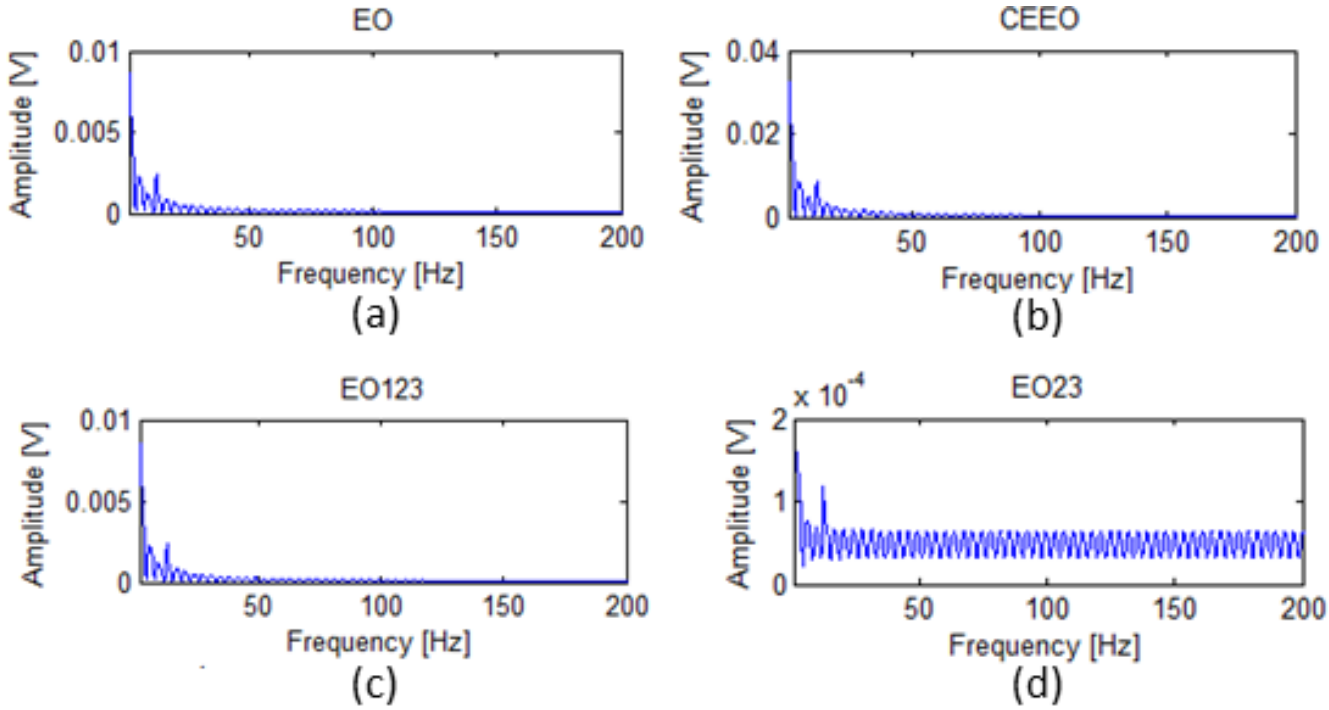

Figure 4.4: Fault detection methods applied to phase modulated faults

As harmonics are added, additional peaks are expected at the meshing frequency. These are present with healthy as well as faulty gears. A fault is indicated by the presence of peaks adjacent to the meshing frequency that are harmonics of the rotational frequency. For example, for a rotational frequency of 12 Hz with a driving gear containing 32 teeth the meshing frequency is 384 Hz (12 Hz x 32 teeth). The faulty features would be situated at 384 Hz plus or minus one, two, three or more times the rotational frequency of 12 Hz, therefore 384±12 Hz, 384±2·12 Hz, etc.

4.1.2.2 Representation of faults

Amplitude and phase modulations of signals are generally used to simulate fractures and cracks, as well as wear [35]. Fractures and cracks are localized faults; however, wear is a distributed fault. In equation (4.2), the more harmonics are used, the more localized the fault. In other words, the more summations M there are, more the fault is localized physically on the gear, like a crack for example. It is important to detect these types of faults early in order to prevent a more serious break in the gear. To detect distributed faults, the sidebands around the meshing frequency of the gear at distances of the rotational frequency and its harmonics need to be observed. The same sidebands are observed around the harmonics of the meshing frequency [35]. This is only for distributed faults. Complicating the fault detection, these faults can also be drowning in noise and interferences.

Table 4.1, Table 4.2 and Table 4.3 are formed to analyse the efficiency of fault detection methods. The following explains how these tables are built. The meaning of "-", "Yes" and "Best" in the tables are explained herein and demonstrated via Figure 4.5 and Figure 4.6. Figure 4.5 shows a small fault that cannot be identified in the presence of a considerable amount of noise (SNR = -10 dB). The large peaks observed in the figure, which are illustrated by the arrow

in Figure 4.5, are at the meshing frequency and its harmonics and therefore give no information on the fault. The smaller peaks do not illustrate faults, they are results of noise. This type of result is the example of when the methods do not work and are represented by a dash "-" in Table 4.2 and Table 4.3.

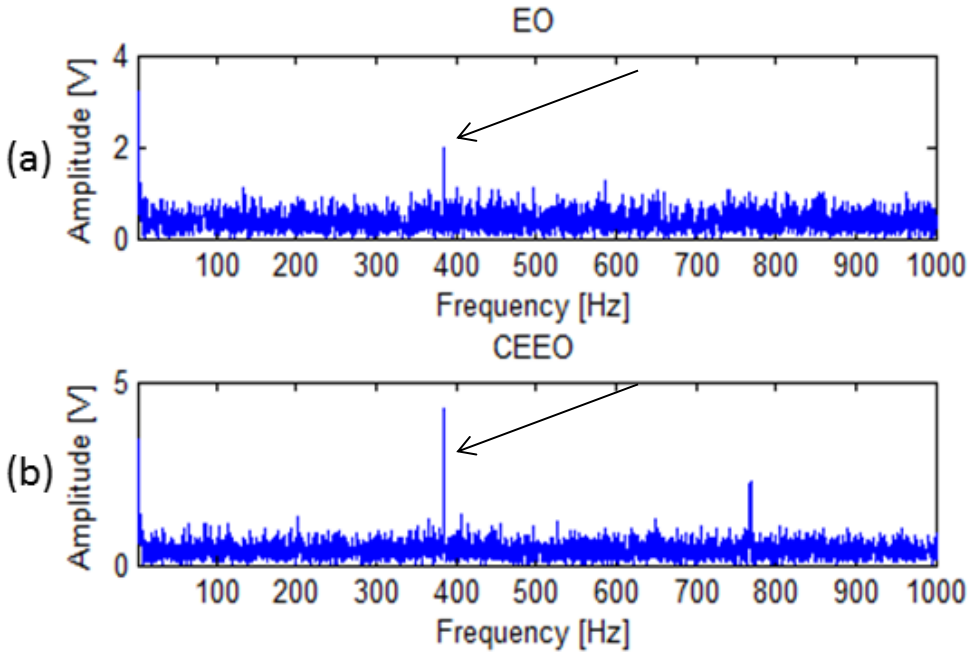

Figure 4.5: Non identifiable fault

Figure 4.6 demonstrates a simulated medium-sized fault to which the EO and the CEEO are applied. It is possible to identify faults from the presence of sideband peaks at one or more harmonics of the rotational frequency around the meshing frequency illustrated by the arrows in Figure 4.6 [35]. Both methods in the figure can detect the fault; however, the noise is handled better by the CEEO method as shown in Figure 4.6 (b). That is why it would be indicated as "Best" for the CEEO and "Yes" next to EO method in Table 4.2 for example.

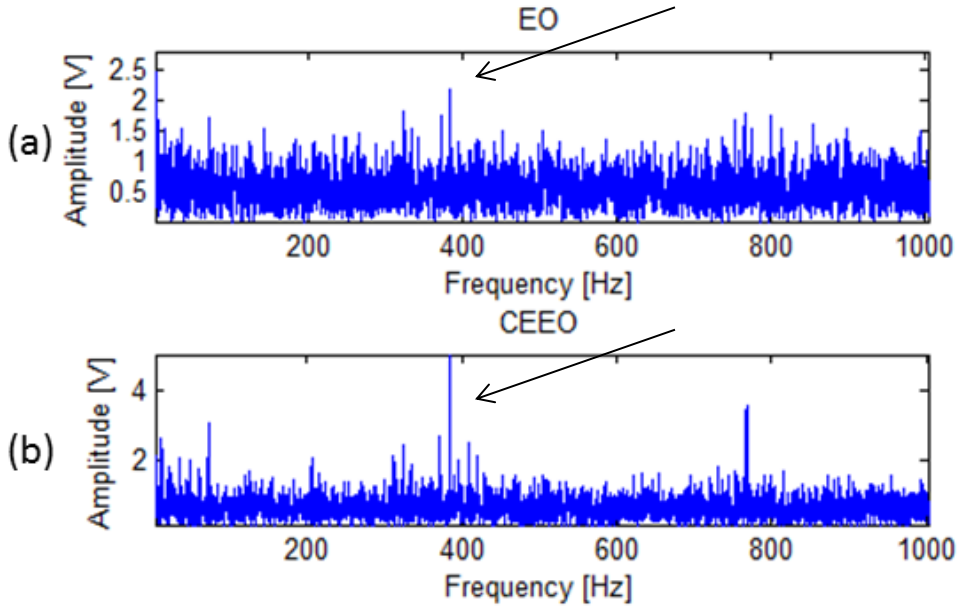

Figure 4.6: Identifiable faults

4.1.3 Clean signal

Considering amplitude modulation, as shown in Table 4.1, analysing a faulty gear with a clean (noiseless) signal, the same result is obtained with all four proposed methods. Here, different sized faults illustrated by a in equation (4.2) (a = 0.1, 0.4 and 0.9) at different frequencies (f_{rt} = 6, 12, 24, 50, 100 Hz) are simulated and tested with all the fault detection methods. The results are the same in this case for different numbers of harmonics (N_a = 3, 6 and 10 from equation (4.3)). All results from Table 4.1 demonstrate that all methods are effective with faults and clean signals. The resulting signals from applying the four methods are all similar plots at different scales. This is expected. As mentioned previously, peaks for all methods are at the distance of the rotational frequency around the meshing frequency and their harmonics.

Rotational frequencies of the pinion f_{rt} (Hz)	Size of fault	EO	CEEO	EO123	EO23
6	a=0.1	Yes	Yes	Yes	Yes
	a=0.4	Yes	Yes	Yes	Yes
	a=0.9	Yes	Yes	Yes	Yes
12	a=0.1	Yes	Yes	Yes	Yes
	a=0.4	Yes	Yes	Yes	Yes
	a=0.9	Yes	Yes	Yes	Yes
24	a=0.1	Yes	Yes	Yes	Yes
	a=0.4	Yes	Yes	Yes	Yes
	a=0.9	Yes	Yes	Yes	Yes
50	a=0.1	Yes	Yes	Yes	Yes
	a=0.4	Yes	Yes	Yes	Yes
	a=0.9	Yes	Yes	Yes	Yes
100	a=0.1	Yes	Yes	Yes	Yes
	a=0.4	Yes	Yes	Yes	Yes
	a=0.9	Yes	Yes	Yes	Yes

Table 4.1: Effect of varying frequency on clean amplitude modulated signal

It is, however, important to analyse the ability of all the proposed methods to handle noise and interference. Phase modulated signals are much more difficult to detect. Phase modulation is

generally caused by a modified rotation condition such as a change of load or speed, for example. Phase modulation is also used to simulate fatigue cracks.

4.1.4 Noise handling

To evaluate a fault detection method, its capability to handle noise is pertinent. Therefore, depending on given fault conditions, the method that can handle the highest SNR will be identified.

Noise handling is investigated at different frequencies for amplitude modulated faults. The effectiveness of distributed fault detection methods varies with rotational frequencies. In Table 4.2, the noise is set to a signal to noise ratio (SNR) of -10 dB. This is a considerably low SNR. Also, the fault is considered to be a distributed fault which is set with N_a from equation (4.3). In this section $N_a = 6$. Table 4.2 illustrates the performance of the methods at different frequencies with different sized faults.

Rotational frequencies ω_{rt} (Hz)	Size of fault	EO	CEEO	EO123	EO23
6	a=0.1	-	-	-	-
	a=0.4	-	-	-	-
	a=0.9	-	-	-	-
12	a=0.1	-	-	-	-
	a=0.4	Yes	Best	Yes	-
	a=0.9	Yes	Best	Yes	-

24	a=0.1	-	Yes	-	-
	a=0.4	Best	Yes	Best	Best
	a=0.9	Best	Yes	Best	Best
50	a=0.1	-	-	-	-
	a=0.4	Yes	Best	Yes	Yes
	a=0.9	Yes	Yes	Yes	Yes
100	a=0.1	-	-	-	-
	a=0.4	Best	Yes	Best	Best
	a=0.9	Yes	Yes	Yes	Yes

Table 4.2: Effect of varying frequency on noisy amplitude modulated signal, SNR = -10 dB

Small faults cannot be detected within a signal containing this much noise. It is interesting to notice that the most effective fault detection method changes depending on the conditions. None of the fault detection methods are effective at very low frequencies. This problem has been investigated in previous work by Wang and Yang [38], and it is known that faults are not detectable by any method at low frequencies. As shown in Table 4.2, at a rotational frequency of 12 Hz, the CEEO method is the best at handling noise. At 12 Hz the fourth method, EO23, cannot be used to identify the fault. However, at rotational frequencies of 24 Hz and 100 Hz, the other three methods EO, EO123 and EO23, appear to handle noise better.

It is now interesting to consider different types of faults. A localized fault can be identified as a crack or a spall. On the other hand, a distributed fault simulates wear. Distributed faults are harder to identify as shown in

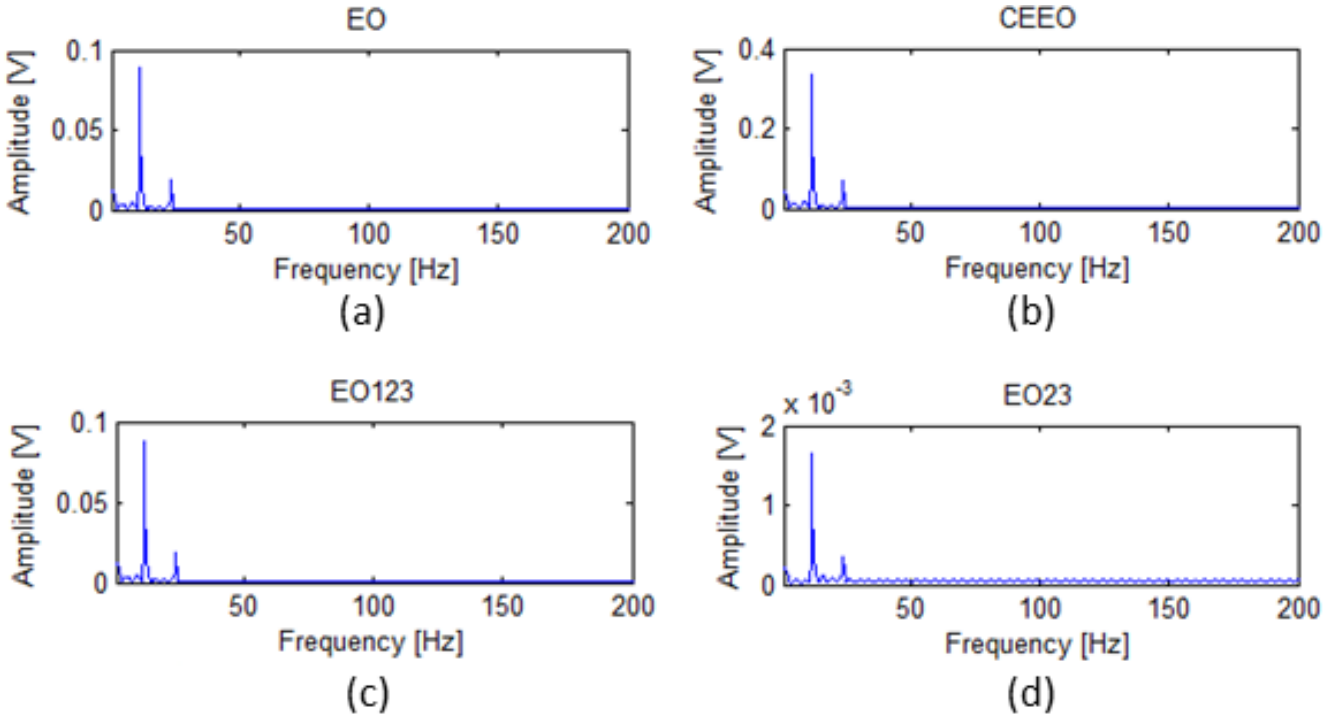

Figure 4.2 and

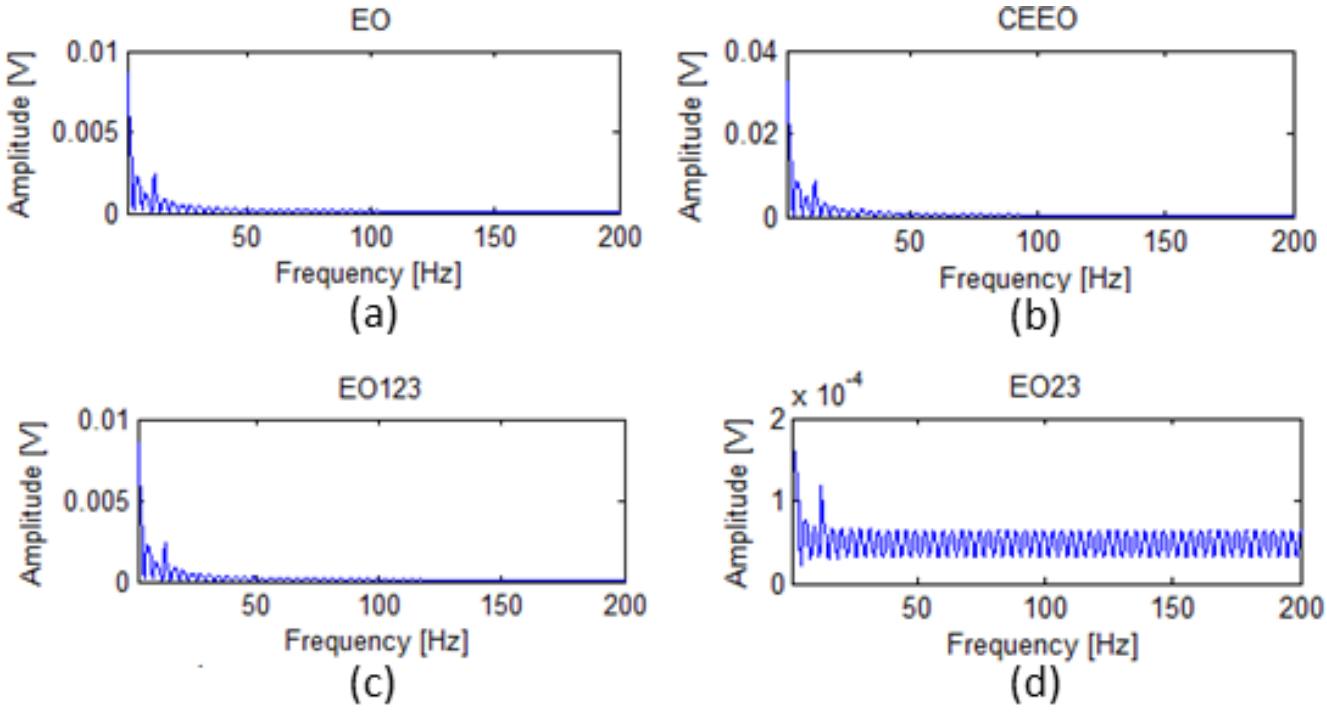

Figure 4.4 where the number of harmonics N is 1. When noise is present, the sidebands closer to the peak are harder to identify. An example of signals is illustrated to show the efficiency of the four proposed fault detection methods. Figure 4.7 shows the vibration signal in time and frequency simulated from equation (4.2). This amplitude modulation is at a frequency of 12 Hz with 3 harmonics ($N_a = 3$).

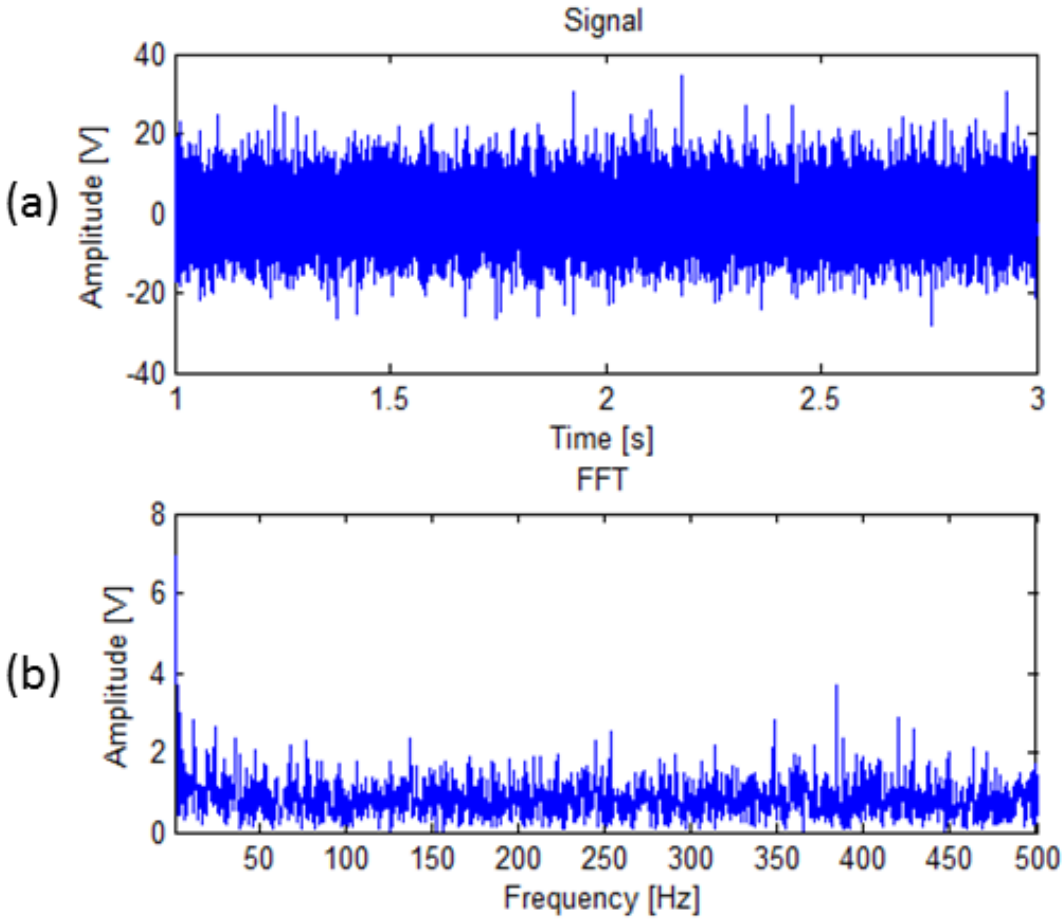

Figure 4.7 : (a) Time and (b) frequency domain signals of an amplitude modulated fault, at a frequency of 12 Hz with 3 harmonics ($N_a = 3$) in presence of noise

It can be seen from Figure 4.7 that the sidebands are not visible in the frequency domain; therefore, the fault cannot be detected from the spectrum alone. Now, the fault detection methods are applied prior to the computation of the spectrum.

As can be observed in

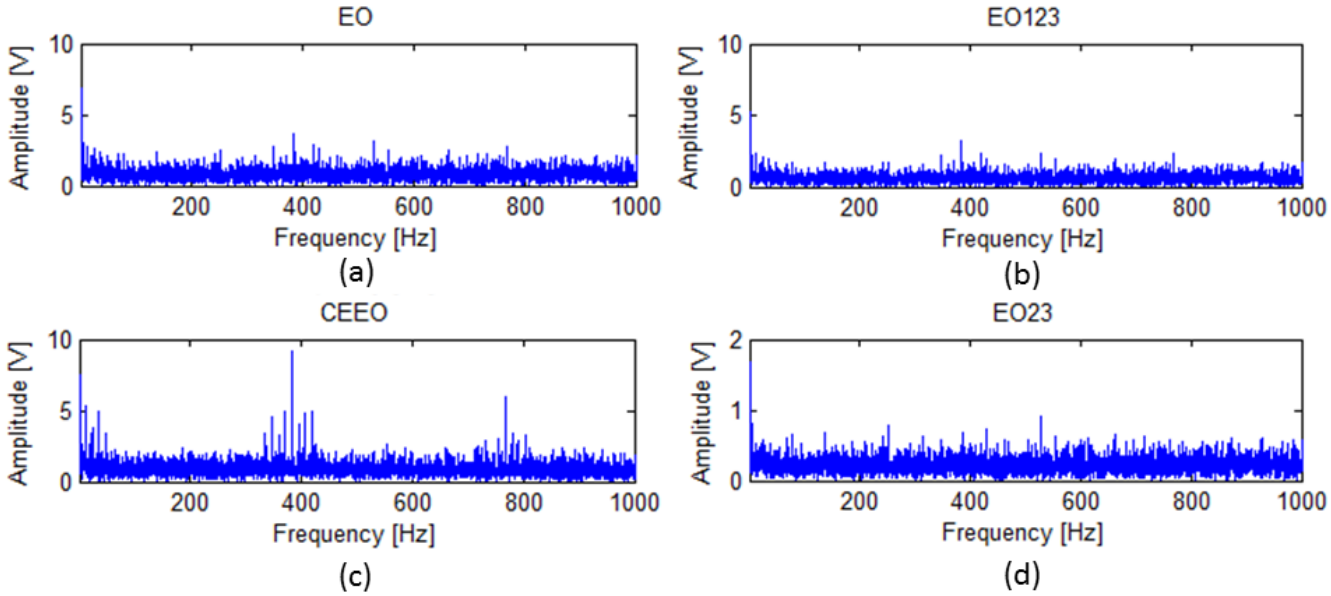

Figure 4.8, all four methods lead to different results. EO, EO123, and EO23 are very similar; however, the fault is not detected. The CEEO fault detection method is the best with noise in this case because all the three sidebands around the meshing frequency are clearly observable. As mentioned previously, considering it is a localized fault, the rotational frequency and its several harmonics are easier to identify.

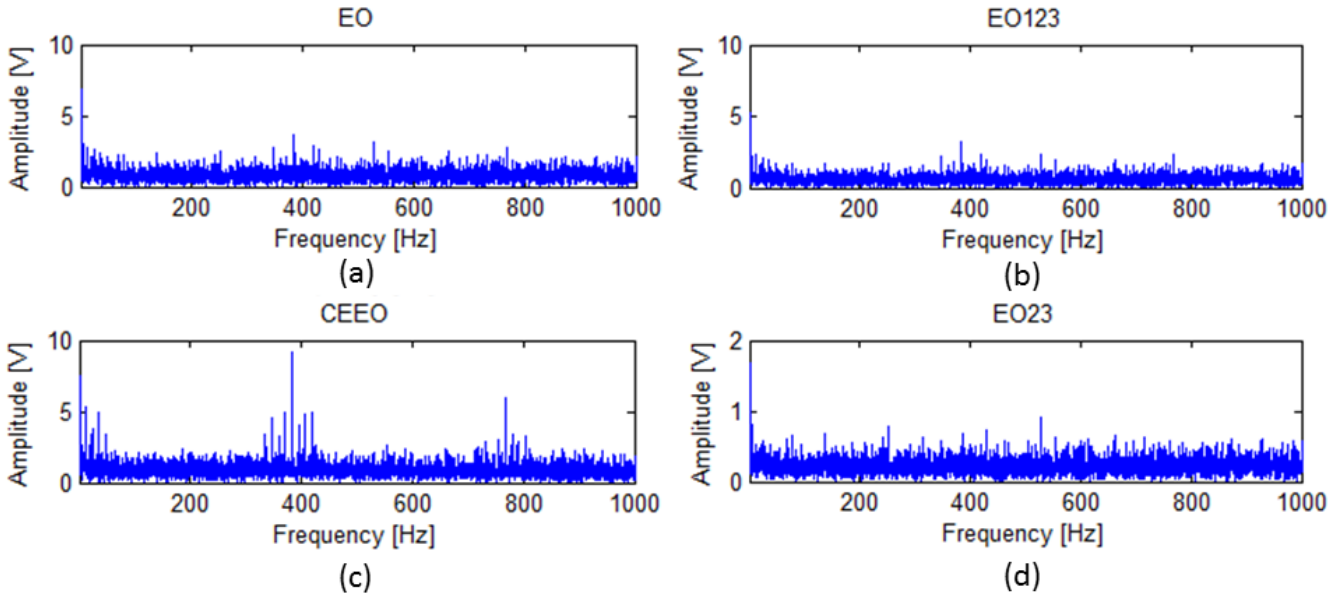

Figure 4.8: Fault detection methods applied to an amplitude modulated fault in presence of noise

4.1.4.1 Noise handling at different frequencies for phase modulation

Similarly to amplitude modulated signals, the capacity for the fault detection methods to handle noise is evaluated for phase modulated signals. As done previously, the methods are tested with a SNR of -10 dB and six harmonics, i.e., N_a=6. The results are shown in Table 4.3.

Rotational frequencies ω_{rt} (Hz)	Size of fault	EO	CEEO	EO123	EO23
6	a=0.1	-	-	-	-
	a=0.4	-	-	-	-

	a=0.9	-	-	-	-
12	a=0.1	-	-	-	-
	a=0.4	-	-	-	-
	a=0.9	-	-	-	-
24	a=0.1	-	-	-	-
	a=0.4	-	-	-	-
	a=0.9	-	-	-	-
50	a=0.1	-	-	-	-
	a=0.4	-	-	-	-
	a=0.9	-	-	-	-
100	a=0.1	-	-	-	-
	a=0.4	-	-	-	-
	a=0.9	-	-	-	-

Table 4.3: Effect of varying frequency on noisy phase modulated signal, SNR=-10 dB

A phase modulated fault cannot be detected with this much noise (SNR= -10dB). As soon as any noise is added, the fault impulses around the meshing frequencies and its harmonics are lost. Phase modulation is therefore not the type of signal feature that will allow fault detection with the proposed methods. Therefore, amplitude modulation will be used in further analysis of these methods for signals containing noise.

4.1.5 Interference handling

Interference is a series of continuous sinusoidal signals that interfere with the signal of the faulty gears. Interference can be caused by shaft misalignment or any other imbalance in the rotational

mechanism. The four proposed fault detection methods are applied to highly interfered signals. An interfering sinusoidal signal is added to the faulty signal. The interfering signal is defined as

$$Int(t) = \sin(c\pi t) + \sin(b\pi t) \tag{4.9}$$

where *Int(t)* is the interfering signal at time *t*, *c* and *b* are constants defining the frequency of the interfering signal in this following case 8 and 8/3 respectively. As for the faulty signal, for example, a simulated case is observed, using equation (4.2), a small fault (a = 0.1), a driving shaft rotational frequency of 12 Hz and an interference with a Signal-to-Interference Ratio (SIR) of -35 dB. The number of harmonics, which determines how localized the fault is, is N_a = 3 and N_b = 6 in Figure 4.9 and Figure 4.10, respectively. The previous values are inserted in equation (4.2). First, an amplitude modulated fault is simulated in Figure 4.9, and then a phase modulated fault is simulated in Figure 4.10. In the two figures, the small peaks between the brackets illustrate the presence of a fault. These are at the driving gear's rotational frequency and its harmonics. The large impulses situated, in this case, at 384 Hz and 768 Hz are the meshing frequency and its harmonic. The arrows show the presence of interference around the meshing frequency. In this case, the peaks at the rotational frequency of the driving gear are still visible; however, if more noise were to be added, the fault would not be detected.

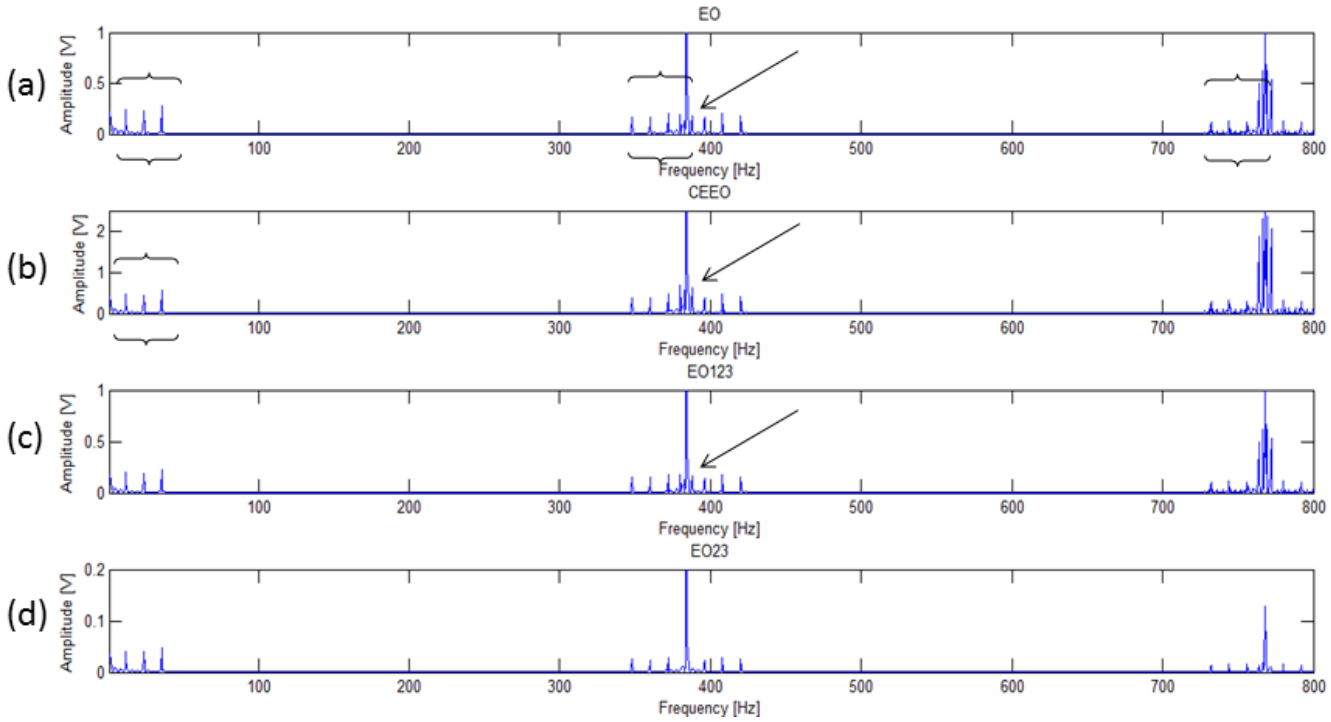

Figure 4.9: Simulated amplitude modulated fault with interference of -35 dB at a shaft rotational frequency of the driving gear of 12 Hz

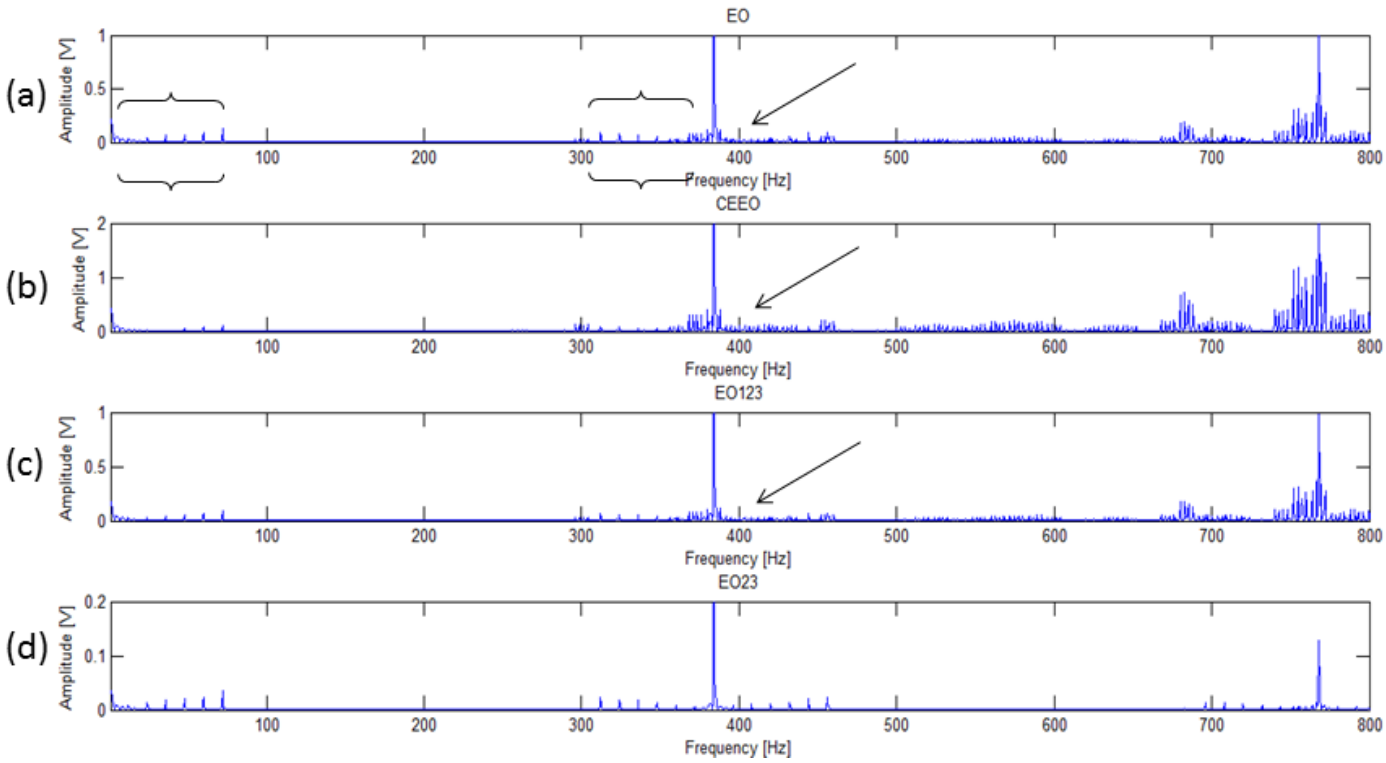

Figure 4.10: Simulated phase modulated fault with interference of -35 dB at a shaft rotational frequency of the driving gear of 12 Hz

In Figure 4.9 and Figure 4.10, it is shown that all methods are effective with such interference. However, the EO23 method stands out with cleaner results. The first three methods show interference peaks around the meshing frequency of the second and third harmonics that falsify the fault identifications. The last method, EO23, completely removes the interfering peaks as shown in Figure 4.9 and Figure 4.10. At all different frequencies and fault sizes, the same phenomenon can be observed. Concerning the EO23 method, the interference starts affecting the signal simply at a later harmonic. As shown in Figure 4.11, the interference falsifies the fault detection results at about the fourth harmonic.

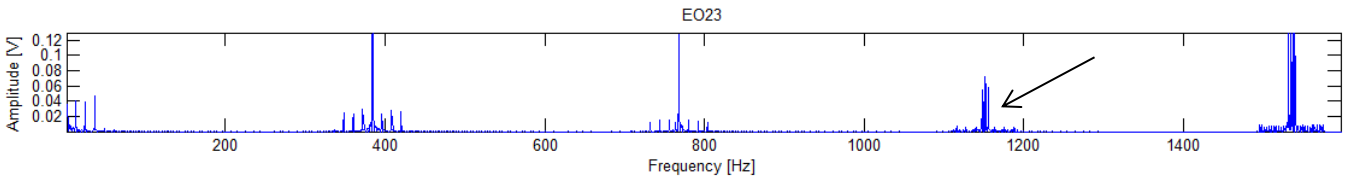

Figure 4.11: Amplitude modulated fault using the EO23 with a larger range of frequencies at a shaft rotational frequency of the driving gear of 12 Hz

It can be concluded that all methods can handle interference, however when there is too much interference, (SIR ≤ - 35 dB) EO23 is the best method to use.

4.1.6 Noise and interference handling

It is more realistic to simulate a signal containing noise in addition to interference in order to test fault detection methods. Considering the conclusion made in Section 4.1.4, about noise handling, that phase modulation could not be detected in the presence of noise, only amplitude modulated signals will be used in this section.

Applying an interference of magnitude -35 dB, fault detection methods are also tested in terms of noise handling. The following tests are done with a rotational frequency of the pinion of 12 Hz, 24 Hz, 50 Hz, and 100 Hz, respectively. In Table 4.4 Table 4.5Table 4.7 the observed fault is a localized fault where N_a = 6 from equation (4.3). The same phenomenon as observed with a noisy signal without interferences occurring here. At certain frequencies, as shown in Table 4.4, CEEO is obviously the best performing method. However, at other frequencies, such as 24 Hz, 50 Hz, or 100 Hz, depending on the amount of interference and noise, the EO, EO123, and the EO23 outperform CEEO for a rotational frequency of the driving gear of 24 Hz or perform equally well when these rotational frequencies increase to 50 and 100 Hz. From previous conclusions, EO23 can handle more interference than the other methods. This is very

clear in Table 4.5 where the fault is easier to detect due to the methods' ability to handle interference.

	SNR (dB)					
	-2	-5	-10	-12	-15	-20
EO	YES	YES	YES	-	-	-
CEEO	YES	YES	YES	YES	-	-
EO123	YES	YES	YES	-	-	-
EO23	YES	YES	-	-	-	-

Table 4.4: Fault detection methods' capability to handle noise and interference at a shaft rotational frequency of the driving gear of 12 Hz

	SNR (dB)					
	-2	-5	-10	-12	-15	-20
EO	YES	YES	YES	YES	-	-
CEEO	YES	YES	YES	-	-	-
EO123	YES	YES	YES	YES	-	-
EO23	YES	YES	YES	BEST	-	-

Table 4.5: Fault detection methods' capability to handle noise and interference at a shaft rotational frequency of of the driving gear 24 Hz

	SNR (dB)					
	-2	-5	-10	-12	-15	-20
EO	YES	YES	YES	YES	-	-
CEEO	YES	YES	YES	YES	-	-
EO123	YES	YES	YES	YES	-	-

EO23	YES	YES	YES	YES	-	-

Table 4.6: Fault detection methods' capability to handle noise and interference at a shaft rotational frequency of the driving gear of 50 Hz

	SNR (dB)					
	-2	-5	-10	-12	-15	-20
EO	YES	YES	YES	YES	-	-
CEEO	YES	YES	YES	YES	-	-
EO123	YES	YES	YES	YES	-	-
EO23	YES	YES	YES	YES	-	-

Table 4.7: Fault detection methods' capability to handle noise and interference at a shaft rotational frequency of the driving gear of 100 Hz

From all these tests, it can be concluded that:

- The EO and the EO123 are mostly efficient up to a SNR of -12 dB for rotational frequencies above 12Hz.
- The CEEO is the most efficient method at very low rotational frequencies, in this case 12 Hz; it detects faults with noise up to -12 dB while none of the other methods can.
- The EO23 has a very particular effect on signals with noise and interference. It is able to detect faults in this case above the rotational frequency of 16 Hz. However, it cannot handle as much noise as the other fault detection methods, as explained in previous sections.

4.2 **Experimental validation**

To confirm the results obtained while doing the simulated study in section 4.1, experimental tests are performed. In this section, the proposed fault detection methods are tested on data acquired

from running a two-stage spur gear gearbox. The input gear has 32 teeth, and the output gear has 96 teeth. For the data gathering, IMI 623C01 ICP accelerometers are placed in order to capture the horizontal lateral vibration. During the test, the accelerometer signals are collected at a sampling frequency of 40000 Hz, and the signals last for 60 seconds. A constant torque of 35 lb-in (2.5/5.0 indicated by the rating plate) is applied to the output shaft by the brake. A few cases are observed, but first, the results of the fault detection methods is applied to this gearbox with an input shaft rotational speed of 16 Hz. In Figure 4.12, the original signal is observed and below, its Fourier Transform can be seen. As explained previously, the pertinent peaks are the sideband peaks, i.e., the ones situated around the meshing frequency of the system at a distance of the rotational frequency and its harmonics. In this case, the rotational frequency of the driving gear is 16 Hz. We therefore expect peaks at the meshing frequency 512 Hz (32 teeth *16 Hz) minus and plus 16 Hz, 32 Hz and so on.

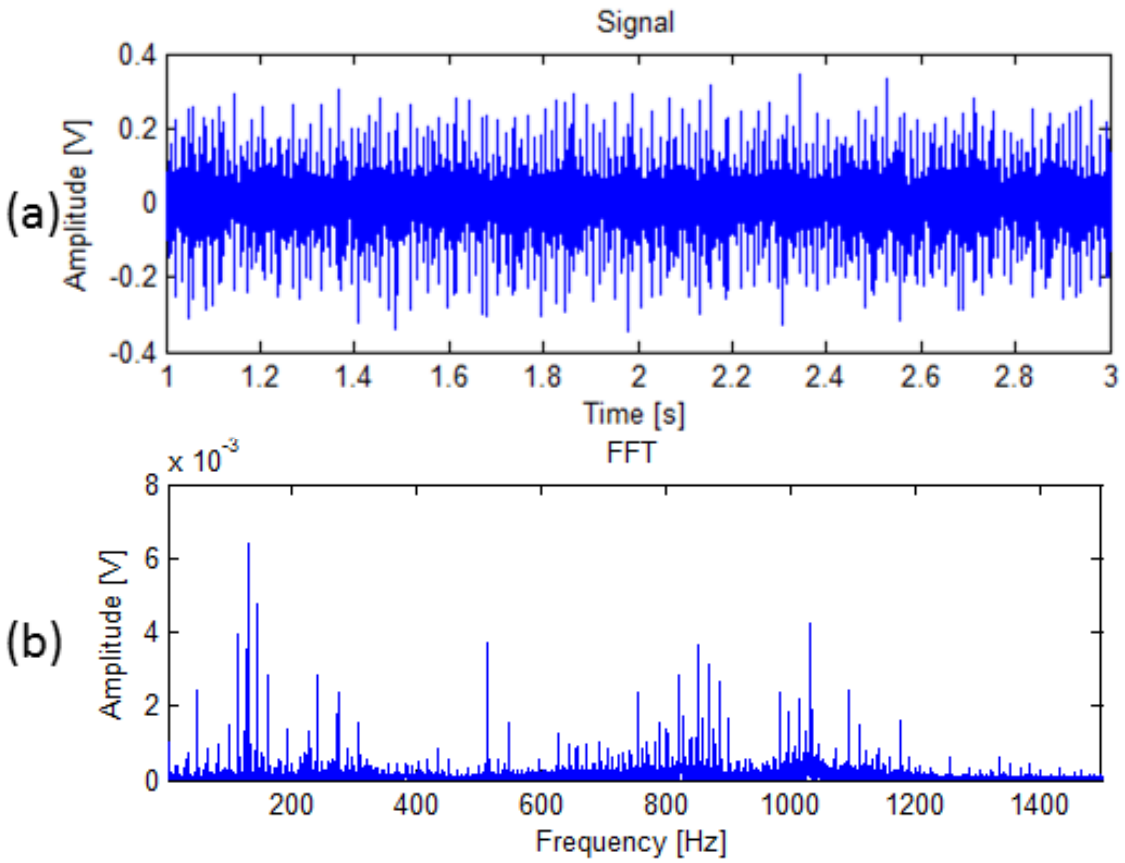

Figure 4.12: (a) Experimental evaluation of a worn gear with a rotational frequency of the pinion of 16 Hz and (b) its Fourier Transform

To compare the results in this present gear to a healthy gear, Figure 4.13 is generated. Figure 4.13 (a) contains the signal generated by a healthy gear and (b) its Fourier Transform. It is already possible to observe a difference between the worn gear signal and the healthy gear signal in the frequency domain seen in Figure 4.13. The impulses, representing the rotational frequency of the driving gear around the meshing frequency are much larger in Figure 4.12 than those in Figure 4.13. We can notice that the meshing frequency is dominant in Figure 4.13, this is expected because it is a healthy gear.

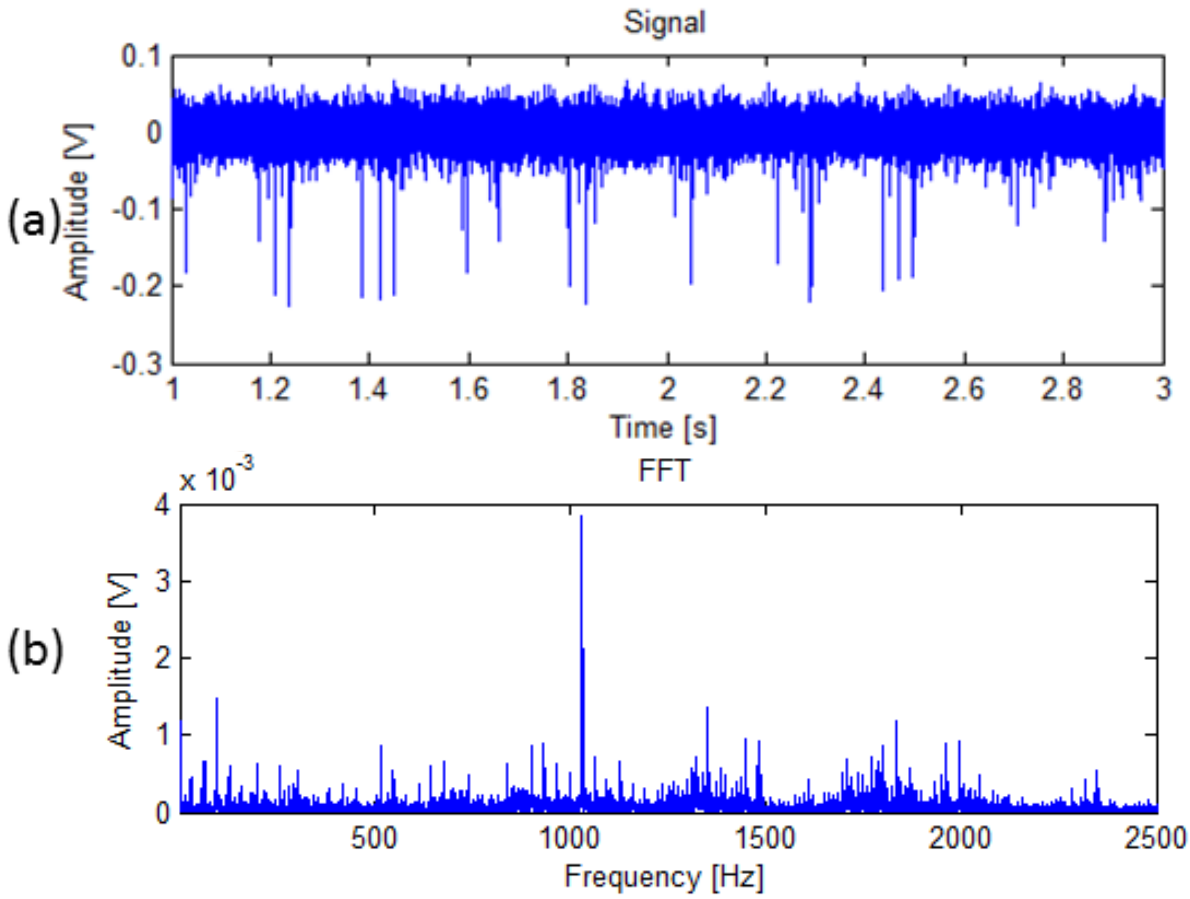

Figure 4.13: (a) Experimental evaluation of a healthy gear with a rotational frequency of the pinion of 16 Hz and (b) its Fourier Transform

In Figure 4.12, the frequency range includes three meshing harmonics. With a rotational frequency of the driving gear of 16.1 Hz and a pinion of 32 teeth, the meshing frequency and its harmonics are situated at 515.2 Hz, 1030.4 Hz, 1545.6 Hz and 2060,8 Hz. The pertinent areas to detect faults surround the meshing frequency and its harmonics [35]. For a worn gear, we would expect the peaks surrounding the meshing frequency to be of the same range of magnitude as the peak at the meshing frequency. These peaks are expected to be distanced at 16.1 Hz, which is the

exact experimental rotational frequency of the pinion. In Figure 4.14 faulty peaks are situated around the meshing frequency. They are situated at distances of 16.1 Hz which is the rotational frequency of the driving gear. Interfering peaks are situated at the rotational frequency of the driven gear which has a rotational ratio of one third. Considering that the amplitude of the meshing frequency peak is in the same scale as its sidebands, this shows the presence of wear. Here, the FFT is able to detect peaks however there is still noise and interference present.

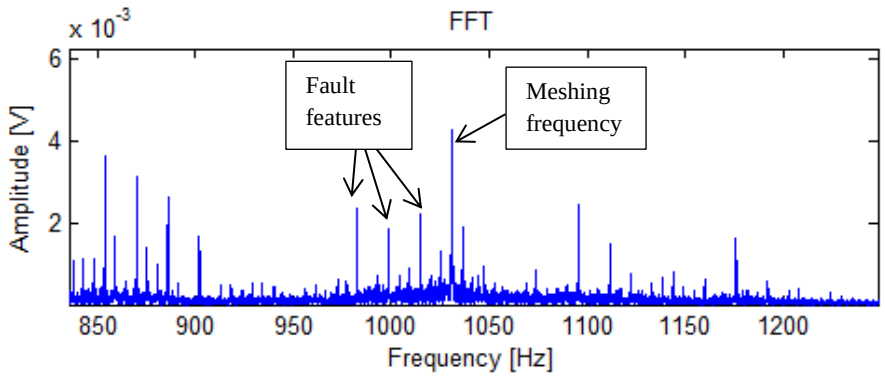

Figure 4.14: Fourier Transform of the experimental evaluation of a worn gear with a rotational frequency of the pinion of 16 Hz with a frequency range of 350 to 800 Hz

Even though the FFT was sufficient to detect the fault, it is interesting to observe the results obtained by applying the EO and its derivatives prior to the FFT. After applying the energy operator and its derivative fault detection methods, noise is reduced as seen in Figure 4.15. The theoretical meshing frequency is 512 Hz but the actual meshing frequency in this system is 515.1 Hz because the 16 Hz reading from the invertor may not be accurate. In all plots shown in Figure 4.15, sidebands can be observed at the same intervals of 16.1 Hz at the rotational frequency of the shaft. Figure 4.16 is generated by the four proposed fault detection methods applied to a healthy gear's signal. Concerning the EO, EO123, and EO23, the results observed in Figure 4.15 and Figure 4.16 are very different. In Figure 4.15, the interferences are

noticeable between the faulty features shown with the arrows. It is obvious in Figure 4.16 that the faulty features for these three fault detection methods are more dominated by the noise in the system. The four proposed methods have shown practically the same effectiveness to detect faults in this specific set of data. The noise and interfering peaks have the same magnitude in all cases in Figure 4.15. However in Figure 4.16 more interfering faults are noticeable as shown with the arrows. There are less interfering peaks in the healthy gear's signal after applying the EO23.

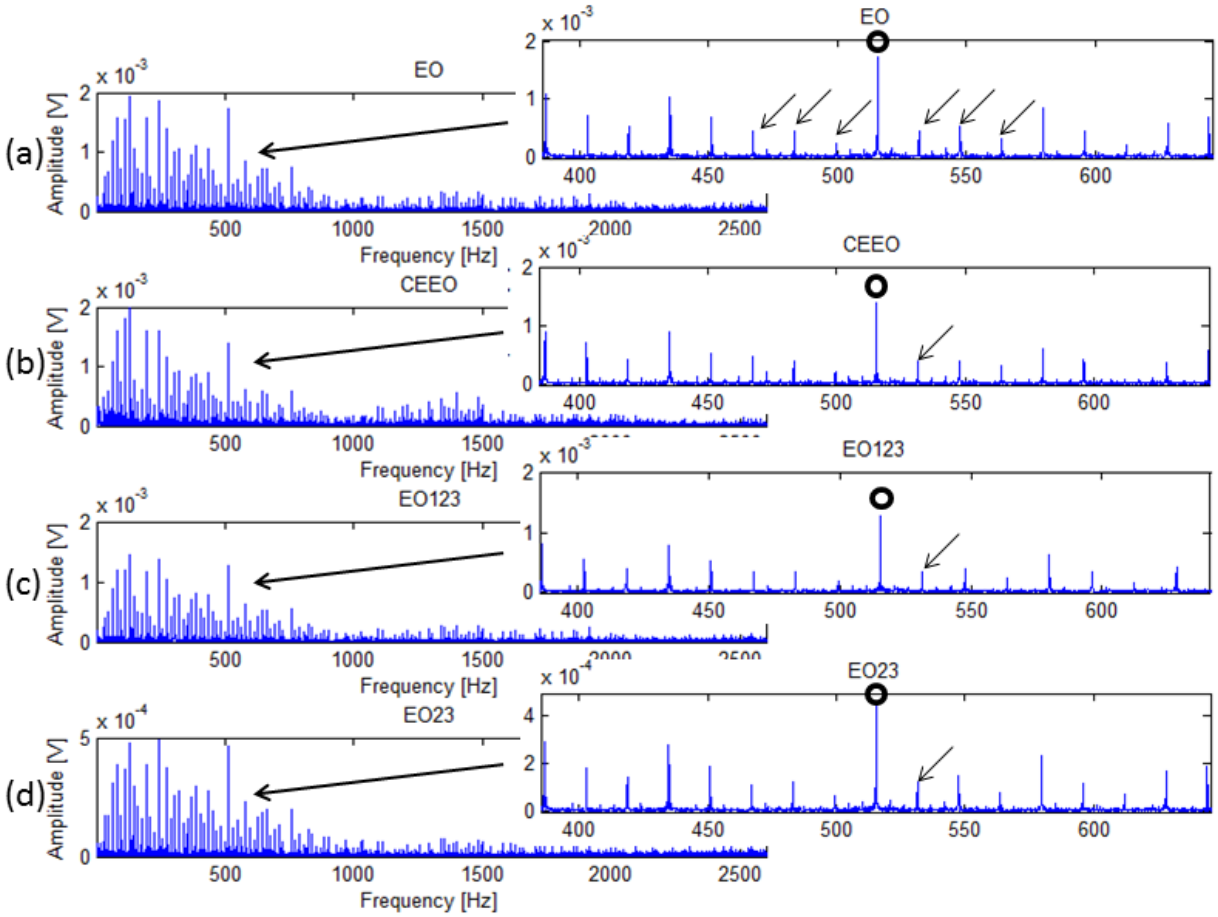

Figure 4.15: Fault detection methods applied to experimental evaluation of a worn gear with a rotational frequency of 16 Hz (a) EO (b) CEEO (c) EO123 (d) EO23

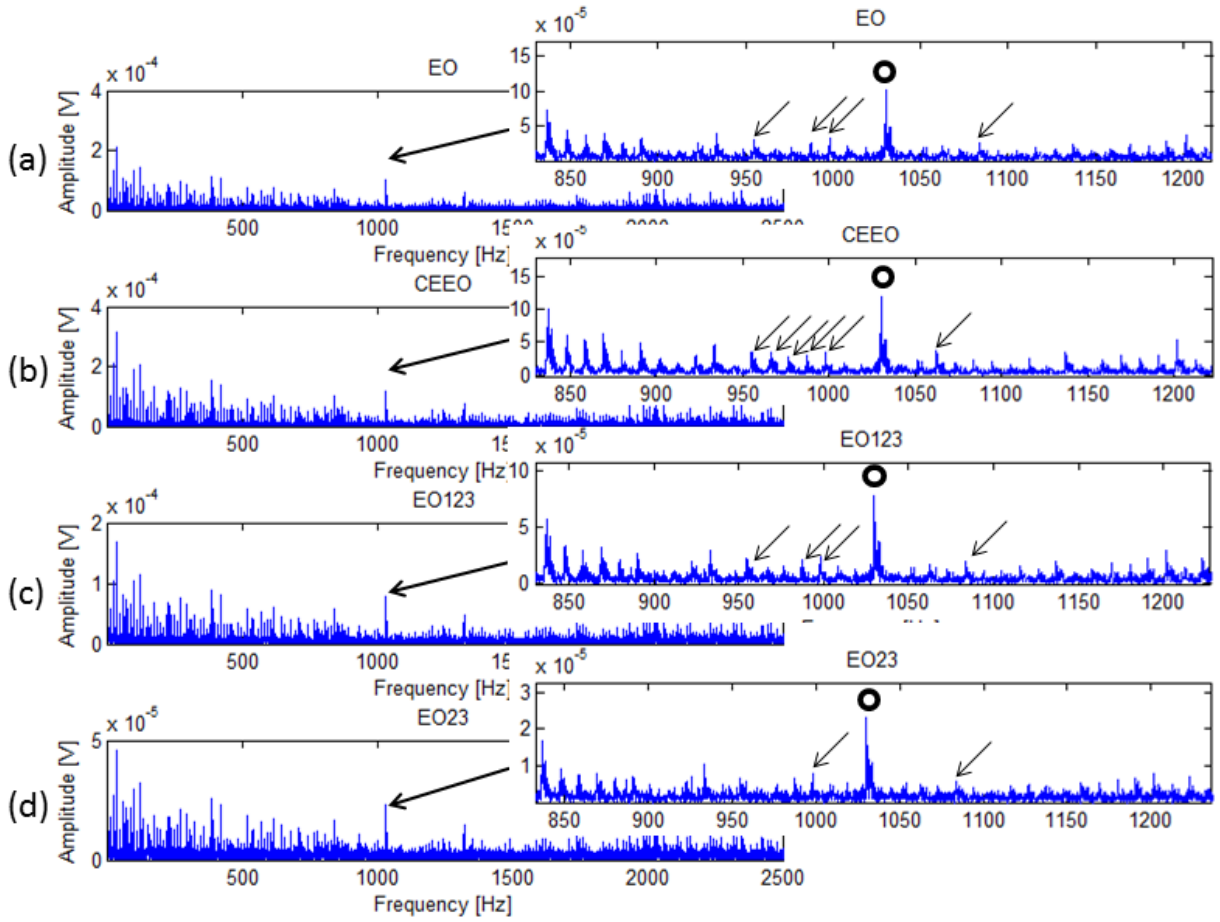

Figure 4.16: Fault detection methods applied to experimental evaluation of a healthy driving gear (chipped driven gear) with a rotational frequency of 16 Hz (a) EO (b) CEEO (c) EO123 (d) EO23

As concluded in the simulation evaluation, the EO23 method seems to handle interference better than the other methods in Figure 4.15. This can be verified at other frequencies with other sets of data.

The fault detection methods are now applied to a different test signal with a driving rotational frequency of 33 Hz with the same gears. The meshing frequency is therefore 1056 Hz (33 Hz x 32 teeth). The time signal is shown in Figure 4.17 (a) and its Fourier Transform in (b). The fault detection methods are used to handle as much as possible the noise and interference present in the signal.

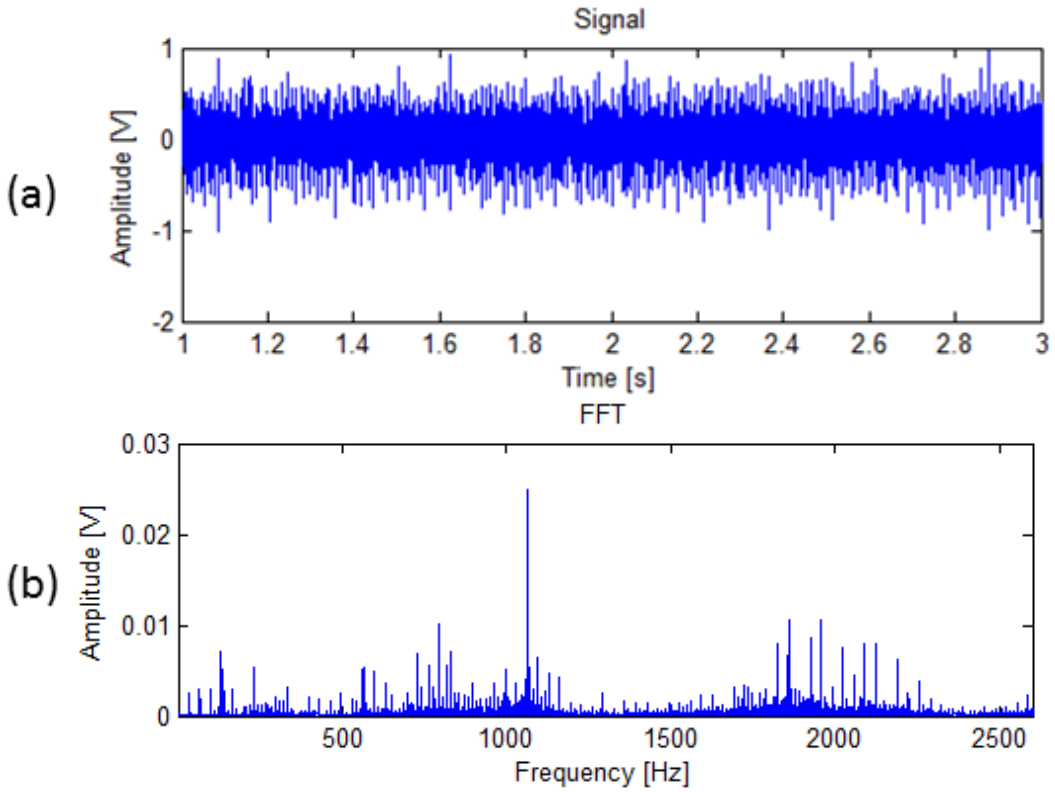

Figure 4.17: (a) Experimental evaluation of a worn gear with a rotational frequency of the pinion of 33 Hz and (b) its Fourier Transform

The frequency domain plot obtained after applying the FFT shows peaks at equidistance to one another around the meshing frequency. The FFT seems to be efficient to detect presence of fault. However, some noise and interferences could be reduced.

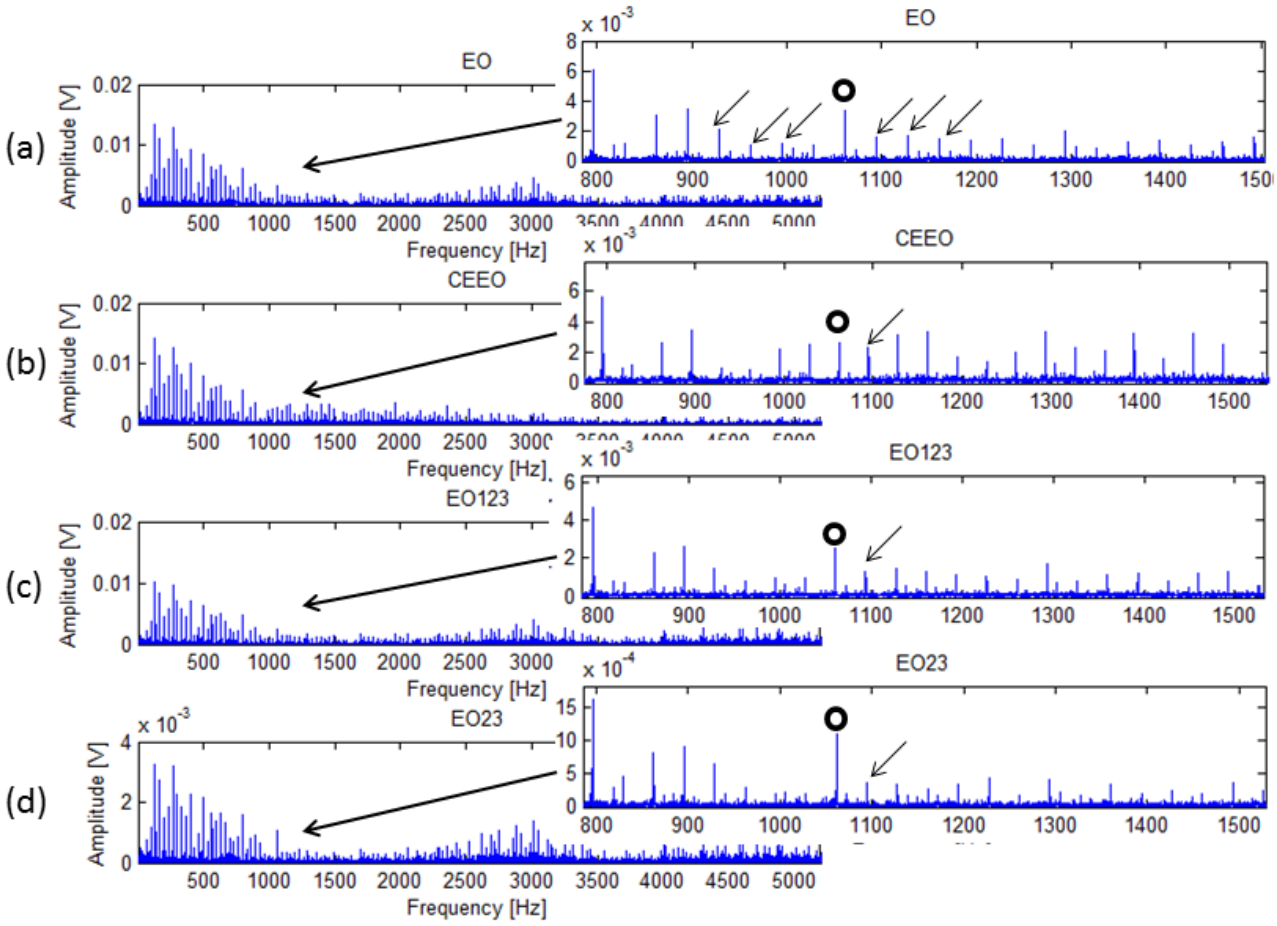

Figure 4.18: Fault detection methods applied to experimental evaluation of a faulty gear with a rotational frequency of 33 Hz (a) EO (b) CEEO (c) EO123 (d) EO23

Figure 4.18 illustrates the four proposed fault detection methods, EO, CEEO, EO123 and EO23 respectively applied to a faulty gear signal with a driving rotational frequency of 33.1 Hz. The second harmonic was chosen to be evaluated because there is less presence of dominant interferences and the faulty peaks are still of a considerable amplitude. All four signals show presence of interferences between the sidebands pointed out with the arrows; however, the result is better than the FFT in Figure 4.17 (b). The meshing frequencies are illustrated by O's. The CEEO's meshing frequency has a little amplitude and the sidebands are enhanced to the same

range of amplitude as the meshing frequency. On the other hand, the other methods, EO, EO123 and EO23 amplitudes of meshing frequency are larger than the sidebands that illustrated presence of wear. Once again, the plots obtained with the EO and the EO123 are very similar. There is presence of interference as well as reduced peaks representing faults. The CEEO fault detection method shown in (b) enhances all presence of faults. The EO23, in (d), is very good at dealing with interferences; however, it also reduced peaks representing faults. As shown in Figure 4.18, most of the interferences in (d) have a smaller magnitude than its adjacent fault frequency. However there is more noise than in the other plots. As mentioned before, the interferences are located at the rotational frequency of the driven gear which is 1/3 of the rotational frequency of the driving gear. In these data, the EO and its modified fault detection methods show better noise and interference handling than the FFT.

It is also interesting to observe the efficiency of the proposed fault detection methods at a low rotational frequency of the pinion, in this case 5.16 Hz. Using the same gears, the meshing frequency of the system is then 165.12 Hz (5.16 Hz x 32 teeth).

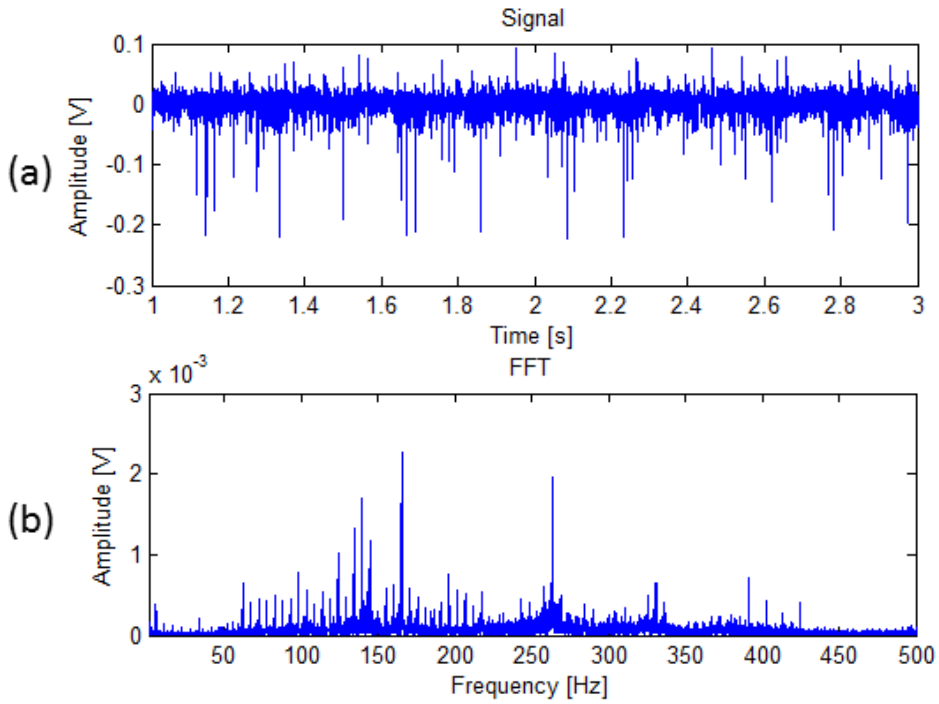

Figure 4.19: (a) Experimental evaluation of a worn gear with a rotational frequency of the pinion of 5.16 Hz and (b) its Fourier Transform

Figure 4.19 (a) is the vibration signal obtained while running the same gears at a driving rotational frequency of 5.16 Hz and Figure 4.19 (b) is its FFT. Compared to the previous figures rotating at higher rotational frequencies, it can be observed in Figure 4.19 that noise is more dominant at a lower frequency. To verify if the proposed methods can identify the worn driving gear, they are applied to the signal as shown in Figure 4.20.

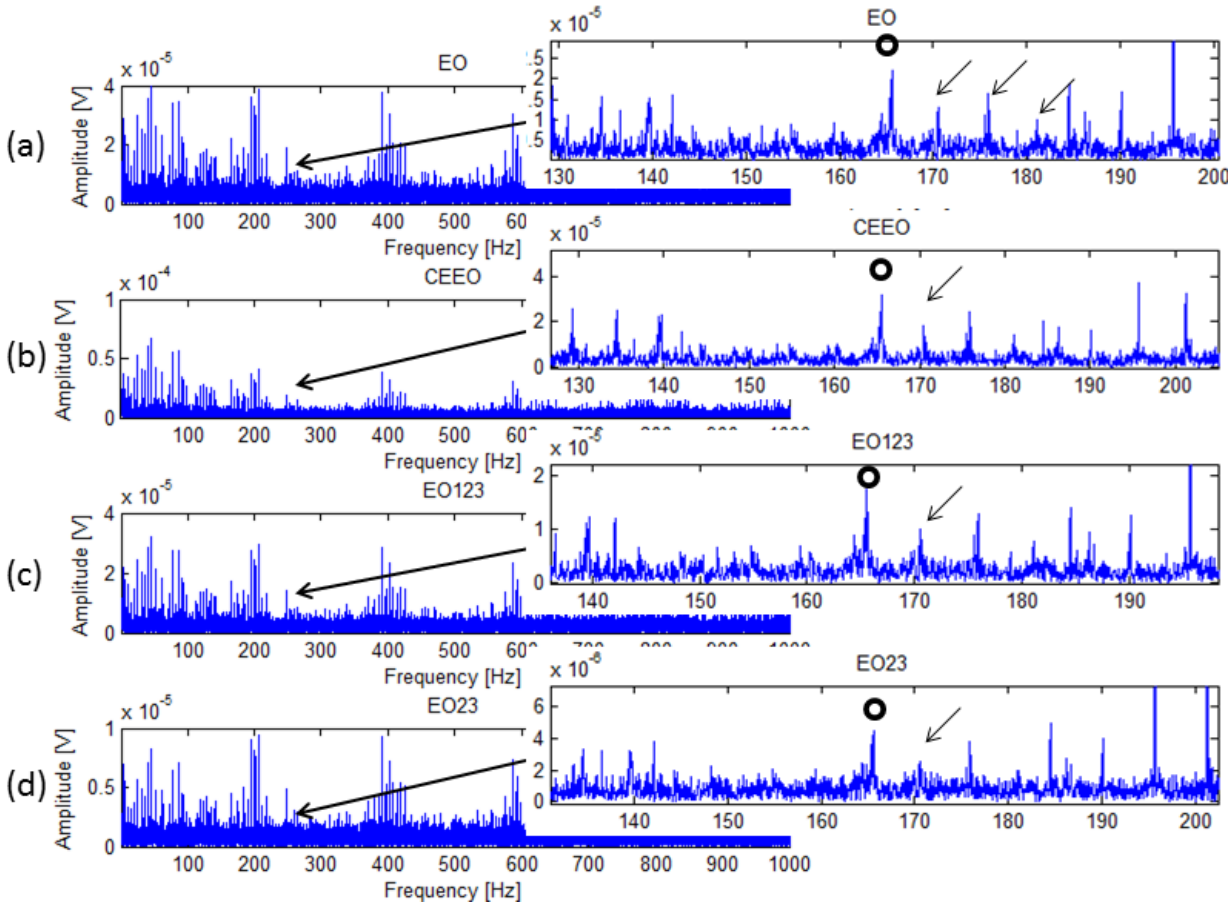

Figure 4.20: Fault detection methods applied to experimental evaluation of a worn driving gear with a rotational frequency of 5.16 Hz (a) EO (b) CEEO (c) EO123 (d) EO23

The CEEO method handles noise the best as seen in Figure 4.20 (b). The CEEO enhances the faults; however, it does the same to interferences. On the other hand, in Figure 4.20 (d) the EO23 reduces interferences considerably; however, it has the disadvantage of also reducing some pertinent faulty peaks. As mentioned before, the EO and EO123 obtain very close results as confirmed in Figure 4.20 (a) and (c). They do not handle noise as well as the CEEO and they do not handle interferences as well as the EO23.

Chapter 5 Signal fault detection methods on localized faults

In this chapter, localized faults are observed. The ability of the proposed fault detection methods to identify a fault and to handle noise and interference is analysed in the following sections. Examples of localized faults are a single cracked, chipped, or broken tooth. First, the equation used to simulate impulsive faults is explained as well as the methods' capability to handle noise and interference. Second, the analysis made with simulations is confirmed with experimental evaluations using the data collected by Professor Zhipeng Feng using a gearbox dynamics test rig in our lab at the University of Ottawa [40].

5.1 Simulated study

To be certain of the effectiveness of a fault detection method, all situations need to be analysed. In this section, the second type of fault is presented; impulsive faults. The simulation of a signal for impulsive faults is explained below, as well as the performance of the methods to detect such a fault. Furthermore, to be realistic, noise and interfering signals are added to the faulty gear vibration signal. To examine the performance of the methods, it is pertinent to know how much noise and interference it can handle.

5.1.1 Signal

As mentioned previously in section 4.1, the simulated signal of a healthy gear is represented by

$$x_{healthy}(t) = \sum_{p=0}^{M} X_p \cos\left(p\omega_m t + \phi_p \right), \tag{5.1}$$

where X_p is the amplitude of the *p*th meshing harmonic, ω_m is the system's meshing frequency, and ϕ_p is the initial phase of the *p*th meshing harmonic. The meshing gear signal $x(t)$ varies with time, *t*, and is summed *M* times depending on the number of harmonics.

Equation (5.1) includes the contact of the gear teeth during the rotation of the gears. A modification needs to be done to this equation to indicate the presence of a single impulsive fault on a gear.

5.1.2 Fault simulation

The equation used to simulate the effect of impulsive faults on the vibration signal is written as a summation of sinusoidal functions [35]. These summations are damped impulses given by

$$q(t) = \sum_{p=0}^{M} A_p e^{-\beta(t-pT_{rt})} \cos(\omega_r (t - pT_{rt}) + \theta_p) u(t - pT_{rt}), \tag{5.2}$$

where A_p is the amplitude of the p^{th} harmonic, β is the damping characteristic, T_{rt} is the period of rotation of the gear, ω_r is the excited resonance frequency, and θ_p is the phase parameter. The function $u(t)$ is a unit step function. These impulsive faults can represent localized faults such as a cracked tooth, a chipped tooth, or a broken tooth [35]. The fault detection methods need to be applied to the signal.

5.1.3 Fault analysis

When the energy operator and its variants are applied to a signal simulating a gear with an impulsive fault, the shape of the signal can be predicted. When the energy operator is applied to equation (5.2), it becomes [35]

$$\Psi\left(q(t)\right) = \sum_{p=0}^{M} A_p^2 \omega_m^2 e^{-2\beta(t-pT_{rt})} u\left(t - pT_{rt}\right). \tag{5.3}$$

The amplitude modulation and the frequency modulation are present in equation (5.3). Considering that local faults, studied in this chapter, cause amplitude and frequency modulation and that the EO extracts these features, it is then possible to say that the EO can detect impulsive faults [35]. From the exponential in equation (5.3), it can be concluded that when a fault is present, it will be situated at the driving gear's rotational frequency and its harmonics in the frequency domain. This is explained by the fact that when the FFT is applied, peaks can be observed at the powered value.

5.1.4 Clean signal

It is interesting to observe the effect of different fault detection methods on the faulty signals. The fault detection methods shown in Chapter 3 are applied to equation (5.2). For this first set of simulations, the effect of variation of the resonance frequency ω (512, 1024, and 2048 Hz) and of the rotational frequencies f_{rt} (6, 12, 24, 50, and 100 Hz) is observed in the signals. The damping of the system β is set to 500 for Table 5.1.

Rotational frequencies of the pinion f_{rt} (Hz)	Resonance frequency (Hz)	EO	CEEO	EO123	EO23
6	ω = 512	YES	YES	YES	YES
	ω = 1024	YES	YES	YES	YES
	ω = 2048	YES	YES	YES	YES
12	ω = 512	YES	YES	YES	YES
	ω = 1024	YES	YES	YES	YES
	ω = 2048	YES	YES	YES	YES
24	ω = 512	YES	YES	YES	YES
	ω = 1024	YES	YES	YES	YES
	ω = 2048	YES	YES	YES	YES
50	ω = 512	YES	YES	YES	YES
	ω = 1024	YES	YES	YES	YES
	ω = 2048	YES	YES	YES	YES
100	ω = 512	YES	YES	YES	YES
	ω = 1024	YES	YES	YES	YES
	ω = 2048	YES	YES	YES	YES

Table 5.1: Effect of varying frequency and resonance frequency on clean signal with impulsive faults

The periodic peaks of the rotational frequency are easily identifiable in all situations tested in Table 5.1. For example, at a rotation frequency of 12 Hz, a damping characteristic of 500 and an excited resonance frequency of 1024 is shown in Figure 5.1.

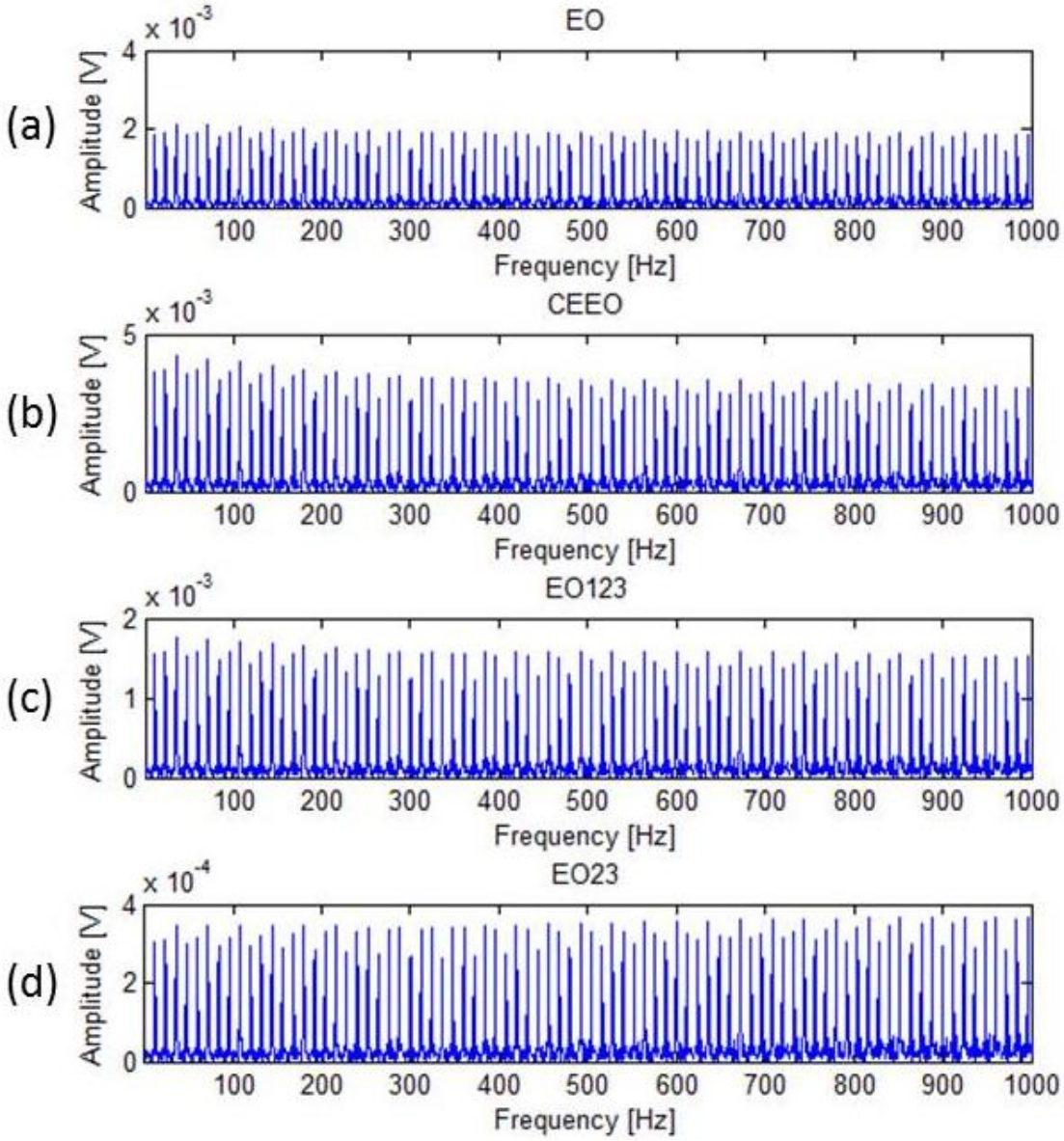

Figure 5.1: Clean signal a rotation frequency of 12 Hz, a damping characteristic of 500 and an excited resonance frequency of 1024

The rotational frequency of the driving gear and resonance frequency do not have an effect on the efficiency of the fault detection methods. However, the shape of the plots varies when the damping characteristic of the system β increases. The plots in Figure 5.2, Figure 5.3, and Figure 5.4 are generated with a rotational frequency of the pinion of 12 Hz and a resonance frequency ω of 2048 Hz. The damping characteristic of the system β is set to 100, 250, and 500 with amplitude A_m equal to 1.

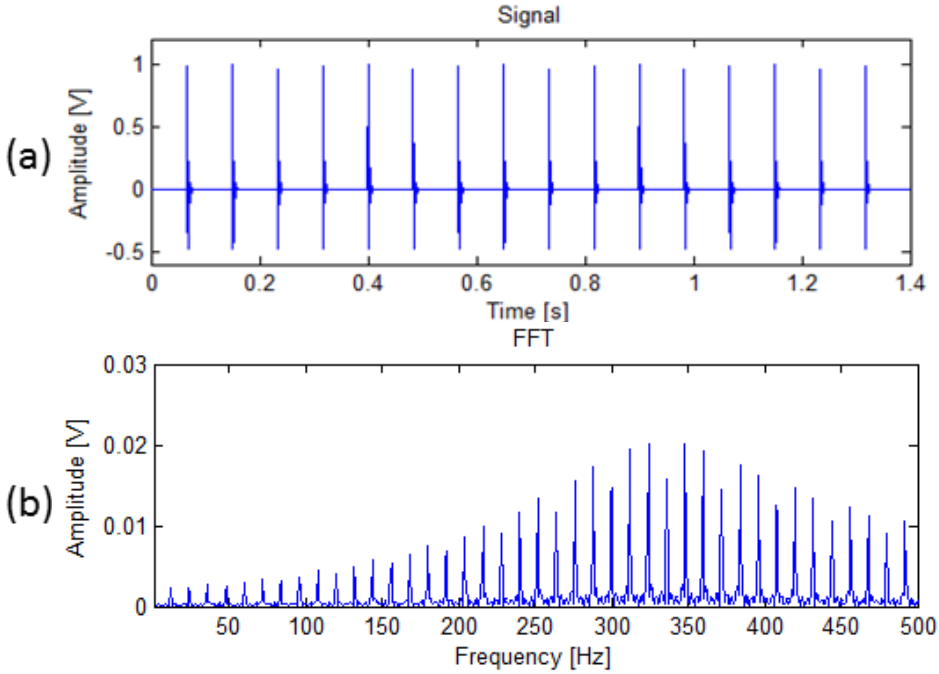

Figure 5.2: (a) Simulated signal and (b) the FFT of an impulsive fault with a damping characteristic of 500

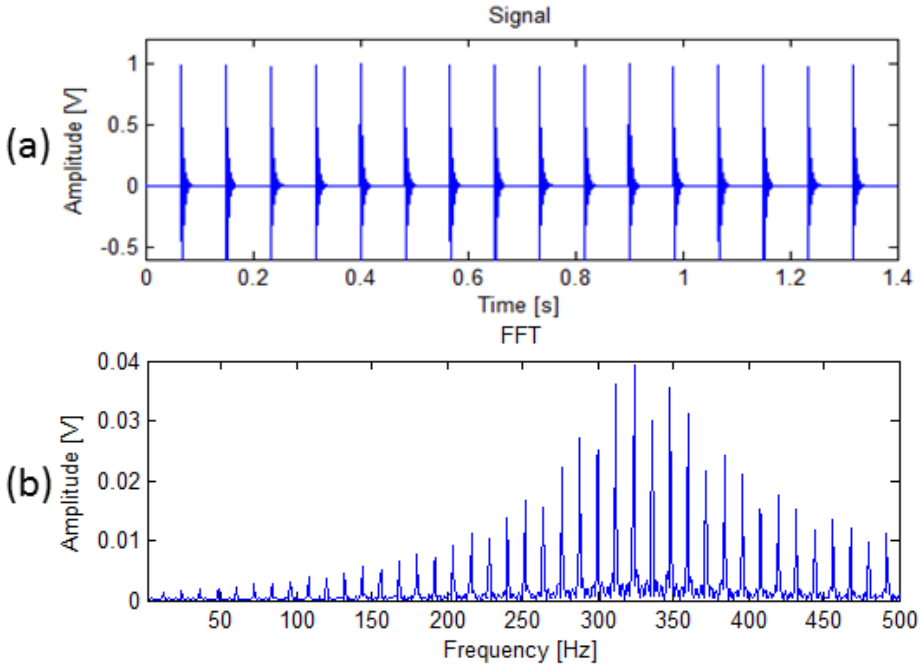

Figure 5.3: (a) Simulated signal and (b) the FFT of an impulsive fault with a damping characteristic of 250

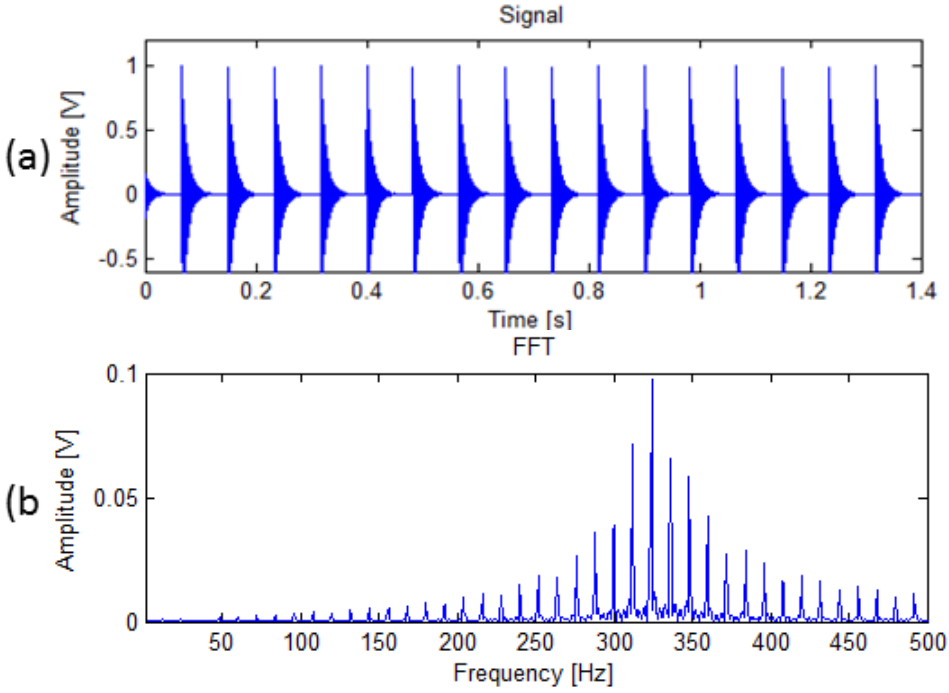

Figure 5.4: (a) Simulated signal and (b) the FFT of an impulsive fault with a damping characteristic of 100

We can see in Figure 5.4 that the peaks in the frequency domain are concentrated around the meshing frequency. With a larger damping characteristic, the peaks are spread out over the frequencies, as shown in Figure 5.2 and Figure 5.3. It could be predicted that this would make it easier to identify a fault in the presence of noise and interference. The four proposed fault detection methods react to the damping differently, as can be seen in Figure 5.5.

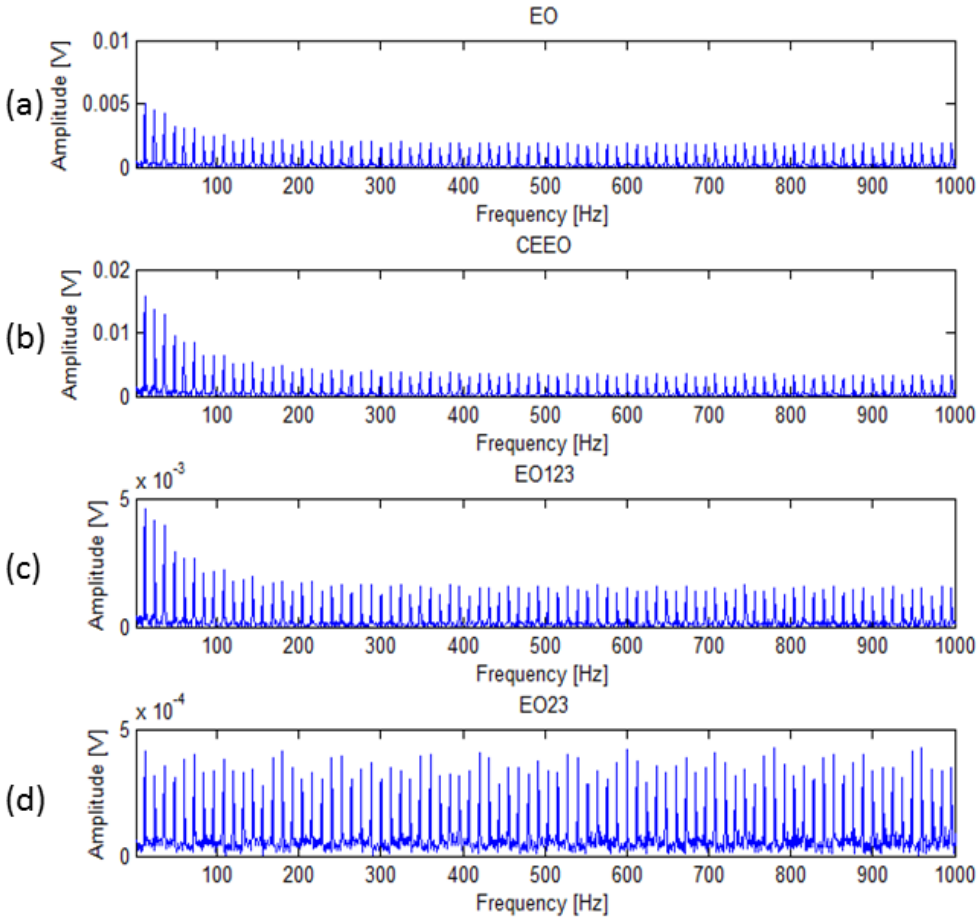

Figure 5.5: Fault detection methods applied to a simulated signal with impulsive faults

It is interesting to see in Figure 5.5 that the EO23 method removes the damping effect on the signal; in Figure 5.5 (d), the amplitude stays constant at all frequencies, while it decreases in all

the other plots (a), (b), and (c). It would be interesting to see how the fault detection methods handle noise and interference.

5.1.5 Noise handling

It is pertinent to determine how the proposed fault detection methods can handle noise. Simulations are done at different frequencies using equation (5.2). In Table 5.2 the damping characteristic of the system is set to 500 and a considerable amount of noise, SNR = -10 dB, is added to the signal. As observed in Table 5.2, the CEEO method appears to handle noise the best. For each method, the ability to detect faults varies at different rotational frequencies of the shaft. However, the EO23, as shown in Chapter 3, does not handle noise well. In Table 5.2, the EO23 cannot detect any faults.

Rotational frequencies of the pinion f_{rt} (Hz)	Resonance frequency (Hz)	EO	CEEO	EO123	EO23
6	ω = 1024	-	-	-	-
	ω = 2048	YES	BEST	YES	-
	ω = 4096	-	YES	-	-
12	ω = 1024	-	-	-	-
	ω = 2048	-	YES	-	-
	ω = 4096	-	-	-	-
24	ω = 1024	-	-	-	-
	ω = 2048	YES	BEST	YES	-
	ω = 4096	-	YES	-	-

50	ω = 1024	-	-	-	-
	ω = 2048	-	YES	-	-
	ω = 4096	YES	YES	YES	-
100	ω = 1024	-	-	-	-
	ω = 2048	-	YES	-	-
	ω = 4096	YES	BEST	YES	-

Table 5.2: Effect of varying frequency and resonance frequency on a noisy signal with impulsive faults with a damping characteristic of 500

Table 5.3 uses the same equation as Table 5.2; however, the damping of the system is changed to 200. The CEEO is still the most efficient method for a noisy signal in this case. As before, the EO23 is not effective at detecting faults in a noisy signal.

Rotational frequencies of the pinion f_{rt} (Hz)	Resonance frequency (Hz)	EO	CEEO	EO123	EO23
6	ω = 1024	-	-	-	-
	ω = 2048	YES	YES	YES	-
	ω = 4096	-	YES	-	-
12	ω = 1024	-	-	-	-
	ω = 2048	-	YES	-	-
	ω = 4096	YES	YES	YES	-
24	ω = 1024	YES	-	YES	-
	ω = 2048	YES	YES	YES	-
	ω = 4096	-	YES	-	-

50	$\omega = 1024$	-	-	-	-
	$\omega = 2048$	YES	YES	YES	-
	$\omega = 4096$	-	YES	-	-
100	$\omega = 1024$	-	-	-	-
	$\omega = 2048$	-	-	-	-
	$\omega = 4096$	-	YES	-	-

Table 5.3: Effect of varying frequency and resonance frequency on a noisy signal with impulsive faults with a damping characteristic of 200

The same observations are made here as in Chapter 3. It is also interesting to determine how much noise the EO23 method can handle.

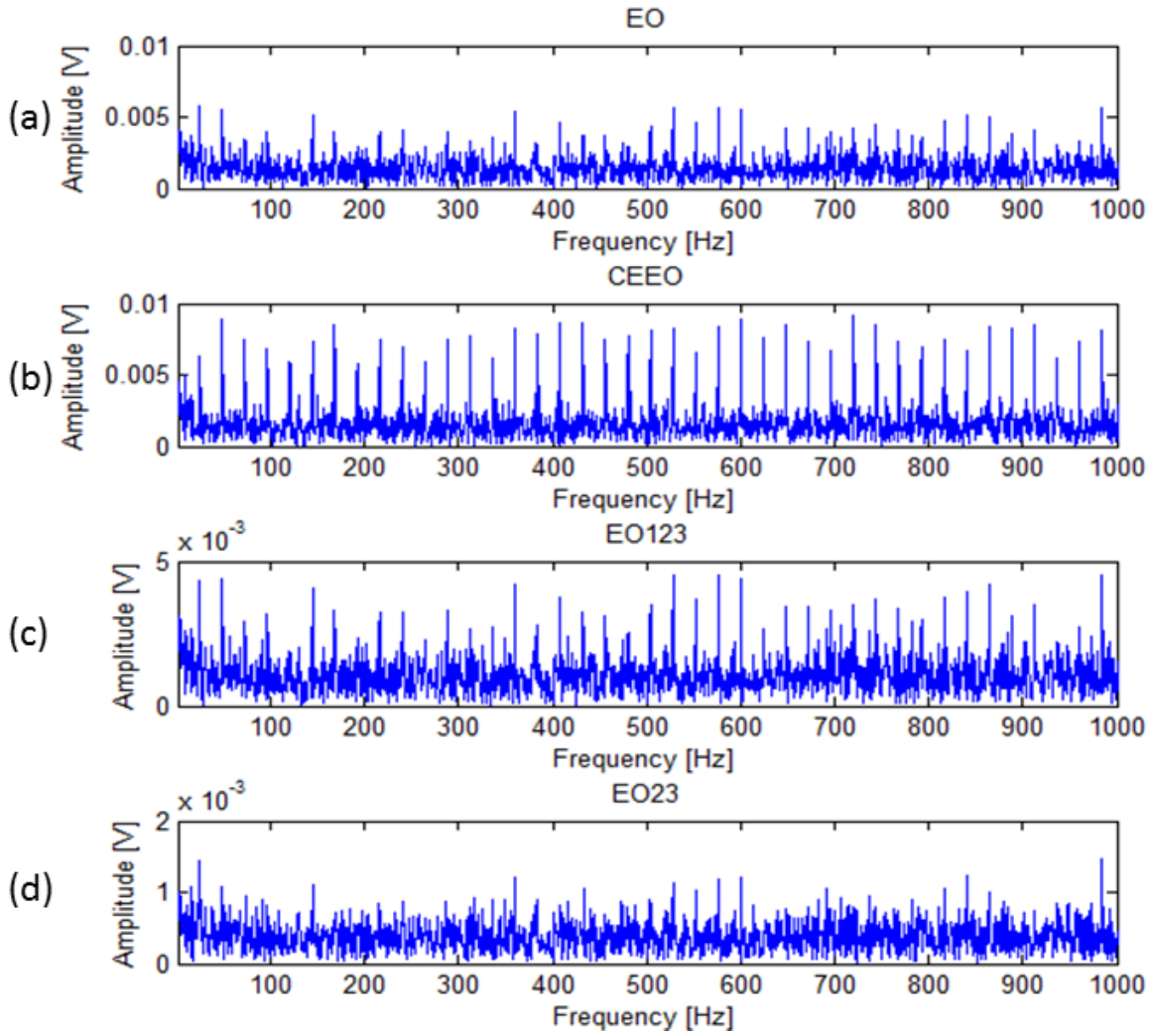

Figure 5.6: Fault detection methods applied to a noisy simulated signal with impulsive faults (SNR = -5 dB)

Figure 5.6 shows that with a SNR of -5 dB, the EO23 method is still effective for detection of faults. However, the other methods are more effective; as more faulty peaks are visible.

5.1.6 Interference handling

The ability of fault detection methods to detect faults in the presence of interference is now considered. This interfering signal consists of a combination of sinusoidal functions that interferes with the faulty signal. The damping characteristic is set to 500 for Table 5.4. The SIR of the signal mixture with the interfering signal is -55 dB.

Rotational frequencies of the pinion f_{rt} (Hz)	Resonance frequency (Hz)	EO	CEEO	EO123	EO23
6	ω = 1024	YES	YES	YES	YES
	ω = 2048	YES	YES	YES	YES
	ω = 4096	YES	YES	YES	YES
12	ω = 1024	YES	YES	YES	YES
	ω = 2048	YES	YES	YES	YES
	ω = 4096	YES	YES	YES	YES
24	ω = 1024	YES	YES	YES	YES
	ω = 2048	YES	YES	YES	YES
	ω = 4096	YES	YES	YES	YES
50	ω = 1024	YES	YES	YES	YES
	ω = 2048	YES	YES	YES	YES
	ω = 4096	YES	YES	YES	YES
100	ω = 1024	YES	YES	YES	YES
	ω = 2048	YES	YES	YES	YES
	ω = 4096	YES	YES	YES	YES

Table 5.4: Effect of varying frequency and resonance frequency on a signal with impulsive faults and interference with a damping characteristic of 200

The results in Table 5.4 show that when the simulated impulsive faulty signal is strictly in the presence of interference (with no noise), all methods are very effective. They can detect faults with large interfering signals. However, the results of the EO23 seem to be more precise than the others.

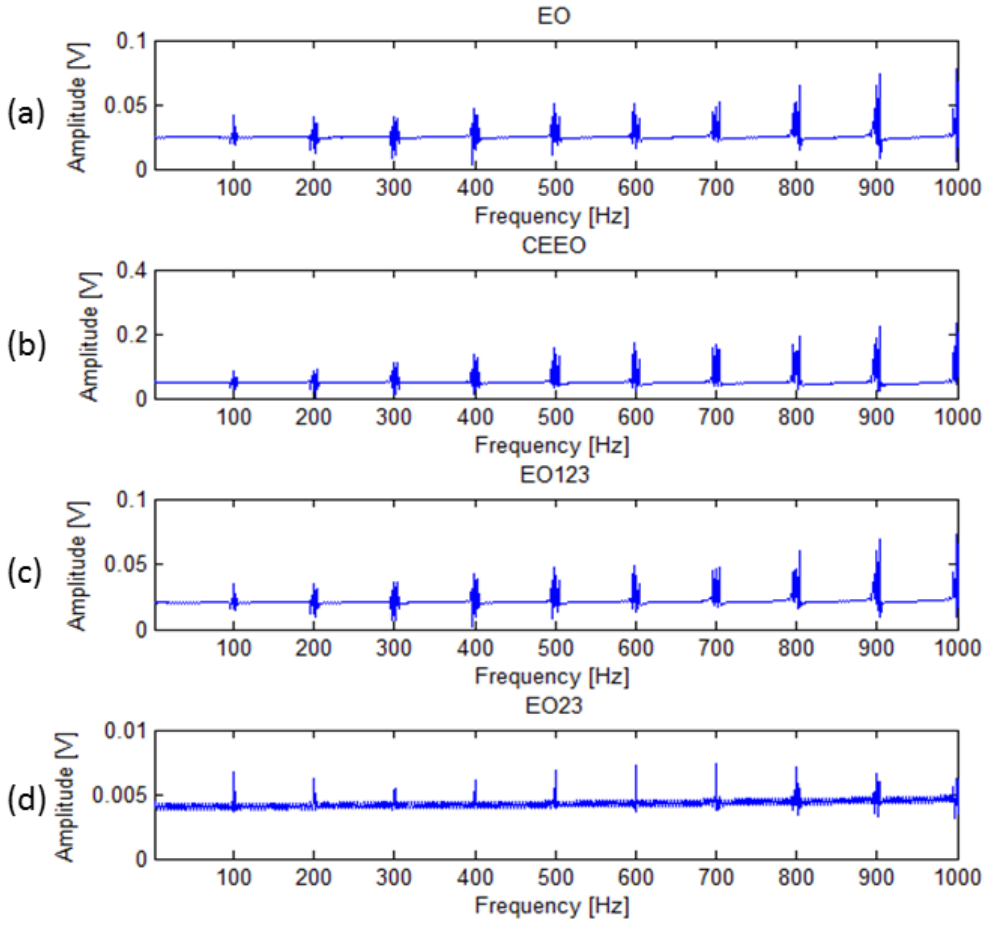

Figure 5.7: Fault detection methods applied to a simulated signal with impulsive faults and interference (SIR = -55 dB)

As mentioned in Chapter 3, the EO23 result shows less interfering peaks around the impulses at the rotational frequency in Figure 5.7. The EO23 method was however the least effective method in the presence of noise. For a more realistic result, it would be interesting to see the results of the proposed methods in presence of both noise and interference.

5.1.7 Noise and interference handling

Previously, the ability of the methods to handle noise and interferences separately has been discussed. Now, it is interesting to observe how the combination of the two, noise and interference, affects the conclusions made previously. Equation (5.2) is used to simulate impulsive faults in the presence of noise and interference. In Table 5.6 Table 5.9, a medium-level damping characteristic and resonance frequency are chosen, $\beta = 500$ and $\omega = 2048$ respectively, to simulate the signal. The SIR is set to -55 dB. The amount of noise is the same as in the previous chapter with an SNR ranging between -2 and -20 dB.

	SNR (dB)					
	-2	-5	-10	-12	-15	-20
EO	YES	YES	-	-	-	-
CEEO	YES	YES	-	-	-	-
EO123	YES	YES	-	-	-	-
EO23	-	-	-	-	-	-

Table 5.5: Fault detection methods' capability to handle noise and interference at a rotational frequency of 6 Hz

	SNR (dB)					
	-2	-5	-10	-12	-15	-20
EO	YES	YES	-	-	-	-
CEEO	YES	YES	-	-	-	-
EO123	YES	YES	-	-	-	-
EO23	YES	YES	-	-	-	-

Table 5.6: Fault detection methods' capability to handle noise and interference at a rotational frequency of 12 Hz

	SNR (dB)					
	-2	-5	-10	-12	-15	-20
EO	YES	YES	-	-	-	-
CEEO	YES	YES	-	-	-	-
EO123	YES	YES	-	-	-	-
EO23	YES	-	-	-	-	-

Table 5.7: Fault detection methods' capability to handle noise and interference at a rotational frequency of 24 Hz

	SNR (dB)					
	-2	-5	-10	-12	-15	-20
EO	YES	YES	-	-	-	-
CEEO	YES	YES	-	-	-	-
EO123	YES	YES	-	-	-	-
EO23	YES	-	-	-	-	-

Table 5.8: Fault detection methods' capability to handle noise and interference at a rotational frequency of 50 Hz

	SNR (dB)					
	-2	-5	-10	-12	-15	-20
EO	YES	YES	-	-	-	-
CEEO	YES	YES	-	-	-	-
EO123	YES	YES	-	-	-	-
EO23	YES	-	-	-	-	-

Table 5.9: Fault detection methods' capability to handle noise and interference at a rotational frequency of 100 Hz

The results, obtained in Table 5.5 Table 5.9, seem to be very similar. The rotational frequency of the driving gear does not affect the ability of the methods to detect faults in these tables. In the listed tables, the EO23 method is the weakest one of the proposed methods.

5.2 **Experimental study**

An experimental study is performed to confirm the results obtained in the simulation evaluation. Herein, tests are done on a two stage gearbox with a driving gear of 32 teeth and with a speed ratio of 1/3 for both stages. In this section, the proposed fault detection methods are tested on data acquired from running a two stage spur gear gearbox. The input gear has 32 teeth, and the output gear has 96 teeth. For the data gathering, IMI 623C01 ICP accelerometers are placed on the case aligned with each gear in order to capture the horizontal lateral vibration. During the test, the accelerometer signals are collected at a sampling frequency of 40 kHz, and the signals last for 60 seconds. A constant torque of 35 lb-in (2.5/5.0 indicated by the rating plate) is applied to the output shaft by the brake. The motor driving the gear to the left shown in Figure 5.8 is rotating at a constant speed. The rotational frequency of the driving gear is set to different values to verify whether rotational frequency affects the fault detection efficiency. The accelerometer is aligned with the first gear, containing 32 teeth.

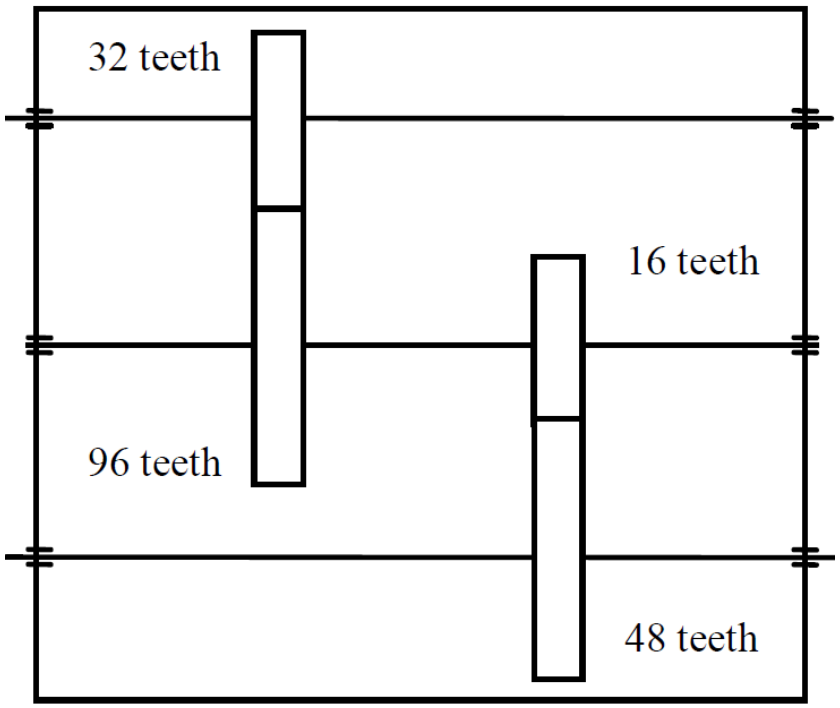

Figure 5.8: Motor driving the 32 teeth gear shaft, and there is a brake on the right connecting the 48 teeth gear shaft [40]

5.2.1 Chipped driven gear and healthy driving gear

Considering the driving gear is healthy, no signal of interest is expected at the rotational frequency of the driving gear and its harmonics. However, because the driven gear is chipped, and its rotational frequency is one third of the rotational frequency of the pinion, peaks are expected at its rotational frequency. For example, experimental data is observed for a rotational frequency of the driving gear of 12 Hz in Figure 5.9 and Figure 5.10.

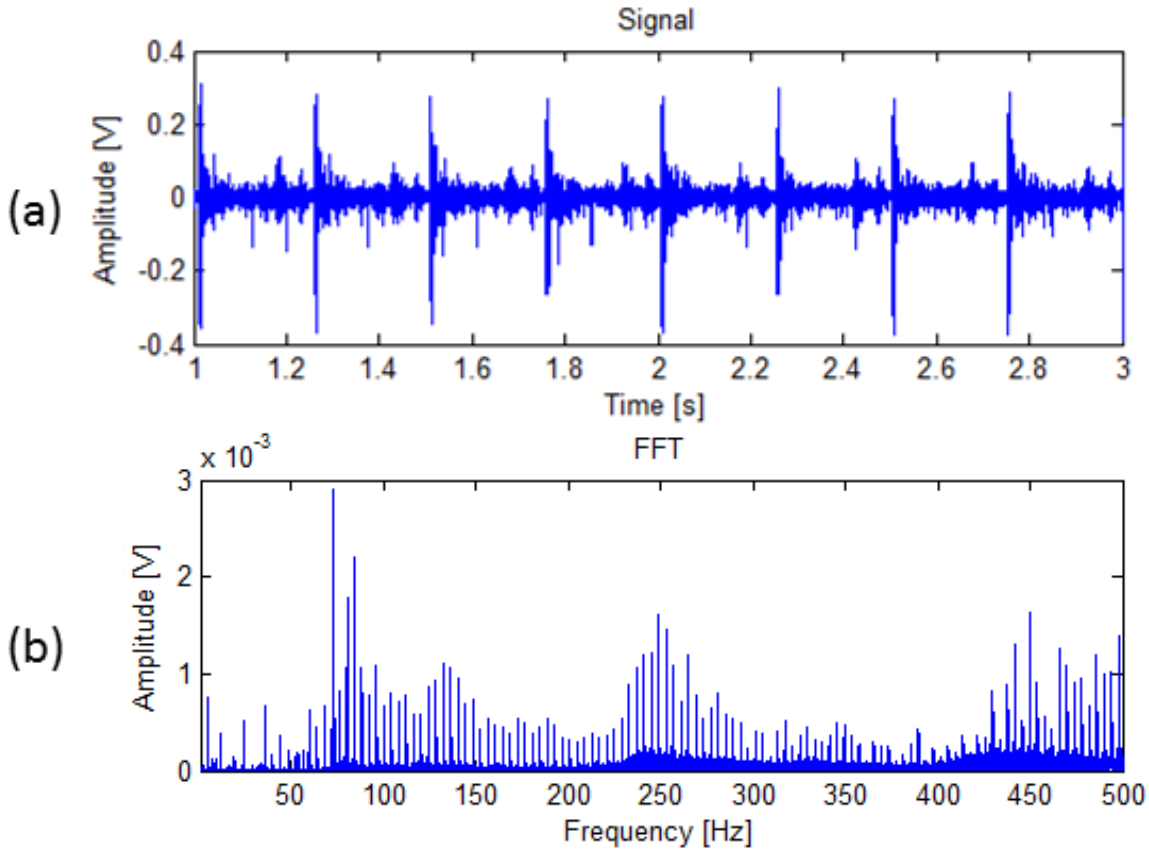

Figure 5.9: Experimental evaluation at a rotational frequency of the driving gear of 12 Hz (a) in the time domain (b) and frequency domain

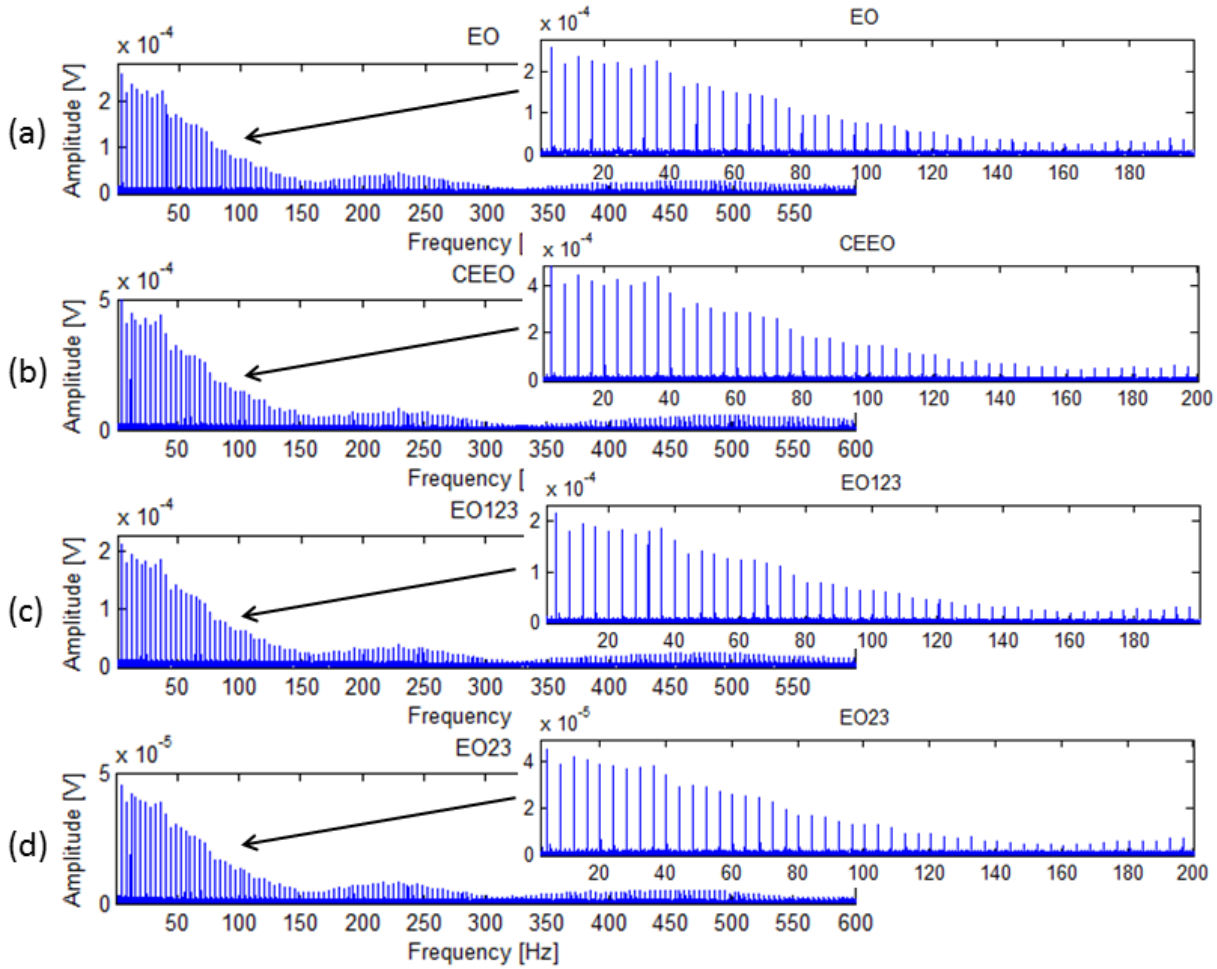

Figure 5.10: Fault detection methods (a) EO (b) CEEO (c) EO123 (d) EO23 applied to experimental data with a rotational frequency of the driving gear of 12 Hz

As expected, the simple FFT in Figure 5.9 (b) shows more noise than the plot obtained with the proposed fault detection methods in Figure 5.10. In Figure 5.10 peaks at 12 Hz (the rotational speed of the chipped driven gear) and its harmonics are easily identifiable. The same result is obtained for most tested frequencies, 9 Hz, 10 Hz, 12 Hz, 15 Hz, 18 Hz, and 20 Hz. At lower frequencies, the fault detection methods handle noise and interference differently as shown in Figure 5.12. As shown in Figure 5.9 (b), applying the FFT makes it possible to identify faults; however, the proposed EO method and its variants handle noise better as seen in Figure 5.10.

The results in this section do not show larger peaks at the meshing frequency. The local faults result in faulty features at harmonics of the rotational frequency. As show in Figure 5.10, these periodic peaks, showing presence of a local fault show very little variation of amplitude between the adjacent peaks. This is expected as demonstrated in the plots in the simulated study.

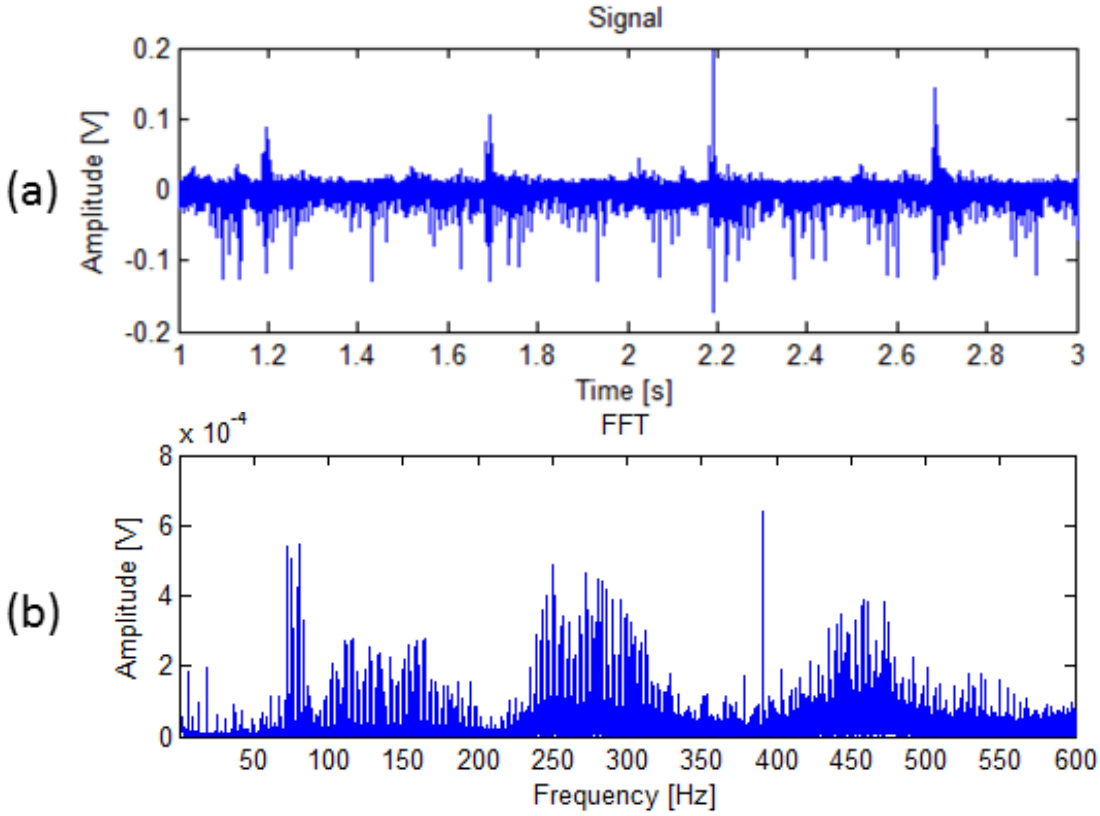

Figure 5.11: Experimental evaluation at a driving shaft rotational frequency of 6 Hz (a) in the time domain (b) and frequency domain

The FFT shown in Figure 5.11 and the fault detection methods in Figure 5.12 are still efficient at a rotational frequency of the driving gear of 6 Hz. However noise and interferences seem to be mixed with the faulty features. The proposed fault detection methods are applied.

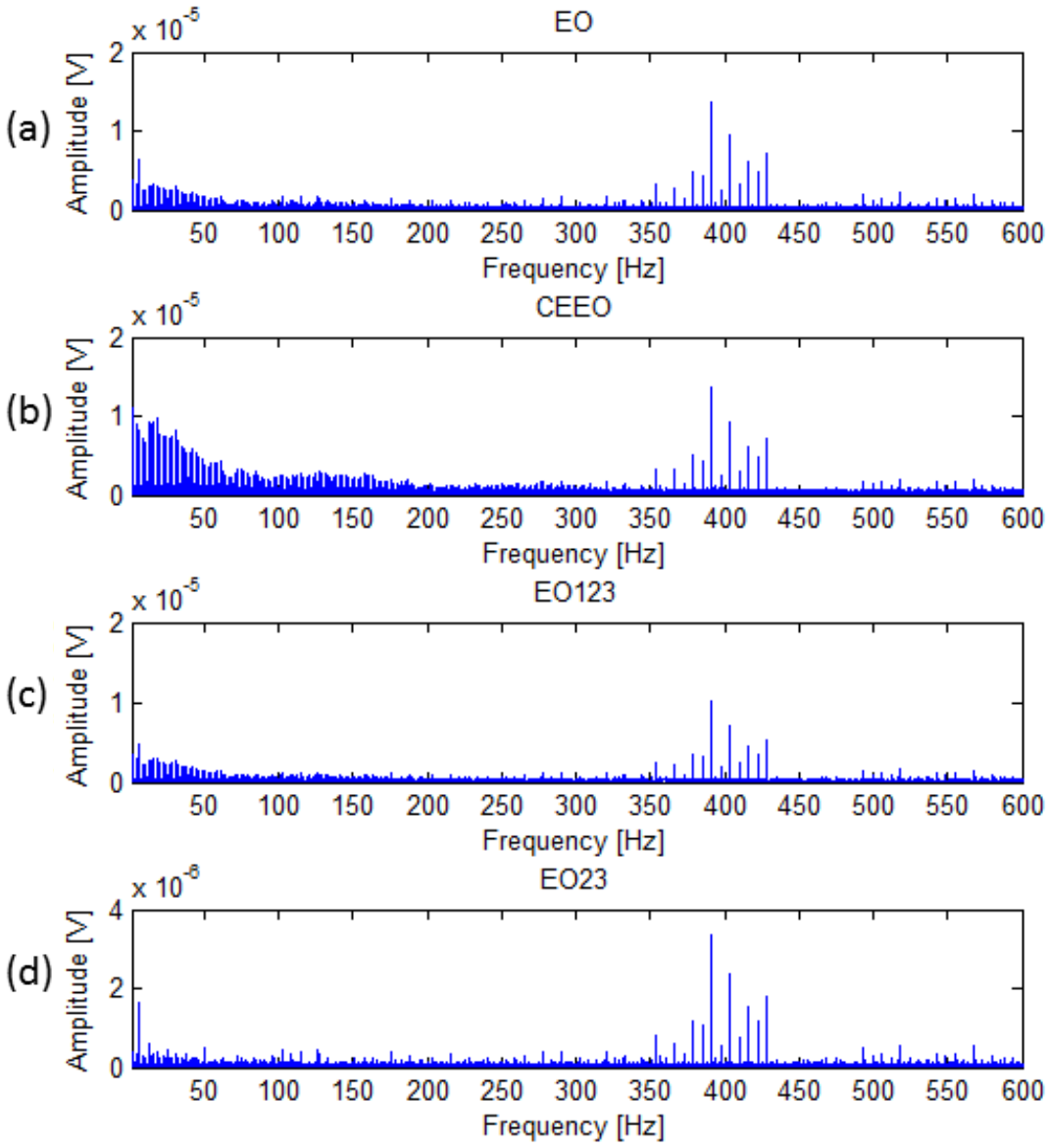

Figure 5.12: Fault detection methods (a) EO (b) CEEO (c) EO123 (d) EO23 applied to experimental data with a rotational frequency of the driving gear of 6 Hz

In this case, the clearest results are around the second harmonic of the meshing frequency (390.9 Hz). There are very little interfering peaks in all cases and the faulty features are much larger than the noise. Around zero, the EO and the EO123 in Figure 5.12 show distinctive peaks at 2 Hz (the rotational frequency of the chipped driven gear at 1/3 the rotational frequency of 6 Hz of the driving gear) and its harmonics; however, they start getting mixed up with noise at about 190 Hz. The EO23 in Figure 5.12 shows peaks at very low frequencies and they start being falsified by

noise at 75 Hz. However the EO23 method is the only method that increases the peaks on the driving gear and reduces the peaks caused by the chipped driven gear. The CEEO is clearly the most efficient method in this case to handle noise as shown in Figure 5.12 (b). This has been predicted in the previous sections. The EO23 cannot handle noise which becomes more dominant at lower rotational frequencies.

5.2.2 Chipped driven gear and cracked tooth on driving gear

Doing tests with two faulty gears, the results will differ from the previous test done on a chipped driven gear and a healthy driving gear. Here, two features will be affecting the results. First, an experimental evaluation is done on data with a rotational frequency of the driving gear of 12 Hz.

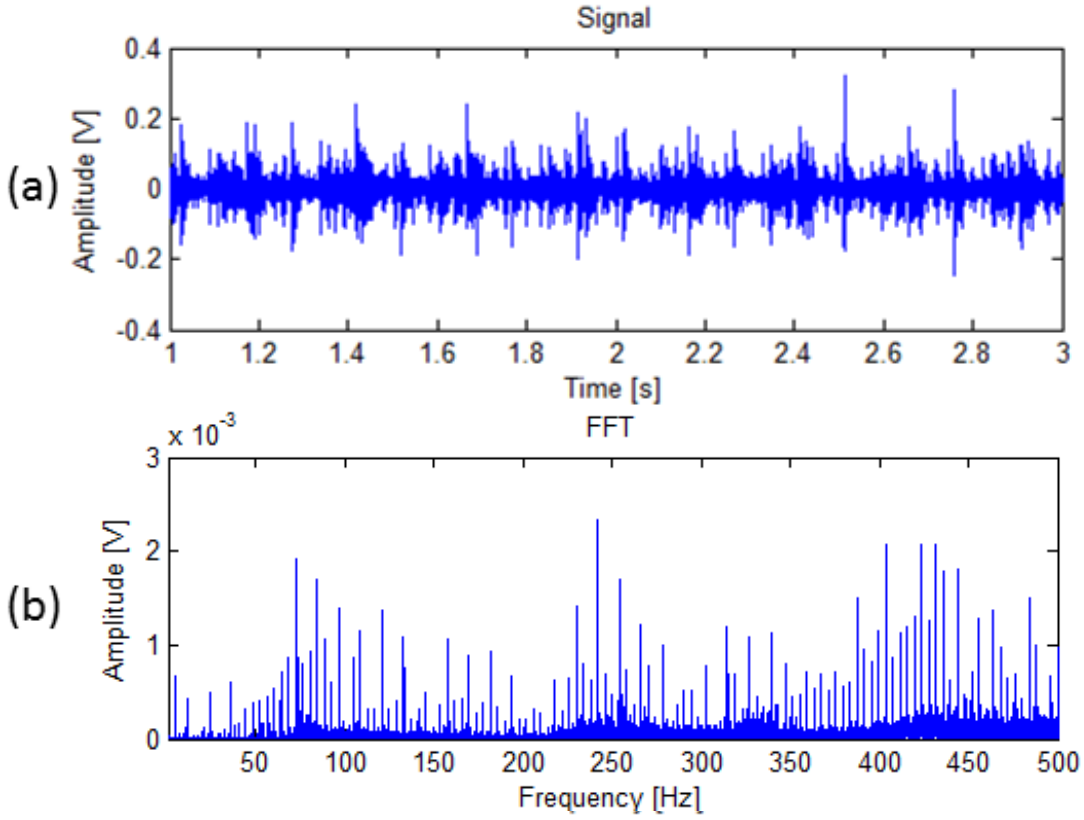

Figure 5.13: Experimental evaluation at a driving shaft rotational frequency of 12 Hz (a) in the time domain (b) and frequency domain

The peaks in the time domain are not regular in Figure 5.13 (a); they resemble those in Figure 5.9 (a) which has only one faulty gear. This is interpreted in the frequency domain with the varying amplitudes of the peaks in Figure 5.13 (b). This is caused by the addition of an impulsive fault at every 12 Hz on the driving gear.

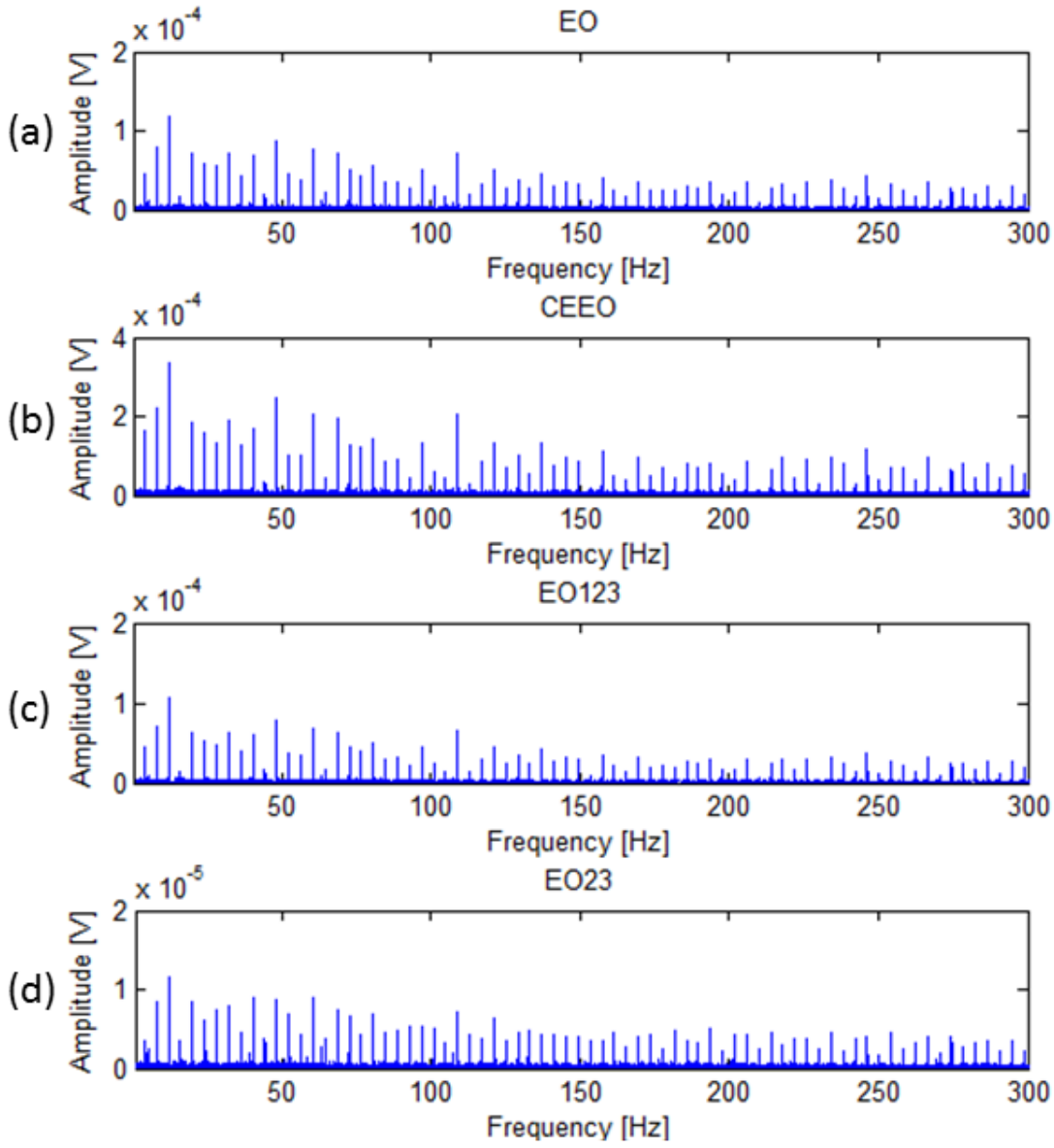

Figure 5.14: Fault detection methods (a) EO (b) CEEO (c) EO123 (d) EO23 applied to experimental data with a rotational frequency of the driving gear of 12 Hz

The proposed fault detection methods are applied to the signal shown in Figure 5.13 (a). The proposed methods, in Figure 5.14, obtain cleaner and more precise results as the simple FFT in Figure 5.13 (b). The CEEO in Figure 5.14 (b) has the effect of reducing smaller peaks and increasing the larger peaks. The disadvantage in this case is that some faulty peaks are reduced when they should be considered in the fault detection. On the other hand, the EO23 method, illustrated in Figure 5.14 (d), levels out the faulty features; therefore, it increases the smaller peaks and reduces the larger ones. This is the optimal result. However the EO23 result does show more noise than those of the other methods. This could be important under different conditions. Experimental evaluations show the same results at different frequencies such as 7 Hz, 9 Hz, 10 Hz, 12 Hz, 15 Hz, 18 Hz, and 20 Hz. The results are observed for tests done at a rotational frequency of the driving gear of 6 Hz.

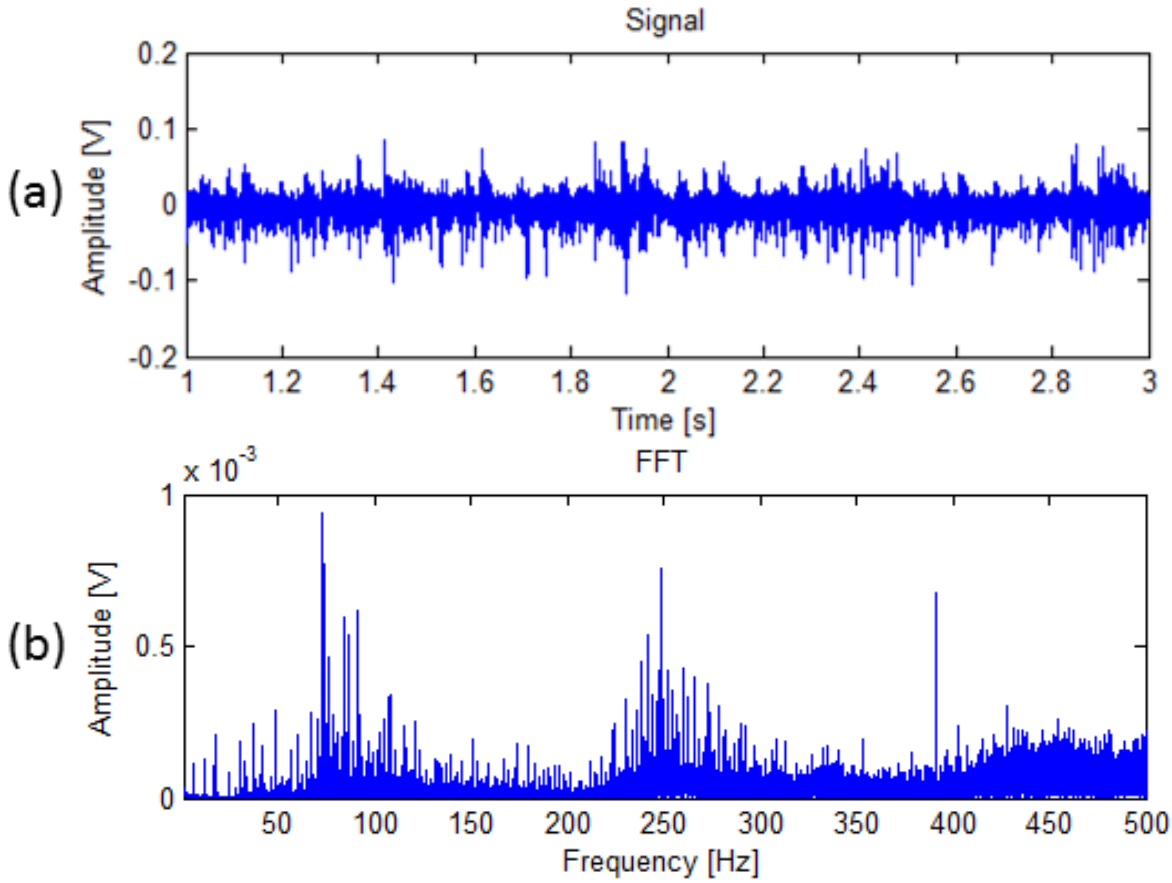

Figure 5.15: Experimental evaluation at a driving gear rotational frequency of 6 Hz (a) in the time domain (b) and frequency domain

At a low rotational frequency, as observed previously, noise is more dominant in the vibration signal as seen in Figure 5.15 (a). The FFT also shows the presence of noise. Some faulty peaks are missing and there are interfering peaks. The EO fault detection method and its variants are tested to see if they will help to provide better results.

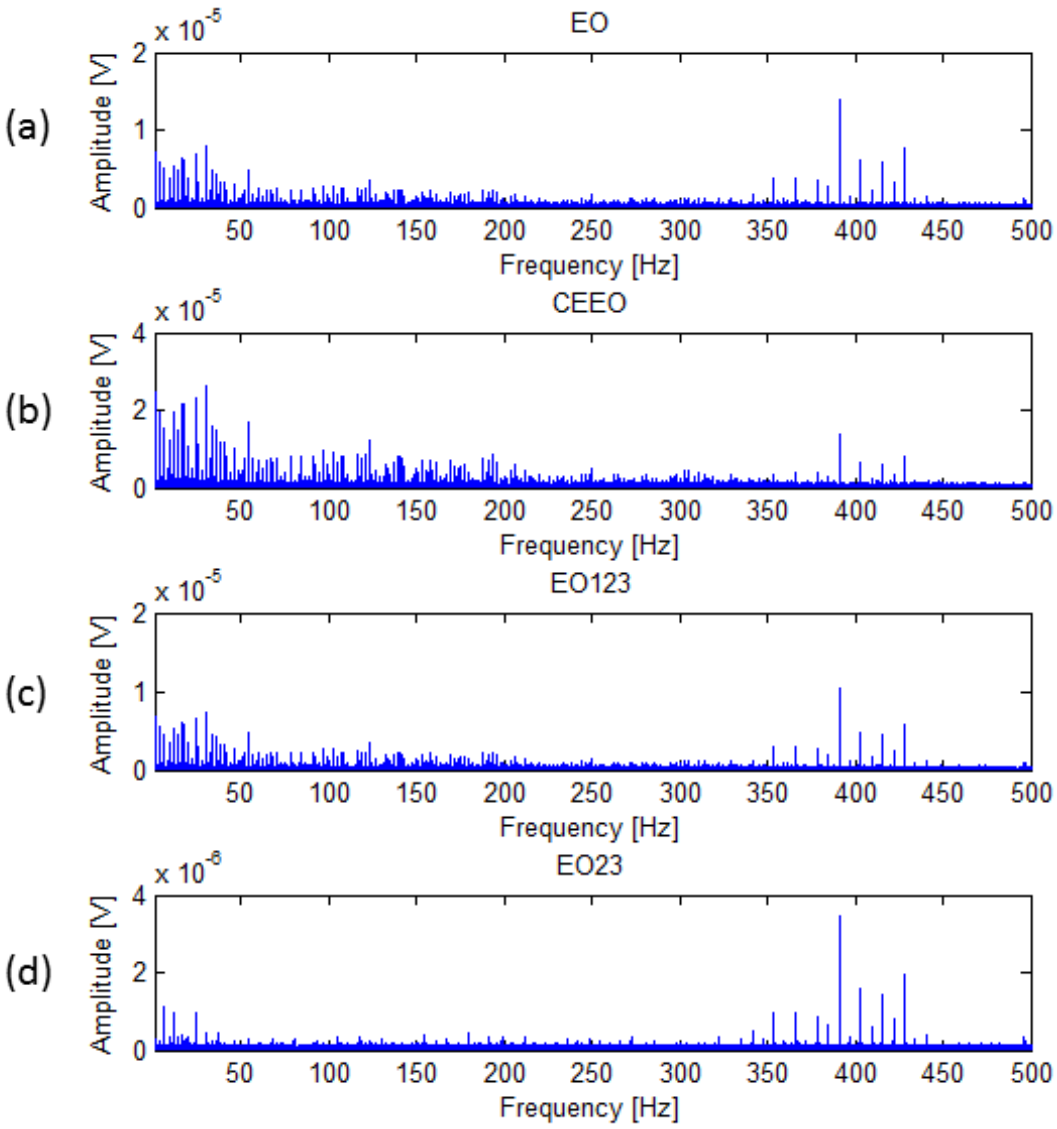

Figure 5.16: Fault detection methods (a) EO (b) CEEO (c) EO123 (d) EO23 applied to experimental data with a rotational frequency of the driving gear of 6 Hz

The plots obtained by applying the EO, CEEO, and EO123 are very similar to each other, as shown in Figure 5.16 (a), (b) and (c). The EO23 results in a very interesting signal. Considering the accelerometer is placed to detect faults on the driving gear, which rotates at a frequency of 6 Hz, the EO23 handles the interfering signal at the 2 Hz harmonics the best. The noise is still the most dominant with this fault detection method.

It is also possible to notice the second harmonic of the meshing frequency (195 Hz) which has a value of 390 Hz. The faulty peaks surrounding 390 Hz are at harmonics of the rotational frequency. As well as around zero and as mentioned previously, faults can be identified around the meshing frequency.

5.2.3 Chipped driven gear and broken (missing or partially missing) tooth on driving gear

Data is compiled from the vibration signal of the rotation of a driving gear with a partially or completely missing tooth driving a gear containing a chipped tooth. At frequencies higher than 7 Hz the results are quite similar to those observed previously with a cracked driving gear. At frequencies lower than 7 Hz some conclusions can be made about the fault detection methods.

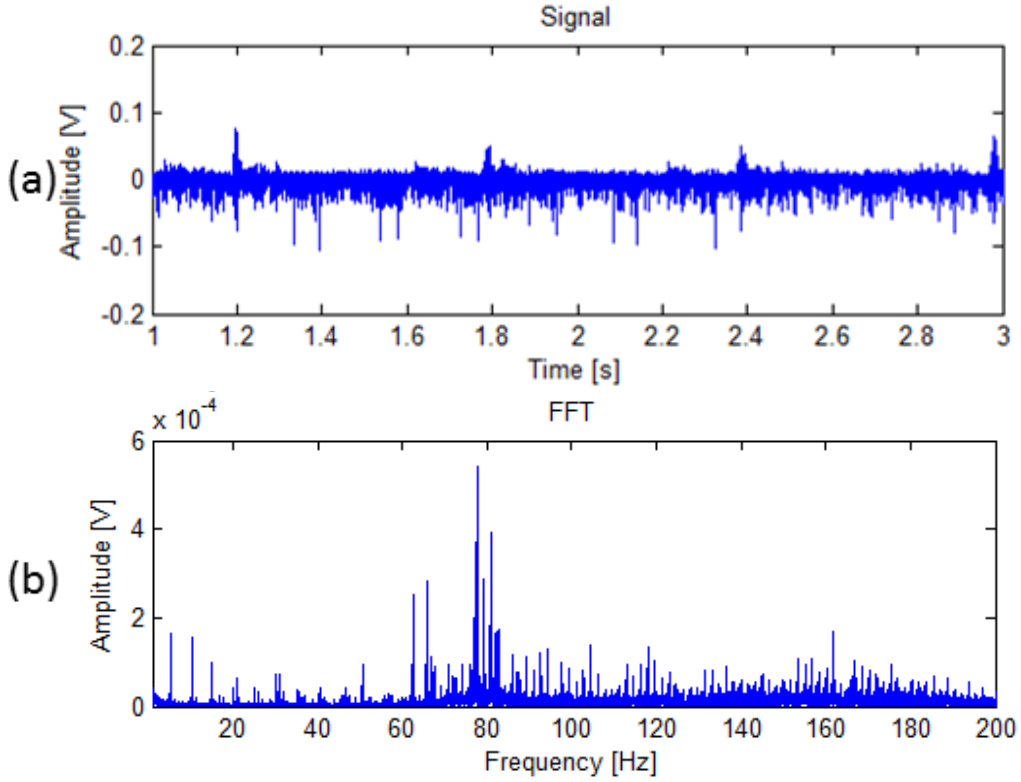

Figure 5.17: Experimental evaluation at a rotational frequency of 5 Hz (a) in the time domain (b) and frequency domain where the driving gear has a partially missing tooth

In Figure 5.17 (a) the time-domain signal is illustrated. The large peaks seen Figure 5.17 (b) are caused by the partially missing tooth on the driving gear at 5 Hz and its harmonics. The chipped tooth on the driving gear is less dominant in the signal than seen in plots at a higher rotational frequency.

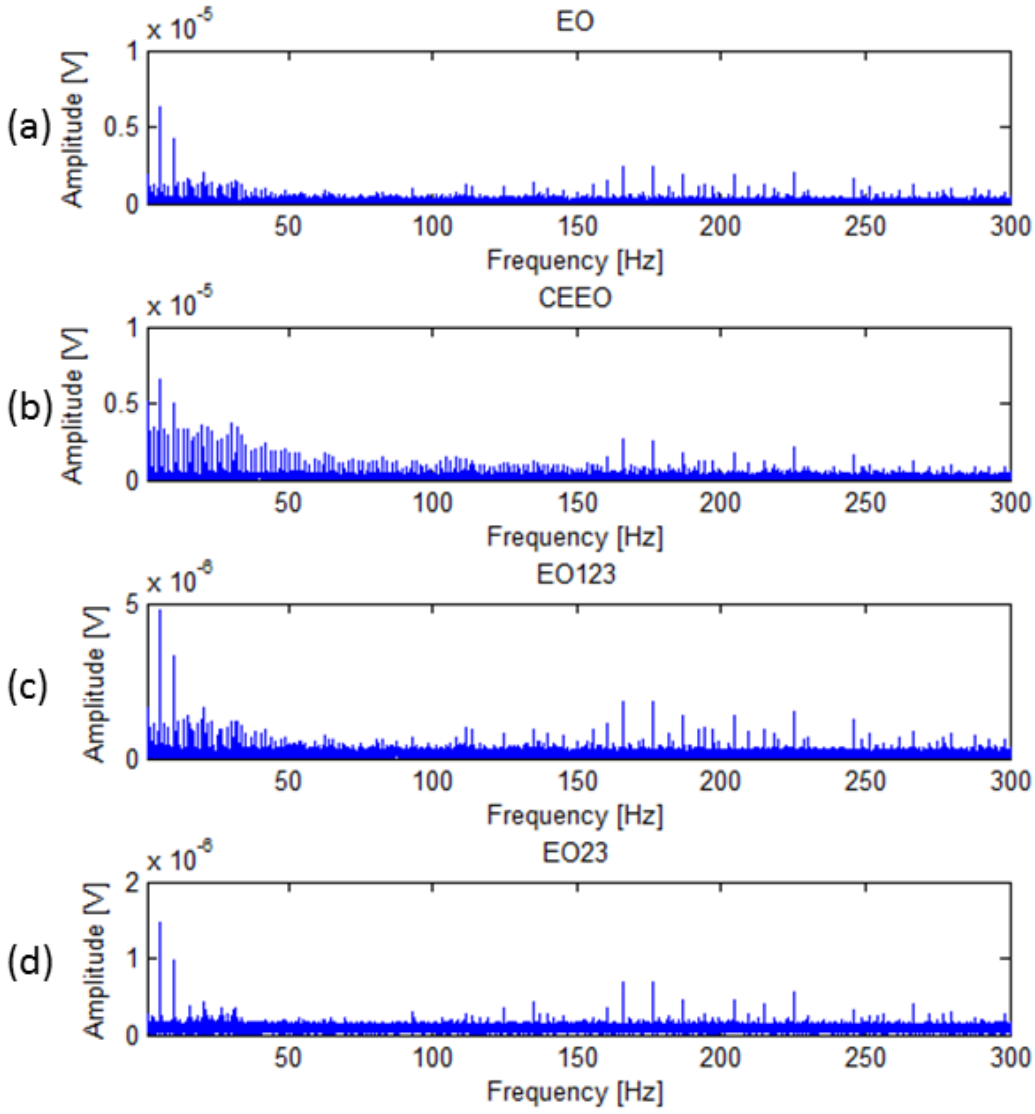

Figure 5.18: Fault detection methods (a) EO (b) CEEO (c) EO123 (d) EO23 applied to experimental data with a rotational frequency of the driving gear of 5 Hz with a partially missing tooth

The fault detection methods each modify the signal differently. The plots in Figure 5.18 (a) and (c) obtained after applying the EO and the EO123 has handled noise and interference better than the FFT shown in Figure 5.17 (b). The CEEO method; however, brings the amplitude of the peaks, caused by the chipped driven gear, closer to that of the partially missing tooth, as observed in Figure 5.18 (b). Interference is therefore more dominant. Finally, the EO23 method shown in Figure 5.18 (d) clearly shows the peaks caused by the fault on the driving gear at a rotational frequency of 5 Hz and reduces the interfering fault of the driven gear. The results differ for the case of the tooth being completely missing. Because it is a larger fault, larger impulses caused by the driving gear are expected.

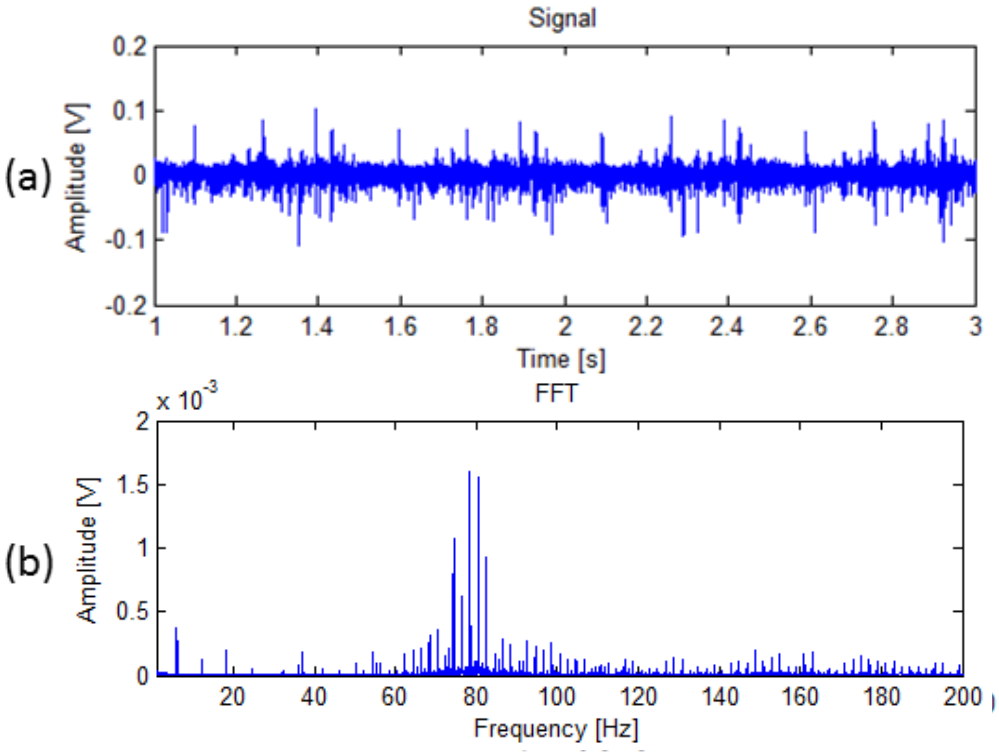

Figure 5.19: Experimental evaluation at a driving gear rotational frequency of 6 Hz (a) in the time domain (b) and frequency domain where the driving gear has a missing tooth

The original signal is shown in Figure 5.19 (a). As expected in Figure 5.19 (b), its FFT shows large peaks caused by the missing tooth at distances of 6 Hz from one another. The chipped tooth on the driven gear shows smaller impulses at 2 Hz and its harmonics. Once again, this is explained by the rotational ratio of one third. This was expected, considering a missing tooth is a large fault.

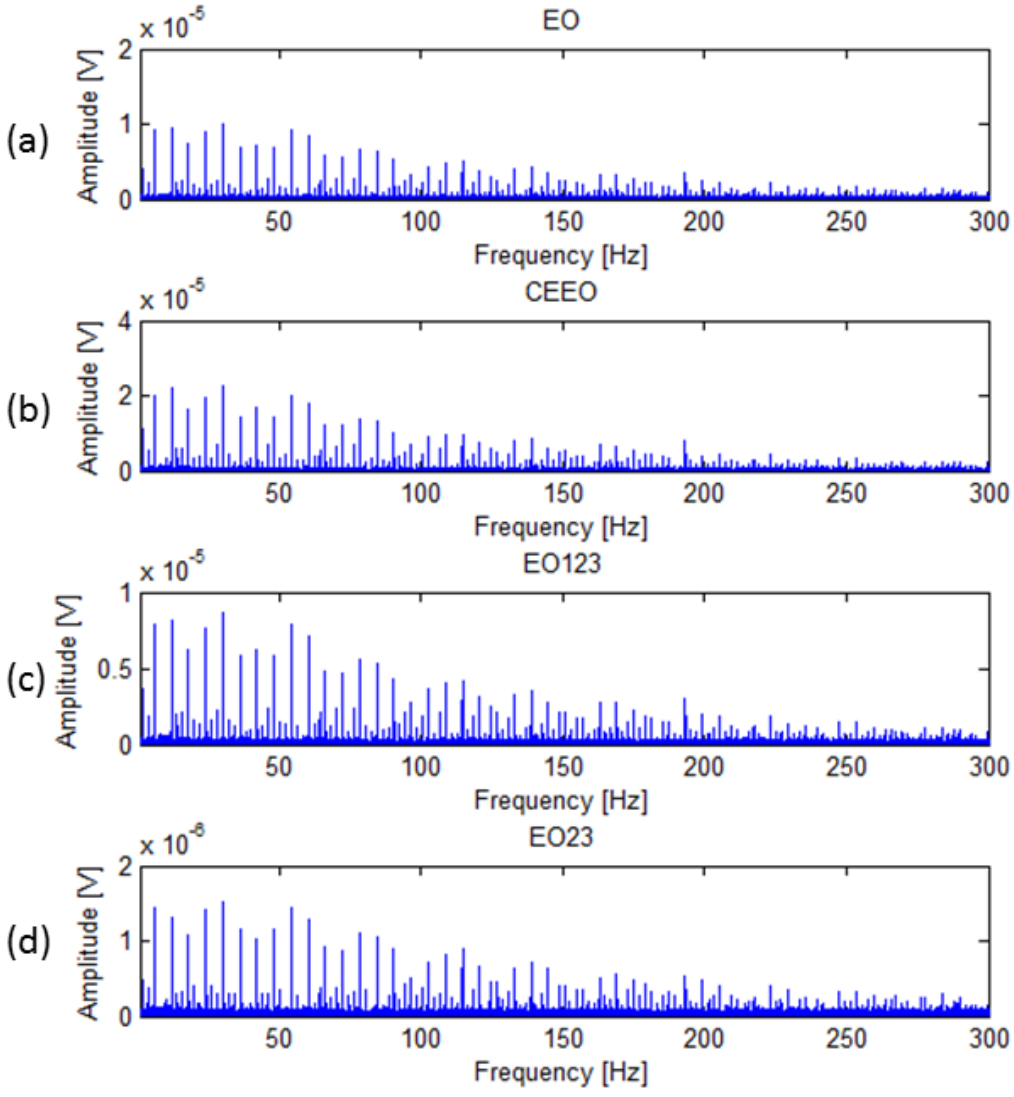

Figure 5.20: Fault detection methods (a) EO (b) CEEO (c) EO123 (d) EO23 applied to experimental data with a rotational frequency of the driving gear of 5 Hz with a missing tooth

All the fault detection methods shown in Figure 5.20 result in larger peaks in the plot caused by the missing tooth on the driving gear and smaller peaks caused by the chipped driven gear.

5.3 **Summary and conclusions**

A few observations can be made on the ability of the proposed methods to detect local faults in presence of noise and interference based on simulated and experimental evaluations.

All methods are effective for the detection of impulsive faults; however, there are differences between the methods:

- The EO and EO123 methods: These two methods are close to being the same. These methods work very well; however, they are weak when it comes to handling interference.
- The CEEO method: This method is the best method in the presence of a lot of noise.
- The EO23 method: This method is weak when a lot of noise is present in the signal; however, it is the best method at handling interferences.

Chapter 6 Conclusion

In conclusion, the intention of this thesis is to find an effective method that can (i) detect both types of gear faults: local and distributed faults; (ii) that does not require information from the gear's healthy state or a reference state; (iii) that handles noise and interference; and (iv) that is as simple as possible. The energy operator (EO) has been used in the past and respects these requirements; however, its ability to handle noise and interference can be improved. The CEEO method has been developed previously for bearing fault detection and was shown to be more effective to handle noise and interference than the EO [25]. Two other methods deriving from the EO were proposed: the EO123 and the EO23.

In Chapter 3 the theory on the EO and its variants is explained. The EO and the CEEO are methods that have been previously developed and are explained here. However, the CEEO has never been proposed nor evaluated for fault detection on gears. The EO123 and EO23 are variants of the EO proposed here for the first time. In Chapter 4, the methods are tested and analysed on distributed faults. Simulated and experimental data is used. As for Chapter 5, the four methods are observed when applied simulated and experimental data of local faults.

The tests and analysis in the current thesis done on the CEEO applied to gears reveal that it is better at handling noise than the EO and the other EO derived methods. The results obtained by applying the EO123 are, as predicted, very close to the results obtained with the EO. The EO23 was shown to handle interferences better than the other EO derived methods. In different situations, different methods have shown to be more effective. A good solution would be to

apply a few of the fault detection methods at the same time to complement each other, as these methods are all computationally efficient.

In future work, it would be interesting to add a code to automatically identify presence of faults by analysing the output signals. It could also be useful to apply the fault detection methods to data in more extreme conditions where the signal contains more noise and interference. This could be a better way to test the limits of the methods experimentally.

References

[1] P. D. McFadden, “Detecting Fatigue Cracks in Gears by Amplitude and Phase Demodulation of the Meshing Vibration,” *J. Vib. Acoust. Stress Reliab. Des.*, vol. 108, no. 2, pp. 165–170, Apr. 1986.

[2] P. D. McFadden, “Examination of a technique for the early detection of failure in gears by signal processing of the time domain average of the meshing vibration,” *Mech. Syst. Signal Process.*, vol. 1, no. 2, pp. 173–183, Apr. 1987.

[3] G. Dalpiaz, A. Rivola, and R. Rubini, “Effectiveness and sensitivity of vibration processing techniques for local fault detection in gears,” *Mech. Syst. Signal Process.*, vol. 14, no. 3, pp. 387–412, May 2000.

[4] R. B. Randall, *Vibration-based Condition Monitoring: Industrial, Aerospace and Automotive Applications*. John Wiley & Sons, 2011.

[5] S. Ebersbach, Z. Peng, and N. J. Kessissoglou, “The investigation of the condition and faults of a spur gearbox using vibration and wear debris analysis techniques,” *Wear*, vol. 260, no. 1–2, pp. 16–24, Jan. 2006.

[6] Z. Peng and N. Kessissoglou, “An integrated approach to fault diagnosis of machinery using wear debris and vibration analysis,” *Wear*, vol. 255, no. 7–12, pp. 1221–1232, Aug. 2003.

[7] Lebold M., McClintic K., Campbell R, “Review of vibration analysis methods for gearbox diagnostics and prognostics,” pp. 623–634, 2000.

[8] J. F. Kaiser, “On a simple algorithm to calculate the 'energy' of a signal,” in , *1990 International Conference on Acoustics, Speech, and Signal Processing, 1990. ICASSP-90*, 1990, pp. 381–384 vol.1.

[9] W. J. Staszewski and G. R. Tomlinson, “Application of the wavelet transform to fault detection in a spur gear,” *Mech. Syst. Signal Process.*, vol. 8, no. 3, pp. 289–307, May 1994.

[10] S. H. Hyunuk Ha, “Fault Detection on Transmission Lines Using a Microphone Array and an Infrared Thermal Imaging Camera,” *Instrum. Meas. IEEE Trans. On*, vol. 61, no. 1, pp. 267 – 275, 2012.

[11] R. Collacott, *Mechanical Fault Diagnosis and condition monitoring*. Springer Science & Business Media, 2012.

[12] G. P. Stachowiak, G. W. Stachowiak, and P. Podsiadlo, “Automated classification of wear particles based on their surface texture and shape features,” *Tribol. Int.*, vol. 41, no. 1, pp. 34–43, Jan. 2008.

[13] M. E. Badaoui, F. Guillet, and J. Danière, “New applications of the real cepstrum to gear signals, including definition of a robust fault indicator,” *Mech. Syst. Signal Process.*, vol. 18, no. 5, pp. 1031–1046, Sep. 2004.

[14] W. J. Wang and P. D. McFadden, “Application of orthogonal wavelets to early gear damage detection,” *Mech. Syst. Signal Process.*, vol. 9, no. 5, pp. 497–507, Sep. 1995.

[15] R. Guilbault, C. Gosselin, and L. Cloutier, “Helical Gears, Effects of Tooth Deviations and Tooth Modifications on Load Sharing and Fillet Stresses,” *J. Mech. Des.*, vol. 128, no. 2, pp. 444–456, May 2005.

[16] R. G. Parker, S. M. Vijayakar, and T. Imajo, “Non-linear dynamic response of a spur gear pair: Modelling and experimental comparisons,” *J. Sound Vib.*, vol. 237, no. 3, pp. 435–455, Oct. 2000.

[17] X. Fan and M. J. Zuo, “Gearbox fault detection using Hilbert and wavelet packet transform,” *Mech. Syst. Signal Process.*, vol. 20, no. 4, pp. 966–982, May 2006.

[18] V. K. Rai and A. R. Mohanty, “Bearing fault diagnosis using FFT of intrinsic mode functions in Hilbert–Huang transform,” *Mech. Syst. Signal Process.*, vol. 21, no. 6, pp. 2607–2615, Aug. 2007.

[19] Z. K. Peng, P. W. Tse, and F. L. Chu, “A comparison study of improved Hilbert–Huang transform and wavelet transform: Application to fault diagnosis for rolling bearing,” *Mech. Syst. Signal Process.*, vol. 19, no. 5, pp. 974–988, Sep. 2005.

[20] B. Liu, S. Riemenschneider, and Y. Xu, “Gearbox fault diagnosis using empirical mode decomposition and Hilbert spectrum,” *Mech. Syst. Signal Process.*, vol. 20, no. 3, pp. 718–734, Apr. 2006.

[21] Z. K. Peng, P. W. Tse, and F. L. Chu, “An improved Hilbert–Huang transform and its application in vibration signal analysis,” *J. Sound Vib.*, vol. 286, no. 1–2, pp. 187–205, Aug. 2005.

[22] P. D. McFadden and J. D. Smith, “Vibration monitoring of rolling element bearings by the high-frequency resonance technique — a review,” *Tribol. Int.*, vol. 17, no. 1, pp. 3–10, Feb. 1984.

[23] D. Yu, Y. Yang, and J. Cheng, “Application of time–frequency entropy method based on Hilbert–Huang transform to gear fault diagnosis,” *Measurement*, vol. 40, no. 9–10, pp. 823–830, Nov. 2007.

[24] K. Guo, X. Zhang, H. Li, and G. Meng, “Application of EMD method to friction signal processing,” *Mech. Syst. Signal Process.*, vol. 22, no. 1, pp. 248–259, Jan. 2008.

[25] H. Faghidi, “Non-parametric and Non-filtering Methods for Rolling Element Bearing Condition Monitoring,” 2014.

[26] W. Wang, “Early detection of gear tooth cracking using the resonance demodulation technique,” *Mech. Syst. Signal Process.*, vol. 15, no. 5, pp. 887–903, Sep. 2001.

[27] J. Shiroishi, Y. Li, S. Liang, T. Kurfess, and S. Danyluk, “Bearing condition diagnostics via vibration and acoustic emission measurements,” *Mech. Syst. Signal Process.*, vol. 11, no. 5, pp. 693–705, Sep. 1997.

[28] Y.-T. Sheen, “3D spectral analysis for vibration signals by wavelet-based demodulation,” *Mech. Syst. Signal Process.*, vol. 20, no. 4, pp. 843–853, May 2006.

[29] I. S. Bozchalooi and M. Liang, “A joint resonance frequency estimation and in-band noise reduction method for enhancing the detectability of bearing fault signals,” *Mech. Syst. Signal Process.*, vol. 22, no. 4, pp. 915–933, May 2008.

[30] I. S. Bozchalooi and M. Liang, “A smoothness index-guided approach to wavelet parameter selection in signal de-noising and fault detection,” *J. Sound Vib.*, vol. 308, no. 1–2, pp. 246–267, Nov. 2007.

[31] J. Lin and M. J. Zuo, “Gearbox fault diagnosis using adaptive wavelet filter,” *Mech. Syst. Signal Process.*, vol. 17, no. 6, pp. 1259–1269, Nov. 2003.

[32] H. Qiu, J. Lee, J. Lin, and G. Yu, “Wavelet filter-based weak signature detection method and its application on rolling element bearing prognostics,” *J. Sound Vib.*, vol. 289, no. 4–5, pp. 1066–1090, Feb. 2006.

[33] F. Combet and L. Gelman, “Optimal filtering of gear signals for early damage detection based on the spectral kurtosis,” *Mech. Syst. Signal Process.*, vol. 23, no. 3, pp. 652–668, Apr. 2009.

[34] J. Antoni, “The spectral kurtosis: a useful tool for characterising non-stationary signals,” *Mech. Syst. Signal Process.*, vol. 20, no. 2, pp. 282–307, Feb. 2006.

[35] M. L. I. Soltani Bozchalooi, “Teager energy operator for multi-modulation extraction and its application for gearbox fault detection,” *Smart Mater. Struct.*, vol. 19, no. 7, p. 075008, 2010.

[36] Safizadeh M. S., Lakis A. A., Thomas M., “Gear fault diagnosis using time-frequency methods,” 2002.

[37] M. Liang and H. Faghidi, “Intelligent bearing fault detection by enhanced energy operator,” *Expert Syst. Appl.*, vol. 41, no. 16, pp. 7223–7234, Nov. 2014.

[38] H. Wang and G. Yang, “Fault Detection Observer Design in Low Frequency Domain,” in *IEEE International Conference on Control Applications, 2007. CCA 2007*, 2007, pp. 976–981.

Appendices

Appendix A – MATLAB Code for distributed faults

```
% Elise Mayo
% University of Ottawa
% 2015

% Main for faulty gear
% Distributed fault

clc
clear all

%% Parametres
Am=1;                                   %Amplitude
phim=0;                                 %Initial phase
M=4;                                    %Number of sumations
%am=sum amn sin(n wrt+phimna)
Nam=1;                                  %Number of sumations a
amn=0.9;                                %Amplitude of a
phimna=0;                               %Phase of a
%bm=sum bmn sin(n wrt+phimnb)
Nbm=1;                                  %Number of sumations b
bmn=0;                                  %Amplitude of b
phimnb=0;                               %Phase of b
%wm = k wrt
Fr=50;
k=32;                                   %Number of teeth
wrt=Fr*pi()*2;                          %Rotational frequency
wm=k*wrt;                               %Meshing frequency

%% Signal Simulation
%The simulated value of x(t)
T=3;
incr=0.0001;
x=zeros(T/incr,1);
time=zeros(T/incr,1);
Fs=1/incr;

for t=0:incr:T
    %The strength of AM
    am=0;
    for n=1:1:Nam
        am=am+amn*sin(n*wrt*t+phimna);
    end;
    %The strength of PM
    bm=0;
    for n=1:1:Nbm
        bm=bm+bmn*sin(n*wrt*t+phimnb);
    end;
```

```
    X=0;
    for m=1:M
        X=X+Am*(1+am)*sin(m*wm*t+phim+bm);
    end;
    x(round(t/incr)+1,1)=X;
    time(round(t/incr)+1,1)=t;
end;

%% Different situations
% 4 signals are extracted from this:
% clean, noise, interference, noise+interference

% Noise
[x]=noise(x);
% Interference
[x]=inter(x,time);

%% Fault detection methods
%energy operator
E = energy(x);
%CEEO
vteo = CEEO(x);
%EO123
E123 = energy123(x);
%EO23
E23 = energy23 (x);

%% Apply fast fourier transforms
L=length(x);
NFFT = 2^nextpow2(L);
Y1 = fft(  E , NFFT)/L;    Y2 = fft(  vteo, NFFT)/L;  Y3 = fft( E123 ,
NFFT)/L;  Y4 = fft( E23,NFFT)/L;
YY1=2*abs(Y1(1:NFFT/2+1)); YY2=2*abs(Y2(1:NFFT/2+1));
YY3=2*abs(Y3(1:NFFT/2+1)); YY4=2*abs(Y4(1:NFFT/2+1));
f = Fs/2*linspace(0,1,NFFT/2+1);

%% Figures
% Original Signal
figure(1)
set(gcf,'color','w');
subplot(2,1,1),plot(time(:,1),x(:,1)),title('Signal'),xlabel('Time
[s]'),ylabel('Amplitude [V]'),xlim([1 3]);
% Apply FFT
spec=abs(fft(detrend(x(:,1)),T/incr))/T/incr;
subplot(2,1,2),plot(f(5:4000),YY1(5:4000)),title('FFT'),xlabel('Frequency
[Hz]'),ylabel('Amplitude [V]'),xlim([1 500]);

figure(2)
set(gcf,'color','w');
% energy operator
subplot(4,1,1),plot(f(5:8000),YY1(5:8000)),title('EO'),xlabel('Frequency
[Hz]'),ylabel('Amplitude [V]'),xlim([1 1000]);
% CEEO
subplot(4,1,2),plot(f(5:8000),YY2(5:8000)),title('CEEO'),xlabel('Frequency
[Hz]'),ylabel('Amplitude [V]'),xlim([1 1000]);
% energy operator2 1+2+3
```

```
subplot(4,1,3),plot(f(5:8000),YY3(5:8000)),title('EO123'),xlabel('Frequency
[Hz]'),ylabel('Amplitude [V]'),xlim([1 1000]);
% energy operator2 2+3
subplot(4,1,4),plot(f(5:8000),YY4(5:8000)),title('EO23'),xlabel('Frequency
[Hz]'),ylabel('Amplitude [V]'),xlim([1 1000]);
```

Appendix B – MATLAB Code for local faults

```
% Elise Mayo
% University of Ottawa
% 2015

% Main for faulty gear
% Local fault

clc
clear all

%% Parametres
Am=1;                                   %Amplitude
M=1;                                    %Number of sumations
Beta=500;                               %Damping caracteristic
wr=512;                                 %excited resonance frequency
phim=0;                                 %Phase

%wm = k wrt
Fr=24;                                  %Rotational frequency Hz
Trt=1/Fr;                               %Period of a rotation
k=32;                                   %Number of teeth
wrt=Fr*pi()*2;                          %Angular Rotational frequency rad
wm=k*wrt;                               %Angulat Meshing frequency rad

%% Signal Simulation
%The simulated value of x(t)
T=3;
incr=0.0001;
x=zeros(1.6/incr,1);
time=zeros(1.6/incr,1);
x1=zeros(T/incr,1);
time1=zeros(T/incr,1);
Fs=1/incr;

for a=1:1:T/Trt
    for t=0:incr:T-incr
        X=0;
        for m=1:M
            X=X+Am*exp(-Beta*(t-M*Trt*a))*cos(wr*(t-M*Trt*a)+phim)*stepfun((t
- Trt*a*M),0);
        end;
        x1(round(t/incr)+1,1)=X+x1(round(t/incr)+1,1);
        time1(round(t/incr)+1,1)=t;
    end;
end;

for o=1:1:1.4*Fs
    x(o,1)=x1(o+1.6*Fs,1);
    time(o,1)=time1(o,1);
end;
```

```
%% Different situations
% 4 signals are extracted from this:
% clean, noise, interference, noise+interference

% Noise
[x]=noise(x);
% Interference
[x]=inter(x,time);

%% Fault detection methods
%energy operator
E = energy(x);
%CEEO
vteo = CEEO(x);
%EO123
E123 = energy123(x);
%EO23
E23 = energy23 (x);

%% Apply fast fourier transforms
L=length(x);
NFFT = 2^nextpow2(L);
Y1 = fft(  E , NFFT)/L;    Y2 = fft(  vteo, NFFT)/L;  Y3 = fft( E123 ,
NFFT)/L;  Y4 = fft( E23,NFFT)/L;
YY1=2*abs(Y1(1:NFFT/2+1)); YY2=2*abs(Y2(1:NFFT/2+1));
YY3=2*abs(Y3(1:NFFT/2+1)); YY4=2*abs(Y4(1:NFFT/2+1));
f = Fs/2*linspace(0,1,NFFT/2+1);

%% Figures
% Original Signal
figure(1)
set(gcf,'color','w');
subplot(2,1,1),plot(time(:,1),x(:,1)),title('Signal'),xlabel('Time
[s]'),ylabel('Amplitude [V]'),xlim([0 1.4]),ylim([-0.6 1.2]);
% Apply FFT
spec=abs(fft(detrend(x(:,1)),T/incr))/T/incr;
subplot(2,1,2),plot(f(5:4000),YY1(5:4000)),title('FFT'),xlabel('Frequency
[Hz]'),ylabel('Amplitude [V]'),xlim([1 500]);

figure(2)
set(gcf,'color','w');
% energy operator
subplot(4,1,1),plot(f(5:8000),YY1(5:8000)),title('EO'),xlabel('Frequency
[Hz]'),ylabel('Amplitude [V]'),xlim([1 1000]);
% CEEO
subplot(4,1,2),plot(f(5:8000),YY2(5:8000)),title('CEEO'),xlabel('Frequency
[Hz]'),ylabel('Amplitude [V]'),xlim([1 1000]);
% energy operator2 1+2+3
subplot(4,1,3),plot(f(5:8000),YY3(5:8000)),title('EO123'),xlabel('Frequency
[Hz]'),ylabel('Amplitude [V]'),xlim([1 1000]);
% energy operator2 2+3
subplot(4,1,4),plot(f(5:8000),YY4(5:8000)),title('EO23'),xlabel('Frequency
[Hz]'),ylabel('Amplitude [V]'),xlim([1 1000]);
```

Appedix C – MATLAB Functions

Energy:

```
function [E] = energy(signal)
% Energy operator
% ENERGY METHOD WITH LENGTH L WHICH IS LENGTH SIGNAL
E= signal;
L=length(E);

e = signal;
for i=2:L-2
    E(i) = e(i).^2-e(i-1)*e(i+1);
end

 E(1)=E(2);
 E(end)=E(end-1);
```

CEEO:

```
function [ vteo] = CEEO( swn )

% CEEO
% k: time shift that for CEEO is 2.
% swn: input signal

L=length(swn);
e= swn;
vteo= zeros(L,1);

for i=1+2:1:L-2
          vteo(i,1)= e(i)*e(i)- e(i-2)*e(i+2);
end
vteo(L-2+1:end,1)= vteo(L-2);
vteo(1:2,1)= vteo(1+2);
```

Energy123:

```
function [E] = energy123(signal)
% EO123
E= signal;
L=length(E);
e=signal;

for ii=3:L-3
```

```
    E(ii) =-1/3*(e(ii).^2-e(ii-1)*e(ii+1))+1/12*(e(ii).^2-e(ii+2)*e(ii-2))+
e(ii+1).^2-e(ii)*e(ii+2);
end
```

Energy23:

```
function [E] = energy23(signal)
% EO23
% ENERGY METHOD WITH LENGTH L WHICH IS LENGTH SIGNAL
E= signal;
L=length(E);
e=signal;

for ii=3:L-3
    E(ii) =-1/3*(e(ii).^2-e(ii-1)*e(ii+1))+1/12*(e(ii).^2-e(ii+2)*e(ii-2));
end
```

Noise:

```
function [x]=noise(x)

%% Add white gaussian noise
% 1, -1, -2, -5, -10, -15, -20 dB
 x = awgn(x,-10,'measured'); % avec snr en dB
```

Inter:

```
function [x]=inter(x,time)
%% Add interference
Sir =  -5;     % Sir: signal to interference ratio
Ai = [];
 if isempty(Ai)
   sigPower = sum(abs(x(:)/10).^2)/length(x(:)/10);
   sigPower = 10*log10(sigPower);
   intPower = sigPower-Sir;
   intPower = 10^(intPower/10);
   intPower = intPower/4;
   Ai = sqrt(intPower*2);
 end;
 x = x  + Ai*sin(2*pi*4*time)+ Ai*sin(2*pi*(4/3)*time);
```